

**Iron Amino-phenolate Complexes as Catalysts
for CO₂ Activation**

by

© Erika D. Butler

A thesis submitted to the
School of Graduate Studies
in partial fulfillment of the requirements for the degree of

Master of Science (M.Sc.)

Department of Chemistry
Memorial University of Newfoundland
St. John's, Newfoundland and Labrador, Canada

March 2018

St. John's

Newfoundland

Abstract

The increase of CO₂ emissions in the atmosphere from the burning of fossil fuels has been linked to global climate change. Therefore, finding methods to utilize CO₂, a greenhouse gas, as a C1 feedstock has become of interest. The utilization of CO₂ is beneficial as it is an inexpensive, abundant feedstock with low toxicity, and it can react with epoxides to produce polycarbonates or cyclic carbonates; both of which have several applications. Cyclic carbonates can act as polar aprotic green solvents as well as chemical intermediates for the synthesis of other small molecules and polymers, while polycarbonates can be used to synthesize several biodegradable plastics. Using iron to catalyze these reactions has its own benefits as iron is inexpensive, abundant, and biocompatible.

Both the formation of cyclic carbonates and polycarbonates was carried out using iron(III) amino-bis(phenolate) complexes. The iron(III) complexes were characterized by UV-vis spectroscopy, MALDI-TOF MS, and elemental analysis. These complexes were capable of selectively producing cyclic carbonate from carbon dioxide and several epoxides, and reaction parameters could be fine tuned to reduce temperature and reaction time. Polycarbonates were also synthesized selectively from CO₂ and cyclohexene oxide (CHO) in high yields with moderate molecular weights and low dispersities. Polycarbonate synthesis could be carried out at low pressures and temperatures, which is not common for iron catalyst systems. Isolated polymers were studied further using NMR spectroscopy, GPC analysis, and MALDI-TOF MS.

Acknowledgements

I would like to first and foremost thank my supervisor Dr. Christopher Kozak for his guidance throughout my Master's program. This experience has been so enjoyable thanks to his constant guidance and passion for chemistry. Dr. Kozak has always been available to answer all questions I may have, and thanks to his positive criticism, and encouragement to always think 'bigger', I am where I am today – a better scientist and person. I would also like to thank Dr. Fran Kerton and Dr. Robert Davis, my committee members, who have supported me throughout my journey with their ideas and advice. Thank you to Dr. Grover as well for helping with my thesis and giving me advice after my departmental seminar.

Thank you to the Green Chemistry and Catalysis members, past and present, who were not only coworkers and lab mates, but who became my family over the years. I would also like to thank NSERC, the School of Graduate Studies, Graduate Students Union, and the Department of Chemistry for funding.

Lastly, I would like to express my thanks to my family who have supported me throughout my entire life and have done nothing but encourage me to chase my dreams. They have believed in me when I have doubted myself and pushed me to become the best version of myself.

Table of Contents

Abstract	i
Acknowledgements	ii
Table of Contents	iii
List of Tables	v
List of Figures	vii
List of Schemes	xii
List of Abbreviations and Symbols	xiii

Chapter 1: Introduction..... 1

1.1 Green Chemistry: Evolution and principles.....	1
1.2 Synthesis and Polycarbonates Industrially.....	4
1.3 CO ₂ and its Applications.....	7
1.4 Polycarbonate Synthesis via the Coupling of CO ₂ and Epoxides.....	9
1.4.1 Propylene Oxide as Common Epoxide: its Appeal and Diversity..	10
1.4.2 Common Catalysts for the Copolymerization of CO ₂ and Epoxides.....	13
1.4.2.1 Co Catalysts used in Copolymerization Reactions.....	13
1.4.2.2 Zn Catalysts used in Copolymerization Reactions.....	16
1.4.2.3 Cr Catalysts used in Copolymerization Reactions.....	22
1.4.2.4 CO ₂ /Epoxide Coupling Studies at Memorial University.....	27
1.4.3 Iron Complexes for the Copolymerization of CO ₂ and Epoxides ..	32
1.4.3.1 Summary of iron catalyzed reactions with CO ₂ and epoxides.....	44
1.5 Objectives for this Thesis.....	46
1.6 References.....	47

Chapter 2: Synthesis and Characterization of Iron Complexes of Diamino-bis(phenolate) Ligands..... 51

2.1 Introduction.....	51
2.2 Synthesis of Tetradentate Amino-bis(phenolate) Ligands.....	51
2.3 Synthesis of Iron(III) Complexes using Tetradentate Amino-bis(phenolate) Ligands.....	53
2.4 Characterization.....	55
2.4.1 NMR Spectroscopy.....	55
2.4.2 Elemental Analysis.....	57
2.4.3 MALDI TOF-MS.....	58
2.4.4 UV-visible Spectroscopy.....	62
2.5 Conclusions.....	63
2.6 Experimental.....	64
2.6.1 General Methods and Procedures.....	64

2.6.2 Instrumentation.....	64
2.6.3 Synthesis.....	65
2.7 References.....	69

Chapter 3: Iron amine-bis(phenolate) complexes for the coupling of CO₂ with propylene oxide.....73

3.1 Introduction.....	73
3.2 Results and discussion.....	76
3.2.1 Catalyst Screening and Parameter Optimization.....	76
3.2.2 Use of an Internal Standard.....	86
3.2.3 Temperature Dependence and Kinetics.....	88
3.2.4 Epoxide Screening.....	91
3.3 Conclusions.....	95
3.4 Experimental.....	97
3.4.1 General Method and Procedures.....	97
3.4.2 Instrumentation.....	97
3.4.3 Preparation of a 2-component Catalyst System for CO ₂ -Epoxide Coupling Reactions.....	97
3.4.4 In situ Monitoring of the Coupling Reactions by IR Spectroscopy.....	98
3.5 References.....	99

Chapter 4: Iron Amino-bis(phenolate) Complexes for the Copolymerization of CO₂ with Cyclohexene Oxide 101

4.1 Introduction.....	101
4.2 Results and Discussion.....	104
4.2.1 Catalyst Screening and Parameter Optimization.....	104
4.2.2 Temperature, Pressure, and Time Effects.....	108
4.2.3 Method of Polymer Isolation.....	112
4.2.4 Characterization of Polymers by MALDI-TOF MS.....	115
4.3 Conclusions.....	116
4.4 Experimental.....	117
4.4.1 General method and procedures.....	117
4.4.2 Instrumentation.....	117
4.4.3 Copolymerization Procedure.....	117
4.5 References.....	119

Chapter 5: Conclusions and Future Work..... 121

Chapter 6: Appendix..... 124

List of Tables

1.1 The 12 Principles of Green Chemistry.....	2
1.2 Observed reaction rates for the formation of poly(propylene) carbonate and propylene carbonate at various temperatures as seen by Darensbourg and coworkers, reference 41	13
1.3 Iron catalysts used in the production of polycarbonates from CO ₂ and CHO; a summary of the literature presented in section 1.4.2.....	45
1.4 Iron catalysts used for the coupling of CO ₂ and epoxides to produce cyclic carbonate; a summary of the literature presented in section 1.4.2.....	46
2.1 Assignment of resonances for H ₂ L3 in the ¹ H NMR spectrum as seen in Figure 2.3	57
2.2 Assignment of resonances for H ₂ L3 in the ¹³ C NMR spectrum as seen in Figure 2.4.....	57
2.3 Elemental analysis data for complexes 1 - 4.....	58
3.1 Catalyst screening for the formation of propylene carbonate	76
3.2 Optimization of parameters for cyclic carbonate formation	79
3.3 Cocatalyst effects on the formation of propylene carbonate	80
3.4 Observed reaction rates for different methods of achieving the desired temperature and pressure conditions.....	85
3.5 Observed reaction rates for various temperatures.....	86
3.6 Various reactions of propylene carbonate formation, using mesitylene as an internal standard to determine yields	88
3.7 Observed rates of reaction for propylene carbonate formation.....	89
3.8 Cyclic carbonate formation using various epoxides.....	92
3.9 Observed reaction rates for cyclic carbonate formation using various epoxides	95
4.1 Catalyst screening for the formation of polycarbonate.....	105
4.2 Temperature and pressure effects on the formation of polycarbonate.....	108

4.3 Reaction time effects on the formation of polycarbonate	112
4.4 The effect of polymer isolation and increasing yield through various precipitation steps.....	114

List of Figures

1.1 Phosgene replacements to produce polycarbonates	7
1.2 Number of publications per year on Web of Science when searching for “CO ₂ epoxide copolymerization” as of September 2017.....	10
1.3 Activation energy diagram for the formation of poly(propylene)carbonate and propylene carbonate from PO and CO ₂ . Image taken with permission from reference 41.....	12
1.4 (Salen)Cr(III)Cl complex used in Darensbourg’s studies, reference 41.....	13
1.5 Co(II)-saly complexes (left) and PPNDNP (right), reference 42.....	14
1.6 Contribution of cationic radical species of Co(II) complexes for the copolymerization of PO and CO ₂ , reference 42.....	15
1.7 Bifunctional salcyCo(III)NO ₃ complex.....	16
1.8 Polycarbonate product from the reaction of PO and CO ₂ using a diethyl zinc catalyst.....	17
1.9 Tetrahedral zinc phenoxide derivatives used as catalysts for the copolymerization of CHO and CO ₂ reference 44	18
1.10 β-Diiminato zinc complexes synthesized by Coates and coworkers, reference 45.....	20
1.11 Acyclic bis(anilido-imine) complexes (top) and their related 30 membered macrocyclic compounds (bottom), reference 46.....	22
1.12 Chromium salen complex, where R ₁ and R ₂ are alkyl substituents	23
1.13 Dinuclear chromium(III) salen complexes, reference 29.....	24
1.14 Asymmetric bifunctional (salen)CrN ₃ complex, reference 49.....	26
1.15 Cr(III) tetremethyltetraazaannulene complex, reference 51	27
1.16 Tetradentate amine-bis(phenolate) ligands	28
1.17 Vacant sites available for coordination an incoming nucleophile, phenolate donors may be either <i>cis</i> (left) or <i>trans</i> (right).....	29
1.18 Dinuclear Cr(III) amine bis(phenolate) complex, reference 37.....	30

1.19 Cr(III) amino-bis(phenolate) complexes to study the effect of pendant group on activity, reference 59.....	31
1.20 First example of an iron catalyst to copolymerize CHO and CO ₂ , reference 25.....	33
1.21 Iron amino-triphenolate complex used for the copolymerization of CO ₂ with epoxides and two common cocatalysts, PPNX and Bu ₄ NX, reference 60	35
1.22 Iron(II) complexes for the copolymerization of CO ₂ with epoxides, reference 61.....	37
1.23 Iron(III) amino-bis(phenolate) complexes for the copolymerization of CHO and CO ₂ , reference 62	39
1.24 Bis(phenoxyiminato)Fe(III)-chloro complexes for the copolymerization of CO ₂ and epoxides, reference 63.....	40
1.25 Square pyramidal iron(III) complexes for the coupling of PO and CO ₂ , reference 24.....	42
1.26 Thioether-triphenolate bimetallic iron(III) complexes for the coupling of CO ₂ with various epoxides, reference 64.....	43
1.27 Effect of cocatalyst on the catalytic activity for the coupling of PO and CO ₂ using complex 1.24f , reference 64.....	44
2.1 Amino-bis(phenol) ligands synthesized.....	53
2.2 Iron amino-bis(phenolate) complexes 2.1-2.4	54
2.3 ¹ H NMR of H ₂ L 3 in CDCl ₃	56
2.4 ¹³ C{ ¹ H} NMR of H ₂ L 3 in CDCl ₃	56
2.5 Experimental (top) and modelled (bottom) MALDI-TOF mass spectrum of 1 ..	59
2.6 MALDI-TOF mass spectrum of 2.4	60
2.7 Magnification of the experimental (top) and modelled (bottom) molecular ion observed in the MALDI-TOF mass spectrum of 2.4	60
2.8 Magnification of the experimental (top) and modelled (bottom) MALDI-TOF mass spectrum of [2.2 -Cl] ⁺	61

2.9 Magnification of the experimental (top) and modelled (bottom) MALDI-TOF mass spectrum of [2.3-Cl] ⁺	61
2.10 Magnification of the experimental (top) and modelled (bottom) MALDI-TOF mass spectrum of [2.4-Cl] ⁺	62
2.11 UV-vis absorption spectrum of 2.2 in CH ₂ Cl ₂ . Expansion of the mid UV to visible region shows peak wavelengths and molar extinction coefficients.....	63
3.1 Iron amine-bis(phenolate) complexes 2.1-2.4 used throughout this study for the coupling of PO with CO ₂	75
3.2 ¹ H NMR spectrum in CDCl ₃ of cyclic propylene carbonate obtained according to the conditions in Table 3.2, entry 2	78
3.3 MALDI-TOF mass spectra of 2.2 (top) with one equivalent of DMAP (middle) and two equivalents of DMAP (bottom)	81
3.4 MALDI TOF mass spectrum of [2.2-Cl+DMAP] ⁺ . Experimental shown on top, isotopic modelling on bottom.....	82
3.5 Effect of cocatalyst on absorbance vs. time for $\nu_{CO} = 1810 \text{ cm}^{-1}$ corresponding to cyclic propylene carbonate formation.....	83
3.6 Initial rates of reaction comparing method of data collection.....	84
3.7 Normalized data demonstrating initial rates of reaction comparing methods of data collection	84
3.8 Initial rates of reaction for cyclic propylene carbonate formation at various temperatures	86
3.9 ¹ H NMR spectrum of cyclic propylene carbonate using mesitylene as an internal standard. Insert showing the 3 peaks analyzed: PO at 1.3ppm, PC at 1.5ppm, and mesitylene at 2.8 ppm.....	87
3.10 Normalized data demonstrating observed initial rates of reaction for propylene carbonate formation at various temperatures	89
3.11 Arrhenius plot for the formation of propylene carbonate to determine the activation energy for the 2.2/PPNCl system.....	90
3.12 Eyring plot for the formation of propylene carbonate to determine Gibbs free energy for the 2.2/PPNCl system.....	91
3.13 Various epoxides studied. Top: epichlorohydrin (left) and allyl glycidyl ether (right). Bottom: phenyl glycidyl ether(left) and styrene oxide (right)	92

3.14 Initial rates of reaction for cyclic carbonate formation using various epoxides	93
3.15 Normalized data for the observed rates of reaction of cyclic carbonate formation for epichlorohydrin and propylene oxide.....	94
3.16 Normalized data for the observed rates of reaction of cyclic carbonate formation for allyl glycidyl ether, phenyl glycidyl ether, and styrene oxide	94
4.1 Activation energy diagram for the copolymerization of CHO and CO ₂ , image taken with permission from reference 6.....	101
4.2 Iron catalysts in the literature used for the copolymerization of CHO and CO ₂ ..	103
4.3 Iron complex 2.4	105
4.4 ¹ H NMR spectrum in CDCl ₃ of polycarbonate obtained according to the conditions in Table 4.1, entry 3	107
4.5 The effect of pressure on overall conversion to polycarbonate	109
4.6 Relationship between the pressure of CO ₂ and TOF for the production of polycarbonate	111
4.7 Relationship between the pressure of CO ₂ and TOF to produce polycarbonate using a Cr salen complex, image taken with permission from ref. 20.....	111
4.8 MALDI-TOF spectrum of polycarbonate, insert demonstrating pattern at high molecular weights with only one end group present.....	115
4.9 Magnified MALDI-TOF spectra from Figure 4.8 demonstrating two potential end groups.....	116
6.1 ¹ H NMR spectrum of H ₂ L1 in CDCl ₃	124
6.2 ¹³ C{ ¹ H} NMR spectrum of H ₂ L1 in CDCl ₃	124
6.3 ¹ H NMR spectrum of H ₂ L2 in DMSO	125
6.4 ¹³ C{ ¹ H} NMR spectrum of H ₂ L2 in DMSO.....	125
6.7 ¹ H NMR spectrum of H ₂ L4 in CDCl ₃	126
6.8 ¹³ C{ ¹ H} NMR spectrum of H ₂ L4 in CDCl ₃	126
6.9 UV-vis spectrum of 2.1 in CH ₂ Cl ₂	127

6.10 UV-vis spectrum of 2.3 in CH ₂ Cl ₂	127
6.11 UV-vis spectrum of 2.4 in CH ₂ Cl ₂	128
6.12 UV-vis spectrum of 2.2 in CH ₂ Cl ₂ overlaid with 2.2 in PO	128
6.13 ¹ H NMR spectrum of isolated polycarbonate (Table 4.1 Entry 3).....	129
6.14 Magnified ¹³ C{ ¹ H} NMR spectrum of isolated polycarbonate (Table 4.1 Entry 3) demonstrating atactic stereoselectivity.....	129
6.15 ¹ H NMR of attempted homopolymerization reactions of CO ₂ and CHO using 2.4 ; from bottom to top: 25 °C, 40 °C, 60 °C, and 80 °C.....	130

List of Schemes

1.1 Industrial route to polycarbonate formation using BPA and phosgene	4
1.2 Polycondensation reaction of bisphenol M with diphosgene to produce cyclic oligomers	6
1.3 Simple schematic demonstrating the coupling of epoxides and CO ₂ to produce cyclic carbonates, or the polymerization process to synthesis polymers.....	9
1.4 Synthesis of polyethercarbonate polyols and cyclic propylene carbonate from propylene oxide, carbon dioxide, and an alcohol.....	11
1.5 Simplified proposed mechanism demonstrating the backbiting reaction formation of propylene carbonate by Darensbourg et al., reference 44.....	19
1.6 Coupling of BEP and CO ₂ to produce polymer and the depolymerization back to monomer at 100 °C	25
1.7 Simplified mechanistic approach to produce both cis and trans cyclic carbonate. Scheme adapted from reference 25	34
1.8 Oxidation of an iron(II) N ₂ O ₂ complex iron(III), reference 30.....	37
2.1 Synthesis of amino-bis(phenolate) ligands	52
2.2 Synthesis of iron amino-bis(phenolate) complexes	54
3.1 A simplified mechanistic cycle for the formation of propylene carbonate	74
3.2 Coordination of DMAP to 2	80
4.1 A simplified mechanistic cycle for the copolymerization/coupling of CHO and CO ₂	102

List of Abbreviations and Symbols

et al.: and others

E_a : activation energy

ATR: attenuated total reflectance

BEP: 1-benzoyloxycarbonyl-3,4-epoxy pyrrolidine

BPA-PC: bisphenol-A polycarbonates

salen: N,N'-bis(salicylidene)-ethylenediamine

PPNCl: bis(triphenylphosphoranylidene)iminium chloride

PPNDNP: bis(triphenylphosphoranylidene)iminium 2,4-dinitrophenolate

CO₂: carbon dioxide

C: Celsius

Cl⁻: chloride

δ : chemical shift

CCS: carbon capture and sequestration

CCU: carbon capture and utilization

CHO: cyclohexene oxide

CPC: cyclic propylene carbonate

(°): degree

CDCl₃: deuterated chloroform

Et₂Zn: diethyl zinc

BDI: β -diketiminat

DCM: dichloromethane

DMAP: 4-dimethylaminopyridine

DMC: dimethyl carbonate and double metal cyanide

DMF: dimethylformamide

DPC: diphenyl carbonate

FT: Fourier transformation

GPC: gel permeation chromatography

GAC: green analytical chemistry

HO: 1-hexene oxide

h: hour

IEA: international energy agency

IR: infrared

K: Kelvin

MS: mass spectrometry

m/z : mass to charge ratio

MALDI-TOF: matrix assisted laser desorption/ionization time of flight

λ_{\max} : maximum wavelength

mmol: millimole (10^{-3} mol)

min: minute

mL: millilitre

NMR: nuclear magnetic resonance

r_{obs} : observed rate

M_n : number average molecular weight

trans: 'on the other side'

cis: 'on the same side'

PC: propylene carbonate

ppm: parts per million

D: dispersity

PPC: poly(propylenecarbonate)

PO: propylene oxide

TBAB: tetrabutylammonium bromide

TBAI: tetrabutylammonium iodide

THF: tetrahydrofuran

TMTAA: tetremethyltetraazaannulene

Et₃Al: triethylaluminum

Et₃N: triethylamine

TOF: turnover frequency

TON: turnover number

UV-vis: ultraviolet-visible

VCHO: 4-vinylcyclohexene oxide

vs: 'versus'

wt%: weight percent

1. Introduction

1.1 Green Chemistry: Evolution and Principles

The overarching aim of green chemistry is to minimize the toxic exposure risk of chemicals not just in their applications but across their life cycle. This means that careful considerations must be made with regard to minimizing the waste and toxicity (i.e., using less hazardous reagents and solvents) created in the synthesis and decommission of any chemical/material.¹⁻⁴ The overall concept of green chemistry can not be explained properly without identifying the twelve principles outlined by Paul Anastas and John Warner in 1998.⁵ These principles, presented in Table 1.1, lay out a conceptual framework and guide for the overall design and manufacturing of chemicals, which includes reagent choice as well as biodegradability and toxicity of the end products. These 12 principles have sparked significant interest from scientists in many areas of chemistry but was applied early on in organic synthesis, dominated by the pharmaceutical industry.^{5, 6}

Table 1.1: The 12 Principles of Green Chemistry

1. Prevention
It is best to prevent waste from happening
2. Atom Economy
Reaction methods should be designed to incorporate all materials into the product
3. Less Hazardous Chemical Synthesis
Process should use substances which have minimal or no toxicity to people or the environment
4. Designing Safer Chemicals
Products should be designed to complete desired function with minimal toxicity concerns
5. Safer Solvents and Auxiliaries
Auxiliary substances should be avoided when possible
6. Design for Energy Efficiency
Economical and environmental impacts of energy requirements should be recognized; ambient temperatures and pressures are preferred
7. Use of Renewable Feedstocks
Raw materials/feedstocks should be renewable, not depleting
8. Reduce Derivatives
Unnecessary derivatives should be reduced/avoided as they create additional steps
9. Catalysis
Catalytic reagents are superior to stoichiometric process
10. Design for Degradation
At the end of a chemical's lifetime, it should break down into innocuous degradation products
11. Real Time Analysis for Pollution Prevention
Analytical process should allow for real time monitoring prior to hazardous substance formation
12. Inherently Safer Chemistry for Accident Prevention
Substance selection should minimize potential for accidents, explosion, etc.

In 2000, Green Analytical Chemistry, GAC, was developed introducing new methods and innovative ideas, while examining further the negative impacts of chemical analysis on the environment.⁷ GAC then developed their own 12 principles, and while there is some overlap between both versions, there are some principles more specific to the analytical chemist, such as minimal sample size/minimal number of samples, multi-parameter methods preferred, direct techniques applied to avoid sample treatment, and *in situ* measurements should be performed when possible.⁷ This new way of approaching

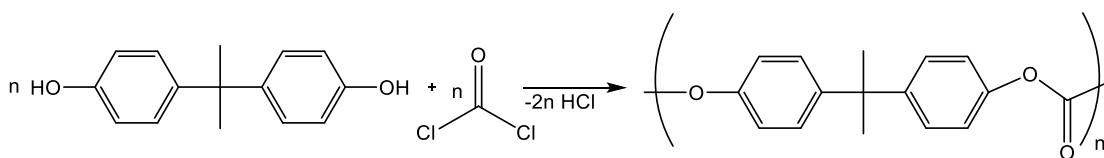
research also sparked interest in those outside of analytical chemistry as well. The entire University of Oregon expressed interest in 1997 to develop tools for other chemists to utilize, if they are interested, in more environmentally aware research.⁸ The goal from the university was to host workshops that could aid and inspire students as well as faculties to modernize curriculum, learn new concepts, adjust lab techniques, etc. In 2001, a new database, Greener Education and Materials for Chemists, was created as a by-product of these workshops giving everyone easy access to these new concepts presented.⁸ Jim Hutchison from the University of Oregon went even further to help develop greener approaches pertaining to four experiments in the undergraduate organic laboratories; these new methods also enhanced the reaction performance.⁹

Although green chemistry has made significant progress over the last 27 years, it also has some drawbacks and concerns that must be addressed when pushing further. For instance, green chemistry only accounts for a small fraction of research currently being investigated, with several concepts being fractured and not cohesive.¹ As well, the principles only outline a conceptual framework as mentioned previously, there are no real quantifiable metrics in place. Thus, while the objectives may be worthwhile, a stricter definition to what Green Chemistry means concretely is necessary.^{3,6} Winterton also touches on other areas of concern when discussing Green Chemistry as a whole. For example, the benefits being offset by a growing population and demand, and understanding that teaching sustainability needs to spread wider than just chemistry.⁶ Perhaps the most important question to take note of is whether or not these principles of Green Chemistry are overshadowing and being given more importance over the basic fundamentals of chemistry, such as the laws of thermodynamics and their practical

significance/consequences.⁶ Anastas has, in the past, touched on key steps he believes are necessary to advance the field: appreciation of the scientific challenges, the basis of any challenge can be impacted positively on a molecular level, design must be exploited, and that life cycle analysis should be considered more often (i.e. biodegradable polymers being synthesized using CO₂, but what do they eventually degrade into).¹

1.2 Synthesis of Polycarbonates Industrially

Bisphenol A polycarbonates, BPA-PC, is the current conventional form of polycarbonates. BPA-PC is synthesized from bisphenol A (BPA) and phosgene, Scheme 1.1.¹⁰ This form of polycarbonate is attractive due to the properties it possesses: high impact capabilities, heat resistant (to a degree), flame retardant, optical transparency, and dimensional stability.¹⁰⁻¹³ The global capacity of these manufactured polycarbonates is in excess of over 6 billion pounds per year,^{14, 15} and is used in several every day common items including epoxy linings in products and packaging materials, toys, dental monomers, medical equipment, water bottles, containers, and much more.¹⁴⁻¹⁶

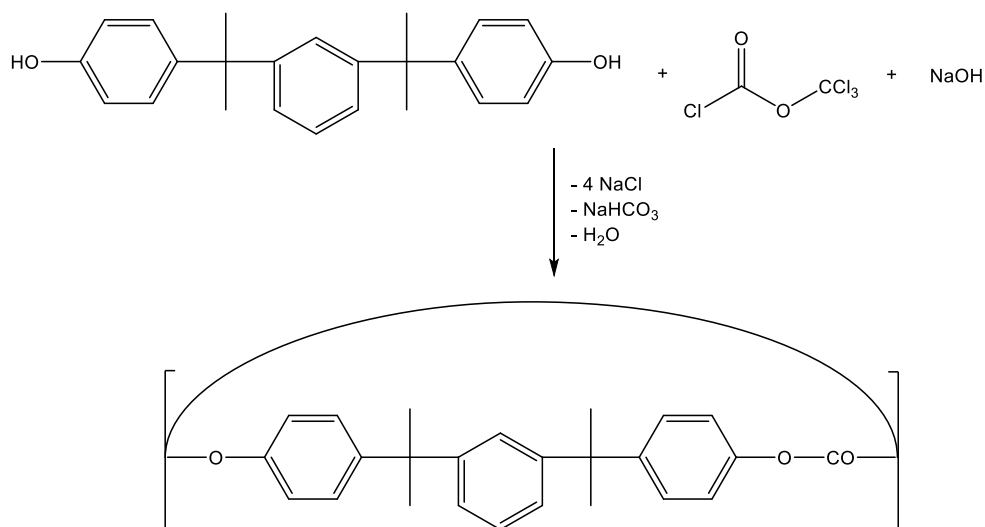


Scheme 1.1: Industrial route to polycarbonate formation using BPA and phosgene

The largest concern surrounding these BPA-PCs is that the ester bonds in the polymer are readily hydrolyzed when heated or when they come in contact with acidic or basic compounds, causing the BPA to leach.^{14,16} Eight billion pounds of BPA is produced annually, with 100 tonnes being released into the atmosphere.¹⁶ Unfortunately, there are several side effects if BPA is metabolized within the body: disruption of

estrogen response mechanisms, altering brain chemistry and structure, lowering the immune system, and acting as an endocrine disruptor.^{14, 16, 17} There has been some effort to remove BPA from some polycarbonates produced, such as in water bottles where leaching can occur readily. Belcher et al. performed a study that examined whether or not various bottles, specifically aluminum water bottles with an epoxy resin, were in fact BPA free.¹⁷ BPA continued to leach from plastics, specifically when heated, which is why it is always up to the consumers to be aware of what they are purchasing and the manufacturers to be able to reliably sell a product based on an attractive feature, such as BPA free.

Bisphenol M has also been studied previously to synthesize cyclic oligocarbonates and polycarbonates; this monomer was selected over BPA as the meta position has two isopropylidene groups, which favour cyclization reactions, Scheme 1.2.¹⁸ By subjecting bisphenol M to polycondensation reactions with monomeric, dimeric, or trimeric phosgene in a mixture of sodium hydroxide and dichloromethane, cyclic oligocarbonates could be readily formed using triethylamine as the catalyst. Dimeric and trimeric phosgene are safer substitutes for phosgene as they are solids at room temperature as opposed to a gas. Changing the catalyst to benzyl ammonium chloride allowed for an increased selectivity towards the linear products. Reaction conditions did not rely on pressure and were performed between 5 – 20 °C for 5 h.



Scheme 1.2: Polycondensation reaction of bisphenol M with diphosgene to produce cyclic oligomers

Phosgene has also been replaced in the literature due to its toxic nature.¹¹ Aside from phosgene acting as a chemical warfare agent and being poisonous gas, the polycarbonates outlined in Schemes 1.1 and 1.2 have several concerns as well: i) a large excess of the phosgene is required, ii) dichloromethane, a known carcinogen, is required in excess as solvent, iii) waste water treatment from the process is extensive and time consuming, iv) corrosion of the equipment readily occurs due to Cl_2 and the chloride anions present, and v) chloride impurities are generally contained within the product and weaken the polymers desired properties, such as heat resistance.^{11,12} Dimethyl carbonate, DMC, and diphenyl carbonate, DPC, Figure 1.1, have both been used to replace phosgene, successfully producing safer polymer products, which eliminate all of the concerns listed above.

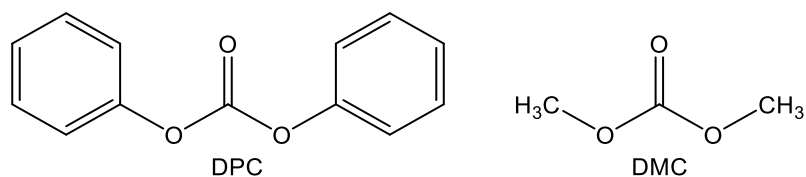


Figure 1.1: Phosgene replacements to produce polycarbonates

1.3 CO₂ and its Applications

Carbon sources are extremely common, existing in many different forms on Earth – the most commonly used by humans as a feedstock is petroleum. Calcium carbonate is the most abundant form and is found in limestone, marble, and the skeletal system of marine life, to name a few sources.¹⁹ Bicarbonates are abundant within the oceans as the second largest reservoir of carbonates.¹⁹ Carbon dioxide, CO₂, in comparison, only represents a small portion of carbon found within the atmosphere, but it is essential to life on Earth. CO₂ plays an important role in the Earth's carbon cycle and is necessary to the life cycle of photosynthetic plants and animals that eat them.^{19, 20} Through photosynthesis, CO₂ and water can be converted into biomass via the Sun's energy (light sources), which in turn is transformed into chemical energy through catalysis by chlorophyll found in plants.¹⁹ These natural methods of capture and generation of CO₂ were in a dynamic equilibrium for a long period of time, however, as the population has increased energy demands have also increased along with the burning of fossil fuels.^{19, 21} If we were to think on a geological timescale about photosynthesis releasing CO₂ and subsequently being converted into biomass, vs. biomass undergoing a fossilization process to form the carbon being mined and refined for fuels, the overall processes are slow. In fact, combustion is a much faster form of CO₂ release, on a scale of 10¹⁰ times greater, when compared to fossilization, creating a large imbalance

between a slow reduction of CO₂ (photosynthesis/fossilization) and combustion.¹⁹ The concentration of CO₂ in the atmosphere has gone from a range of 270-300 ppm during the latter half of the 18th century,^{19, 21} up to 315 ppm in the mid 1900s,²⁰ 377 ppm in 2004,²⁰ and to date has reached and exceeded the threshold of 400 ppm.¹⁹

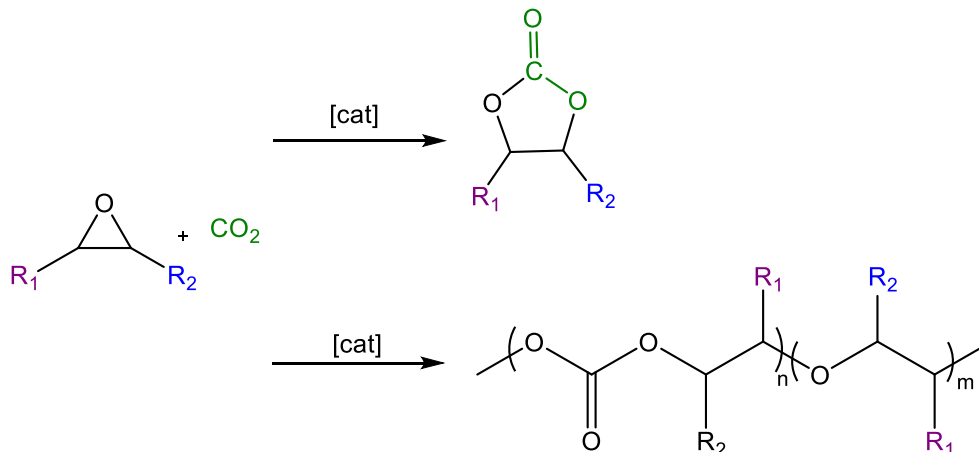
The combustion of substances containing carbon, e.g. fossil fuels, will produce CO₂ thus increasing its concentration in the atmosphere.²⁰ The three main sources of CO₂ emissions include:²⁰

1. Stationary sources: including residential/commercial buildings, military/government facilities, manufacturing plants in industry, and independent power producers
2. Mobile sources: including cars, trucks, buses, trains, construction vehicles, and so many other forms of transportation
3. Natural sources: including humans, animals, plant/animal decay, volcanos, earthquakes, and land emission/leakage

A recent publication has addressed the need for more efficient CO₂ capture and storage, CCS, and the potential contribution of carbon capture and utilization, CCU.²² This century has seen a steady rise in CO₂ emissions annually therefore the International Energy Agency, IEA, has projected the possibility of a maximum 2 °C warming over pre-industrial levels if CO₂ emissions are reduced to less than 20 GT per year by 2050; this has been labelled the two degree scenario, or 2DS. If emissions continue to increase to 60 GT per year on the same scale, warming will increase to 6 °C, creating a six degree scenario, 6DS.²²

1.4 Polycarbonate Synthesis via the Coupling of CO₂ and Epoxides

The first published result of polycarbonate formation utilizing CO₂ was in 1969 by Inoue, Koinuma, and Tsuruta.²³



Scheme 1.3: Simple schematic demonstrating the coupling of epoxides and CO₂ to produce cyclic carbonates, or the polymerization process to synthesize polymers

Copolymerization of CO₂ with epoxides is a growing area of research as it demonstrates an efficient method to form polycarbonates in a safe manner with fewer toxicity concerns than the industrial method. A search of Web of Science for the topic “CO₂ epoxide copolymerization” since 2000 shows the field has grown steadily in importance, Figure 1.2. This could be due in part to the specific need to find methods of utilizing CO₂ when captured. It is of interest to note that since 2005, the number of publications with the same search has more than doubled just ten years later. In the current year, 2017, there have already been 46 publications, which is more than any year prior to 2011. This simple search demonstrates the growing interest in this field making it a ‘hot’ research topic for chemists worldwide. Although finding efficient methods to utilize CO₂ can be a challenge, its coupling with epoxides has shown to be a promising reaction and way to develop polymeric materials.^{11, 24-30} Not only is this process

important for activating thermodynamically stable CO₂, but using CO₂ as a C1 feedstock has several advantages; it is abundant, inexpensive, and non-toxic.³¹⁻³⁴

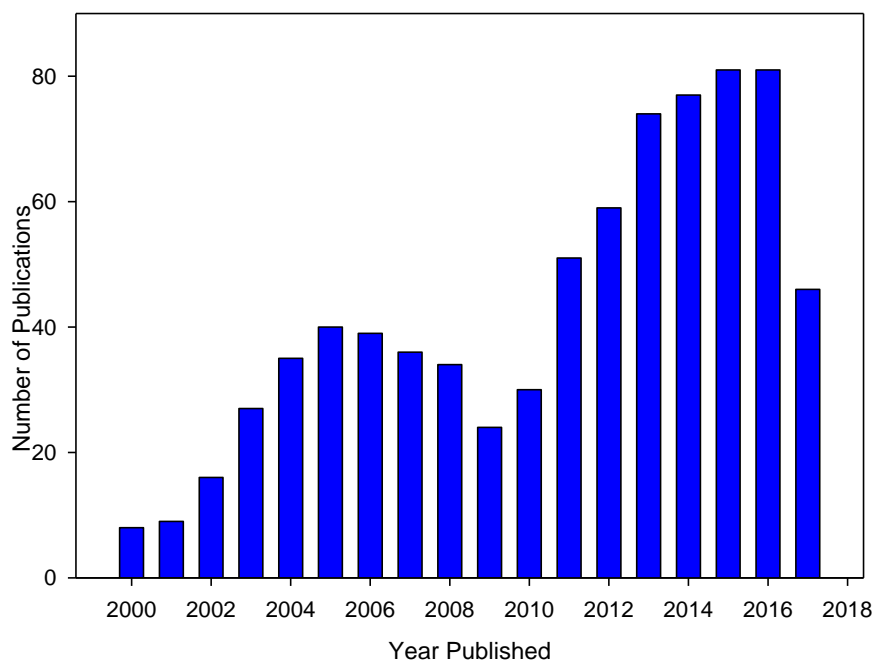


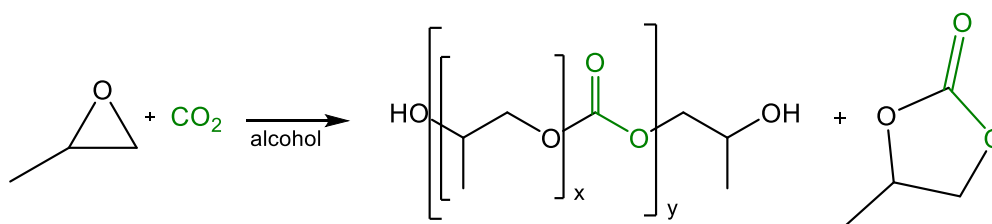
Figure 1.2: Number of publications per year on Web of Science when searching for “CO₂ epoxide copolymerization” as of September 2017

1.4.1 Propylene Oxide as a Common Epoxide: Its Appeal and Diversity

With respect to epoxide selection, propylene oxide is common for many catalytic systems.^{31-33,35-37} Propylene oxide tends to favour formation of cyclic product vs. polymer when coupled with CO₂. These cyclic carbonates have been found to be useful in several applications to date: high boiling point non-toxic solvents, degreasers, reactive intermediates for ring opening polymerizations, and fine chemical production.^{32, 38}

Polymer formation is also industrially important. The synthesis of poly(propylenecarbonate), PPC, is being investigated as a replacement for poly(propyleneoxide) polyols, PPPs, in the production of polyurethane.³⁹ An example

of this is shown in Scheme 1.4 where PO and CO₂ are polymerized, typically using a double metal cyanide, DMC, catalyst in the presence of a multifunctional alcohol, producing polyethercarbonate polyols which are readily processed into polyurethane foams.³⁴



Scheme 1.4: Synthesis of polyethercarbonate polyols and cyclic propylene carbonate from propylene oxide, carbon dioxide, and an alcohol

The synthesis of polyethercarbonate polyols is also important as they could be substitutes for polyether polyols, utilizing up to 1.6 Mt y⁻¹ of CO₂ as a feedstock. This is assuming an average CO₂ content of 20 weight percent, wt%, being incorporated into the polymer.³⁴ Bayer uses similar polymers for rotor blades of wind turbines which consist of dozens of layers of thin glass fibres. These fibres are more durable than previous models created using epoxy resins. They also use polycarbonates as lightweight, high performing plastics to produce mini rotor blades which can generate electricity for homes in remote areas.⁴⁰

The activation barrier for cyclic propylene carbonate formation is only about 30 kJ mol⁻¹ greater than that of copolymer formation. Therefore, it is not surprising to most commonly see cyclic product formed specifically at elevated temperatures, Figure 1.3.⁴¹

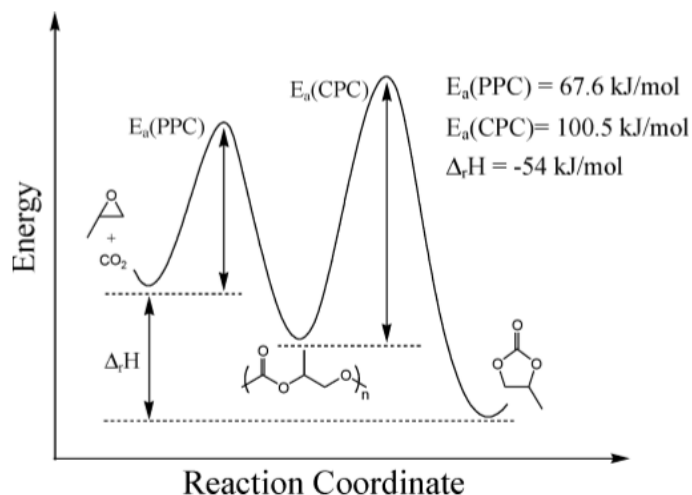


Figure 1.3: Activation energy diagram for the formation of poly(propylene)carbonate and propylene carbonate from PO and CO₂.
Image taken with permission from reference 41.

A Cr(III) salen complex, **1.1** in Figure 1.4, was used throughout Darensbourg's studies. Several reactions were run under 60 bar CO₂ pressure at 80 °C for 24 h, but the concentration of Cr was varied. There was a linear response seen for the formation of polymer as the concentration of catalyst was increased, these data were collected by using in situ infrared spectroscopy. Temperature effects were also studied, and polymer formation is evident at lower temperatures, i.e. 30 °C, however when the temperature is increased to 80 °C, propylene carbonate becomes the dominant product as no absorbance is evident for polymer formation as previously seen. This is speculated to be due to depolymerization processes of the polymer.⁴¹

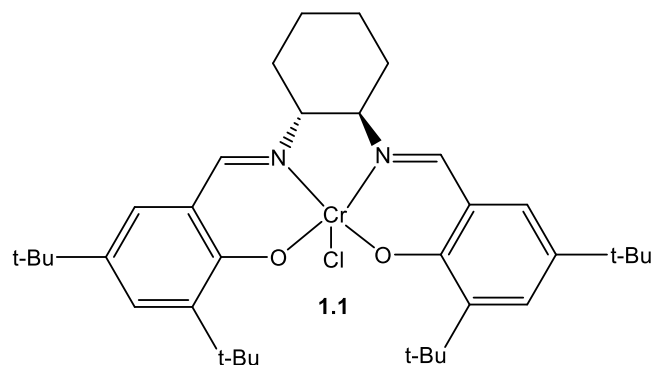


Figure 1.4: (Salen)Cr(III)Cl complex used in Darensbourg's' studies, reference 41

The rates in which polymer was formed, compared to cyclic carbonate, is outlined in Table 1.2. It is not until the reaction reaches 65 °C that there is any cyclic carbonate formation observed, and by the time the reaction reaches 100 °C there is only evidence of cyclic carbonate product.

Table 1.2: Observed reaction rates for the formation of poly(propylene) carbonate and propylene carbonate at various temperatures as seen by Darensbourg and coworkers, reference 41

Temperature (°C)	Rate (r_{obs}) (abs/s x 10^5) Polymer	Rate (r_{obs}) (abs/s x 10^5) Cyclic
30	3.9	-
50	20.7	-
65	64.4	3.2
80	172.3	15.5
100	-	92.7

1.4.2 Common Catalysts for the Copolymerization of CO₂ and Epoxides

1.4.2.1 Co Catalysts Used in Copolymerization Reactions

In 2016, Nozaki and coworkers reported the copolymerization of propylene oxide and CO₂ using in situ generated Co(III) salicy complexes and bis(triphenylphosphine)iminium 2,4-dinitrophenolate, PPNDNP.⁴² The Co(II)

complexes, **1.2** (Figure 1.5), were either i) reacted with either a ferrocenium salt prior to the reaction and sequentially isolating the Co(III) species, or, ii) during the reaction in situ. They found that either of these methods worked effectively giving similar TON for the production of poly(propylenecarbonate), PPC: 729 ± 43 and 703 ± 1 for the in situ generated and isolated catalysts respectively. The only notable difference was the decrease in molecular weight when using the isolated complexes ($28\,900\text{ g mol}^{-1}$ to $18\,700\text{ g mol}^{-1}$) which was attributed to water contamination in the reaction system when isolating the complexes.

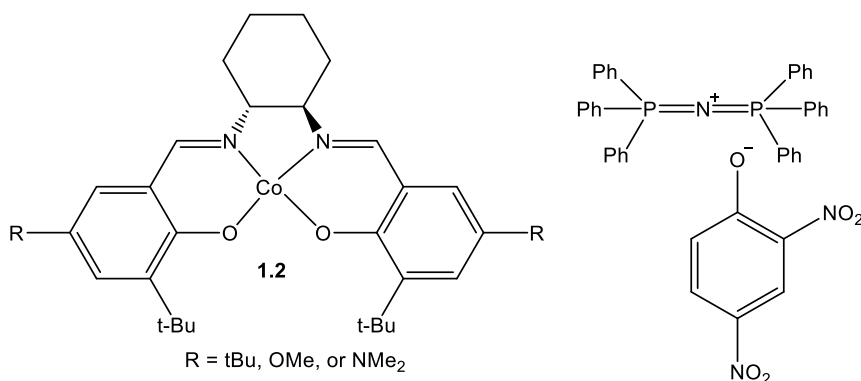


Figure 1.5: Co(II)-salicyl complexes (left) and PPNDNP (right), reference 42

When attempting in situ oxidation using a silver salt, AgPF₆, no product was obtained indicating that any silver particles remaining inhibited the polymerization (or coupling) process. With respect to the ferrocenium salts, the anion had no drastic effect on the polymerization process. However, the choice of anion for the cocatalyst played a larger role. Replacing bis(triphenylphosphine)iminium chloride, PPNCI, with PPNDNP increased overall TON (802 to 976) as well as selectivity. No cyclic product was observed. This is suspected to be due to the higher leaving ability of chloride, increasing the nucleophilic ring opening of PO and this insertion of CO₂ which increases the

probability of cyclic product formation. There is suspected to be an equilibrium between [Co(III)-salcy], **1.3.a/1.4a**, and [Co(II)-salcy]⁺, **1.3b** and **1.4b**, as shown in Figure 1.6. For the methoxy substituted complex, the Co(III) has a stronger contribution to the reaction system than the Co(II), but the opposite is observed for the dimethylamino substituted complexes. The dimethylamino groups are more strongly electron donating, thus increasing the contribution of the Co(II) radical complex; Co(II) is inactive for the synthesis of PPC therefore explaining the low reactivity of this complex compared to the others.

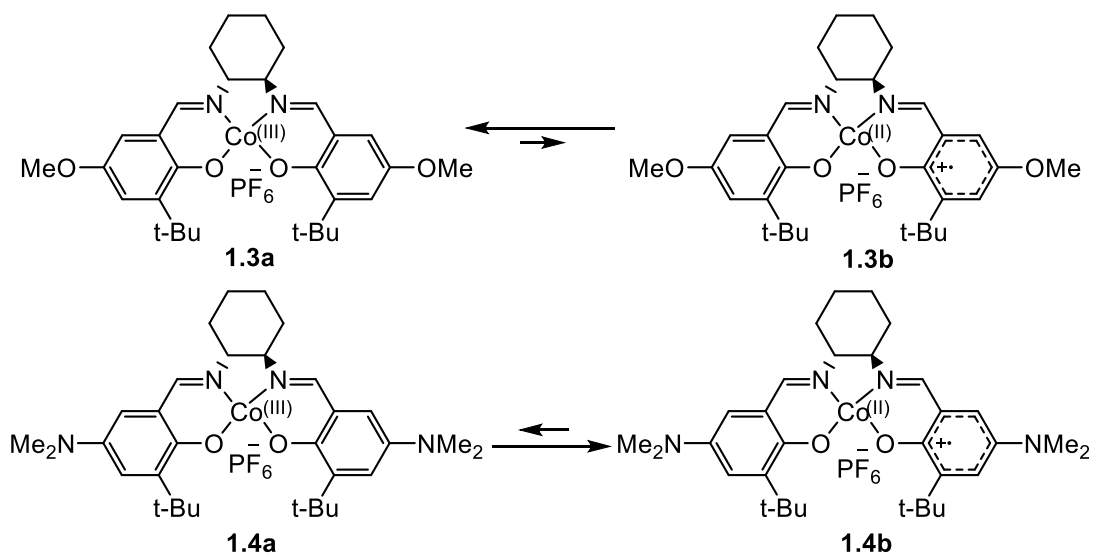


Figure 1.6: Contribution of cationic radical species of Co(II) complexes for the copolymerization of PO and CO₂, reference 42

In 2017, Liu and coworkers were successful in developing polycarbonates from PO, CO₂ and vinyl cyclohexene oxide, VCHO, catalyzed by a bifunctional salcyCo(III)NO₃ complex, **1.5** in Figure 1.7.⁴³ In this case, bifunctional relates to the catalyst having ionically tagged ligands therefore the catalyst can also act as the cocatalyst. At a catalyst loading of 0.15 mol%, when only PO was present, there was a

72% overall conversion seen after 4 h at 70 °C and 30 bar CO₂ pressure. The resulting polymer had high molecular weight 83 000 g mol⁻¹ with a broad dispersity of 1.44. When a ratio of VCHO to propylene oxide was employed at a 2:8 ratio under the same conditions, the conversion of each monomer was 67% and 94% respectively. A large decrease in molecular weight was noted giving 39 000 g mol⁻¹ with an even broader dispersity of 1.85. A 50/50 mixture of the two epoxides resulted in lower conversions of each, now less than 50%, with a molecular weight of only 18 600 g mol⁻¹, but having a relatively narrow dispersity of 1.25. VCHO in the absence of PO was inactive for polymerization.

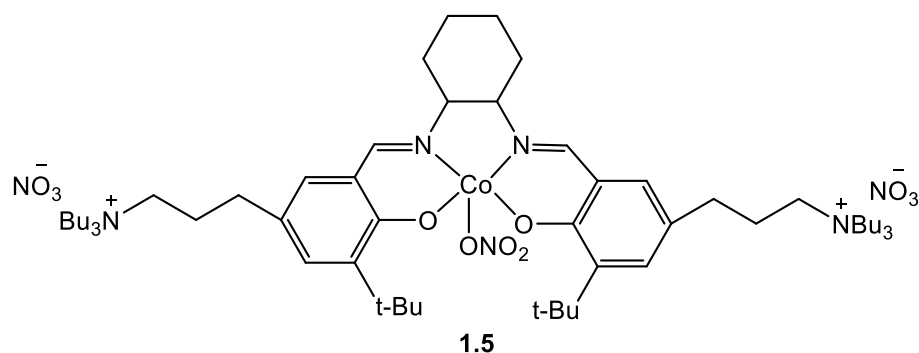


Figure 1.7 Bifunctional salcyCo(III)NO₃ complex, reference 43

1.4.2.2 Zn Catalysts Used in Copolymerization Reactions

As mentioned previously, the first real report for the copolymerization of carbon dioxide with epoxides was in 1969 by Inoue, Koinuma and Tsuruta.²³ They reasoned the success of this reaction by understanding two fundamental reactions necessary for copolymerization to take place; the reaction between carbon dioxide and a metal alkoxide being the propagating chain end, and the other being the reaction between an epoxide and a metal carbonate. They first looked at propylene oxide and CO₂ with a mixture of diethyl zinc, Et₂Zn, and ethanol. After 58 days, at 30 °C using benzene as the

solvent, there was an absorption in the infrared spectrum at 1740 cm^{-1} which could have been indicative of the carbonyl chain end group of the polymer, or of carbon dioxide reacting with the zinc alkoxide. Under atmospheric pressure, there was success in producing some polymer using both $\text{Et}_2\text{Zn-H}_2\text{O}$ and $\text{Et}_2\text{Zn-EtOH}$, as well as triethylaluminum, Et_3Al . By taking the methanol insoluble portions of this polymer, they could determine the ratio of carbonate to propylene oxide units, Figure 1.8, through elemental analysis and NMR.

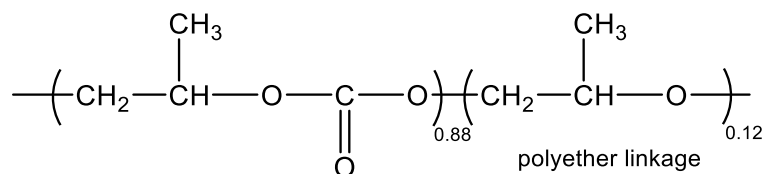


Figure 1.8: Polycarbonate product from the reaction of PO and CO_2 using a diethyl zinc catalyst

Using the Et_3Al catalyst, however, demonstrated a different pattern in the IR spectrum. This product was characteristic of polypropylene oxide only with weak absorptions in the carbonate region, 1740 and 1250 cm^{-1} . Increasing the CO_2 pressure to 50 bar led to an increase in polymer yield using $\text{Et}_3\text{Zn-H}_2\text{O}$, and the polyether linkages became nearly negligible. The Et_3Al catalysts system once again gave a product which was almost entirely polypropylene oxide.

Darensbourg et al. developed distorted tetrahedral zinc phenoxide derivatives having bulky substituents on the phenolate ligands, (1.6) Figure 1.9.⁴⁴ The THF ligands are labile and can be replaced with other bases such as epoxides (which they were unable to fully characterize due to their weak binding ability), pyridine, and phosphines. Non-interacting solvents were therefore ideal to perform these reactions so that there would

be no competitive binding to the metal centre; the reactions with cyclohexene oxide were carried out in the absence of any solvent.

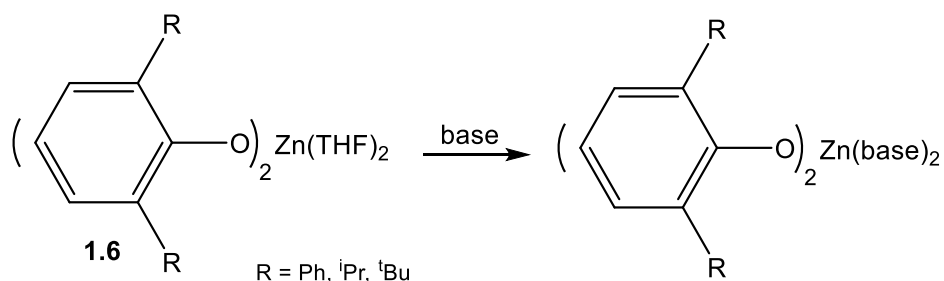
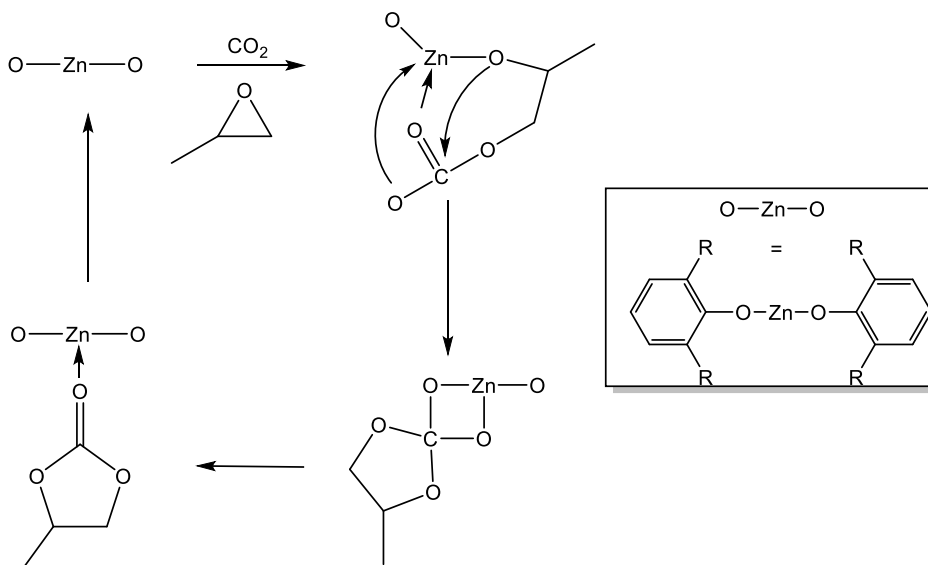


Figure 1.9: Tetrahedral zinc phenoxide derivatives used as catalysts for the copolymerization of CHO and CO₂, reference 44

With respect to the phenolate substituents, the yield of high molecular weight polymer was increased from 477 to 1441 g_{polymer}/g_{Zn} when R was changed from isopropyl groups to smaller methyl groups. Phenyl and *tert*-butyl substituents were not significantly different giving 607 and 677 g_{polymer}/g_{Zn} respectively. Using the (2,6-diphenylphenoxy)₂Zn(Et₂O)₂ catalyst, time temperature, and pressure were also assessed. Yields of 270, 602, and 1198 g_{polymer}/g_{Zn} were achieved after 24, 60, and 144 h respectively, while performing the reaction at only 40 °C led to the lowest yield achieved, 90 g_{polymer}/g_{Zn}. An increase of pressure to supercritical conditions did not enhance the yield substantially. The (2,6-di-*tert*-butylphenoxy) derivative was extremely active to homopolymerization producing high molecular weight polyethers. To slow down or stop this homopolymerization process, the reactor was initially pressurized with carbon dioxide. The catalyst was introduced to the pressurized reactor by being placed in a sealed glass ampule which was broken by the mechanical stirrer once the reaction started. These catalysts were also effective for reactions between

propylene oxide and CO₂, although the propylene carbonate was predominant with the copolymer only favoured at 40 °C. Their proposed process is depicted in Scheme 1.5.



Scheme 1.5: Simplified proposed mechanism demonstrating the propylene carbonate forming backbiting reaction by Darensbourg et al., reference 44

In 2002 Coates and coworkers screened a series of β -diimine zinc complexes, Figure 1.10, for their activity towards CO₂ and PO copolymerization at a loading of 1:2000, zinc to monomer.⁴⁵ At 50 °C and 20 bar CO₂, complex **1.7b** was 100% selective for propylene carbonate formation, but by decreasing the temperature to 25 °C, the system favoured polymer formation with 85% selectivity; the remaining reactions were therefore all run at room temperature. Complex **1.7a**, having a symmetrical backbone, was found to be inactive for PC and PPC production making ligand design a crucial step.

This is further demonstrated through electronic effects as having the electron withdrawing CF₃ substituent on the same side as the diisopropyl aniline, complex **1.7d**,

resulted in a tenfold increase in activity, versus when the CF₃ and diethyl aniline were in close proximity, complex **1.7c**, the TOF increased from 26 h⁻¹ to 212 h⁻¹. By placing two electron withdrawing groups on the ligand backbone as seen in complex **1.7e**, there is complete deactivation of the complex with no product being formed. By decreasing the temperature, greater selectivity could be achieved for polymer formation, with a loss of activity and a decrease in molecular weight. On average, high molecular weight polymers were seen ranging from 21 900 to 43 300 g mol⁻¹, and all catalyst systems demonstrated good control over polymerization having dispersities of 1.1.

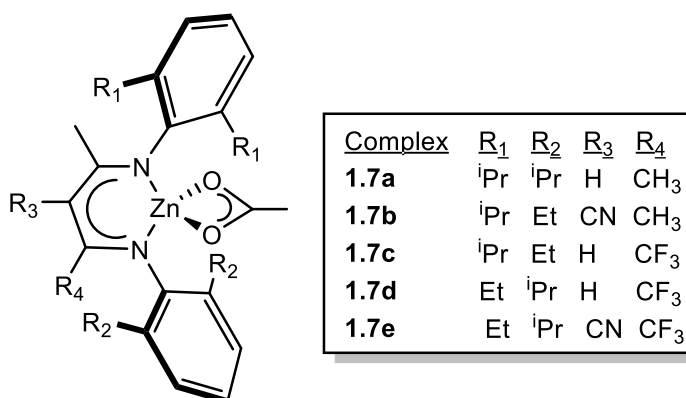


Figure 1.10: β -Diiminato zinc complexes synthesized by Coates and coworkers, reference 45

Lee and coworkers synthesized several dinuclear μ -methylsulfinato zinc complexes, Figure 1.11, in hope of achieving the cooperative action of two metal centres, such as is exhibited by natural metalloenzymes.⁴⁶ The polymerization of CHO and CO₂ was carried out under dilute conditions to determine the activity of Zn at a low mol ratio; 1:5800 of Zn to CHO. The acyclic bis(anilido-imine) complexes showed high activity, aside from the diisopropyl substituted analogue. After only 5 h, the complexes

bearing methyl/isopropyl groups as well as ethyl/isopropyl demonstrated the highest activity and highest molecular weight polymers, between 200 000 and 290 000 g mol⁻¹, at 80 °C, and 12 bar CO₂ pressure. By reducing the Zn:CHO ratio twofold, the TON can be almost doubled, 1 560 – 2 720, but reducing it threefold only increases the TON to 2 980. This was attributed to protic impurities within the epoxide deactivating the catalyst under such dilute conditions. The macrocyclic complexes, **1.8b**, demonstrated negligible activity due to the strength of the methylsulfinato ligand binding, hindering the initiation step. This theory of bond strength is supported by the short Zn-O bonds in the crystal structure and the ideal O-Zn-O tetrahedral bond lengths.

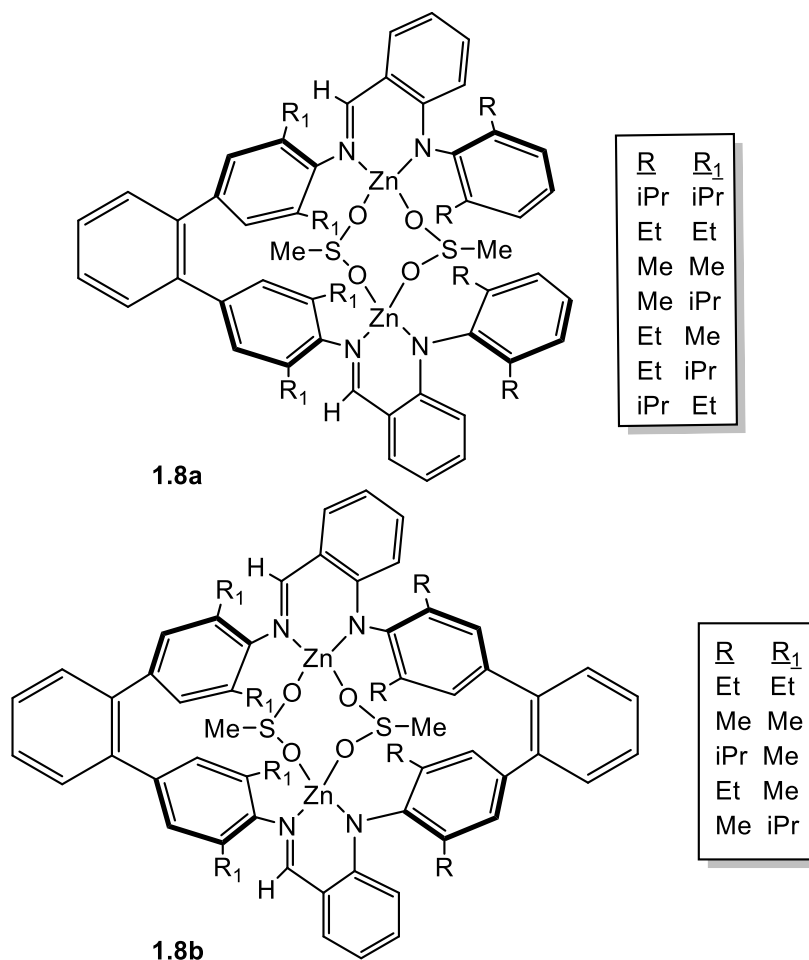


Figure 1.11: Acyclic bis(anilido-imine) complexes (top) and their related 30 membered macrocyclic compounds (bottom), reference 46

1.4.2.3 Cr Catalysts used in Copolymerization Reactions

Nozaki and coworkers explored a series of chromium complexes with salen ligands, Figure 1.12, for the copolymerization of cyclohexene oxide.⁴⁷ A series of cocatalysts were examined using a 0.1 mol% catalyst loading at 70 °C and 13 bar CO₂ pressure, to determine which led to highest activity. Using one equivalent of PPNCl led to optimal results under these conditions with a 37% yield of polymer and a TOF of 170 h⁻¹. Other PPNX salts resulted in very similar activities, while using bulkier cocatalysts, such as Bu₄NX, led to only trace amounts of product.

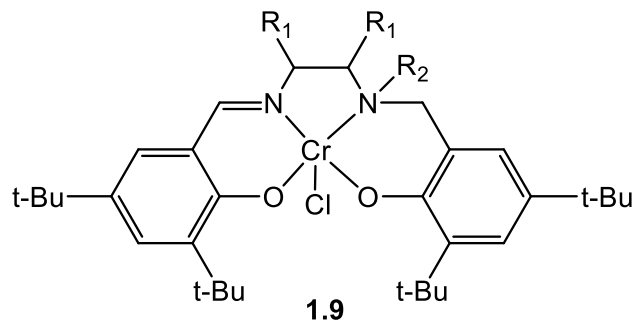


Figure 1.12: Chromium salalen complex, where R_1 and R_2 are alkyl substituents, reference 47

Ligand design was also assessed using a variety of complexes by changing the R groups. R_2 was either H, Me, or bulkier groups such as i Pr and phenyl. Having a methyl group on the nitrogen atom resulted in the highest yields and TOF (52%, 170 h^{-1}) while increasing the steric bulk further decreased activity to only trace amounts of product. The steric bulk at this atom hinders nucleophilic attack from the epoxide lowering catalytic activity which is why the use of isopropyl and phenyl groups were disfavoured. No matter which complex was used, molecular weights were relatively the same with no visible trend, averaging 6500 g mol^{-1} with moderate dispersities of 1.12. Increasing the CO_2 pressure from 1 bar to 34 bar increased the reaction efficiency from a 26% yield (100 h^{-1}) to a 46% yield (230 h^{-1}), while increasing the pressure further to 56 bar CO_2 decreased reactivity, 17% yield (83 h^{-1}).

Lu and coworkers developed a method to completely recycle polycarbonate synthesized from 1-benzyloxycarbonyl-3,4-epoxy pyrrolidine (BEP) and CO_2 utilizing dinuclear Cr(III)-salen complexes, **1.10** in Figure 1.13.²⁹

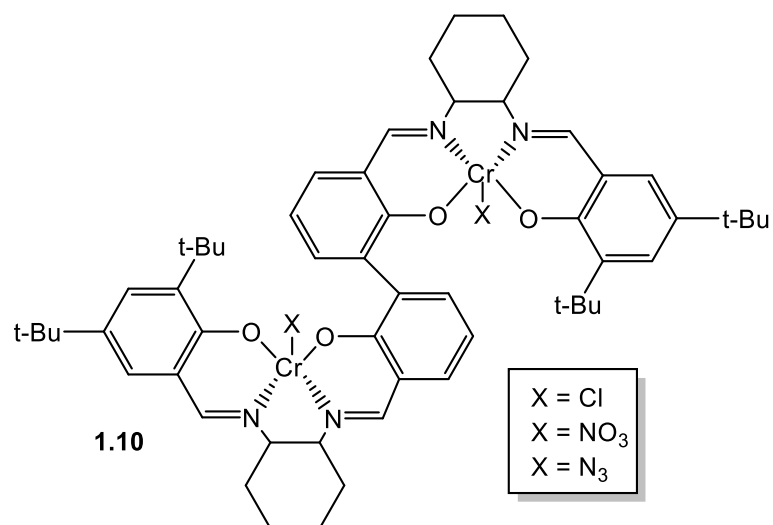
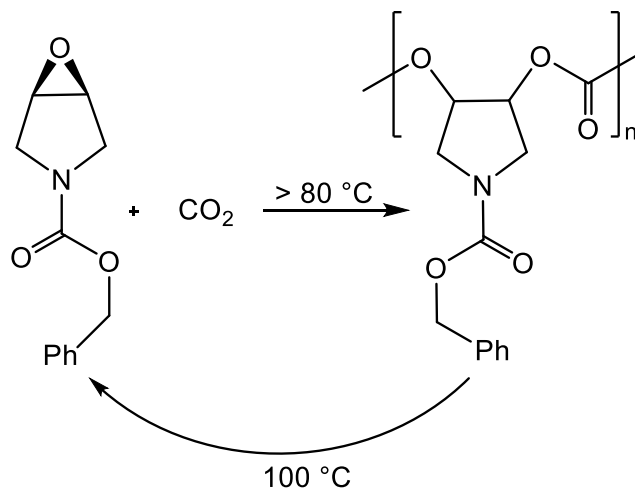


Figure 1.13: Dinuclear chromium(III) salen complexes, reference 29

Using these dinuclear chromium catalysts in the presence of PPNX salts (X = Cl, F, NO₃, or N₃), BEP could be efficiently copolymerized with CO₂ in toluene. Changing the axial group on each chromium metal centre, as well as the cocatalyst choice, had no apparent effect on the reaction. With a catalyst loading of 0.2 mol%, per complex, and half an equivalent of cocatalyst, per complex, each system gave a TOF of 42 h⁻¹ with molecular weights ranging from only 6.7 - 7.1 kg mol⁻¹ with dispersities between 1.29 - 1.31; reactions were run for 12 h at 60 °C and 20 bar CO₂ pressure. Increasing the temperature from 60 to 80 °C decreased the TOF to 13 h⁻¹ and dropped the molecular weight to 2.8 kg mol⁻¹, while increasing the temperature to 100 °C resulted in a complete loss of polymerization. Interestingly, if the reaction was increased to 100 °C after complete conversion of BEP to polycarbonate, depolymerization was observed and complete conversion back into the BEP monomer was achieved within ten

minutes, Scheme 1.6. The monomer could thus be recycled and in the presence of catalyst, copolymerized repeatedly; the formation of the cyclic species is not observed.



Scheme 1.6: Coupling of BEP and CO₂ to produce polymer at 80 °C and the depolymerization back to monomer at 100 °C

Darensbourg has published many papers on CO₂ and epoxide copolymerization over the years, the most of which utilize chromium complexes and study the effect of certain factors such as the cocatalyst choice and ligand systems.^{39,41,48-56} In 2013, he developed a bifunctional Cr(III) complex, **1.11** in Figure 1.14, which was capable of polymerizing cyclopentane oxide with > 94% selectivity and a conversion of 25% after 5 h at 100 °C and 20 bar CO₂.⁴⁹ The molecular weight of the polymer was high, 16 064 g mol⁻¹ with a narrow dispersity, 1.10.

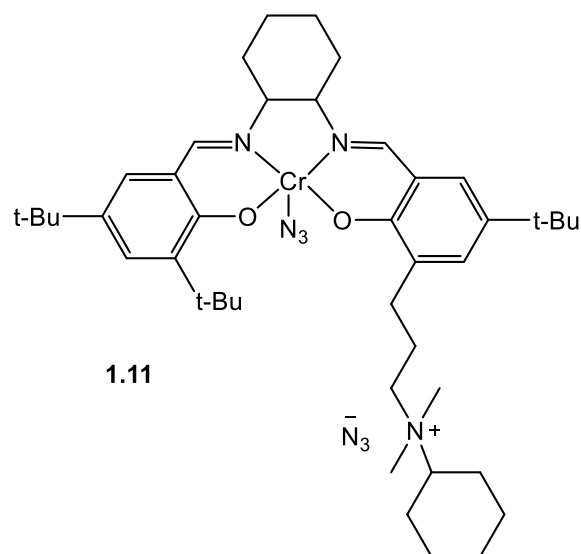


Figure 1.14: Asymmetric bifunctional (salen)CrN₃ complex, reference 49

One of the least common ligand systems used by Darensbourg and coworkers was a tetremethyltetraazaannulene (TMTAA) macrocycle.^{50,51} The methyl groups and aromatic hydrogens create a slight steric repulsion which allows the ligand to take on a saddle shape; the shape results in having a bound metal atom above the donor plane of the ligand. These complexes have an increased solubility in organic solvents which makes them desirable in several catalytic systems. Complex **1.12** shown in Figure 1.15 was used to screen several copolymerization reactions with CO₂ and epoxides. Part of the study assessed PPNX salts as the cocatalyst of choice to determine which led to the highest TOF values; 2 equivalents of the cocatalyst were used at 80 °C and 34 bar CO₂ pressure. PPNC1 gave optimal results with a TOF of 1 478 h⁻¹, however PPNN₃ was also quite effective (1 482 h⁻¹). PPNBr and PPNOBzF₅ were the least active for polymerization with TOFs reported of 795 h⁻¹ and 656 h⁻¹ respectively.

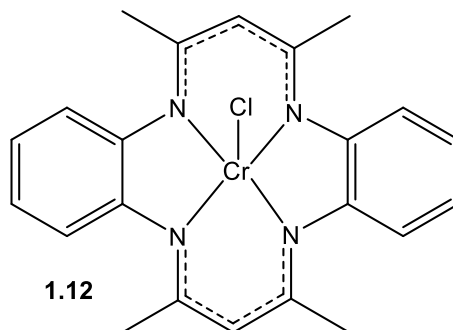


Figure 1.15: Cr(III) tetramethyltetraazaannulene complex, reference 51

Another key aspect to this study was to determine the rate of copolymer and cyclic carbonate production in both solvent, and solventless conditions. Under the same conditions, reactions were run from 60 – 100 °C in 10 mL dichloromethane, and again without the addition of a cosolvent. There is a similar trend seen for each, the large increase in the rate of cyclic carbonate formation as the temperature is increased, however, without the addition of solvent the viscosity of the mixture allows only for qualitative data to be collected during the initial stages of the reaction. A conclusion could be made that cyclic carbonate formation is retarded in the absence of a cosolvent; this idea is supported by the theory that cyclic carbonate formation is due to chain dissociation from the metal centre followed by cyclization which is slightly favourable in aqueous media. Reactions with propylene oxide were also attempted, to less successful results. Using two equivalents of PPNN₃ at 60 °C and 34 bar CO₂ pressure resulted in a 49% conversion after 3 h, with a 15% selectivity towards polycarbonate.

1.4.2.4 CO₂/Epoxide Coupling Studies at Memorial University

In 2012, the Kerton and Kozak groups at Memorial University published their first work on the coupling of CO₂ and epoxides.⁵⁷ Saunders et al. explored various Co(II)

and Co(III) complexes paired with tetradentate amine-bis(phenolate) ligands, Figure 1.16, for the coupling of PO and CO₂. These ligands are desirable for their readily tunable sterics and electronics by varying the pendant donor as well as the phenolate substituents.

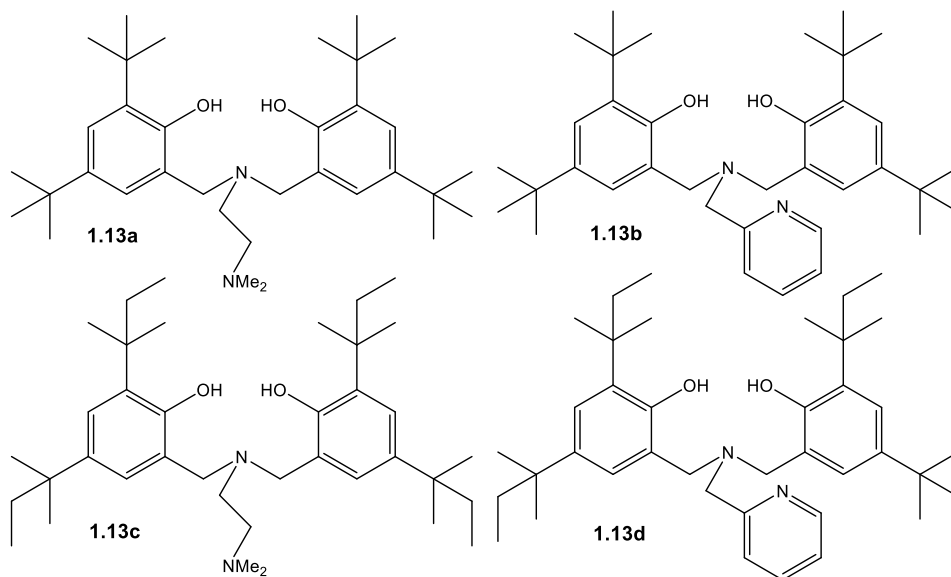


Figure 1.16: Tetradentate amine-bis(phenolate) ligands

In general, it was found that Co(II) complexes were much more active than the Co(III) analogues, with the optimal ligand being the bulky *t*-amyl substituted phenolates with a pyridyl pendant arm, complex **1.13d**. The pyridyl is thought to be a superior pendant when compared to the dialkylamine as it is less bulky and a stronger σ donor. At a 2000:1:1 loading of [PO]:[Co]:[TBAB], at room temperature and 34 bar CO₂ pressure, a TON of 2025 was reached. A decrease in the TON, to 950, was found when using ligand **1.13b** which dropped further to 800 using PPNN₃ as the cocatalyst, and

again to 0 when using DMAP. Throughout these reactions, no polypropylene carbonate was seen in the NMR spectra.

Also in 2012, Dean had success working with chromium complexes for the copolymerization of CHO and CO₂.⁵⁸ Since there had been success using the amine-bis(phenolate) ligands **1.13b** and **1.13d** with the cobalt work, these ligands were also employed in this work. The suspected advantage of using these catalysts is their ability to direct the incoming nucleophile (monomer) to bind *cis* to the X group in six coordinate complexes, as shown in Figure 1.17, and *trans* to either the neutral pendant donor or the anionic phenolate ring. This is different than the salen/salen systems where the systems are planar and the nucleophile will preferentially bind *trans* to the X ligand.⁵⁸

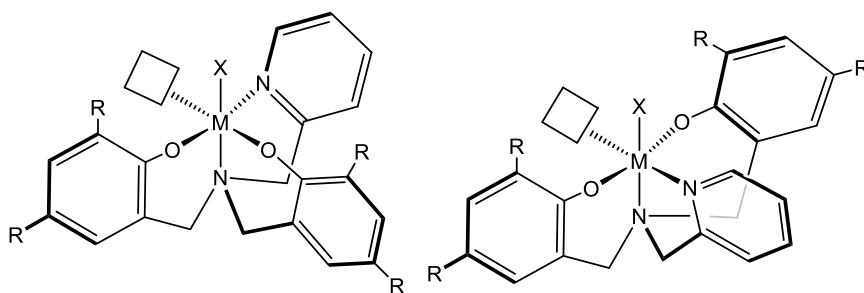


Figure 1.17: Vacant sites available for coordination of an incoming nucleophile, phenolate donors may be either *cis* (left) or *trans* (right)

The standard conditions used were a 500:1:0.5 ([CHO]:[Cr]:[PPNCI]) loading and 40 bar CO₂ pressure. Over a 24 h period at room temperature, there was only a 13% conversion of CHO seen, but with an increase in temperature to 60 °C, the conversion rose to 72%. With respect to cocatalyst selection, PPNN₃ and DMAP demonstrated similar activity, while also increasing the yields of polycarbonate slightly. Increasing

the DMAP loading to 1 equivalent also increased the TOF from 116 – 219 h⁻¹, but 2 equivalents shut down the polymerization process completely.

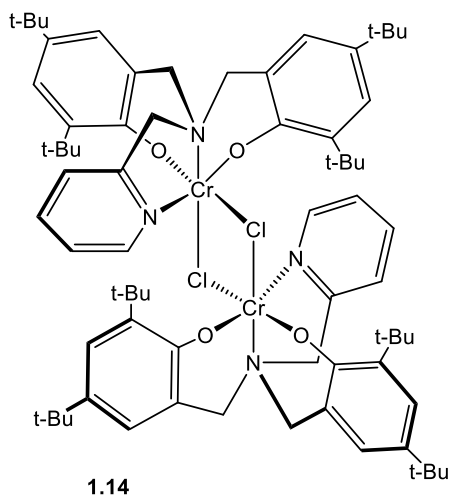


Figure 1.18: Dinuclear Cr(III) amine-bis(phenolate) complex, reference 37

Using chromium complex **1.14** (Figure 1.18), the polymerization of propylene oxide and styrene oxide were also investigated.³⁷ At 60 °C and 45 bar CO₂ pressure, cyclic product could be formed selectively without the aid of a cocatalyst. Decreasing the temperature to 25 °C allowed polymer to form with greater than 80% selectivity. Cocatalyst selection once again was not detrimental to the study as both PPNC1 and PPNN₃ led to similar results with PPNN₃ generating the highest molecular weight polymer, 21.1 kg mol⁻¹, and having a dispersity of 1.14, after 24 h. 100% conversion (93% selectivity) was seen with PPNC1 under the same conditions, but with a lower molecular weight and broader dispersity, 13.3 kg mol⁻¹ and 1.4 respectively. Conversion remained at 100% using DMAP, but the selectivity dropped to 73%. The worst results stemmed from using TBAB as a cocatalyst after which there was only 65% conversion of CHO with a 46% selectivity to polycarbonate formation.

In 2014, Chen further investigated chromium complexes for the polymerization of CHO and CO₂, however, new ligand sets were examined.⁵⁹ Instead of the tetradentate amine-bis(phenolate) ligands seen previously, tridentate ligands were used having no coordinating atom on the pendant arm, as well as one tetradentate ligand having a tetrahydrofuranyl group, **1.16** in Figure 1.19. This was a way to assess if it is favourable to have nitrogen donors coordinated to the metal centre instead of using oxygen donors.

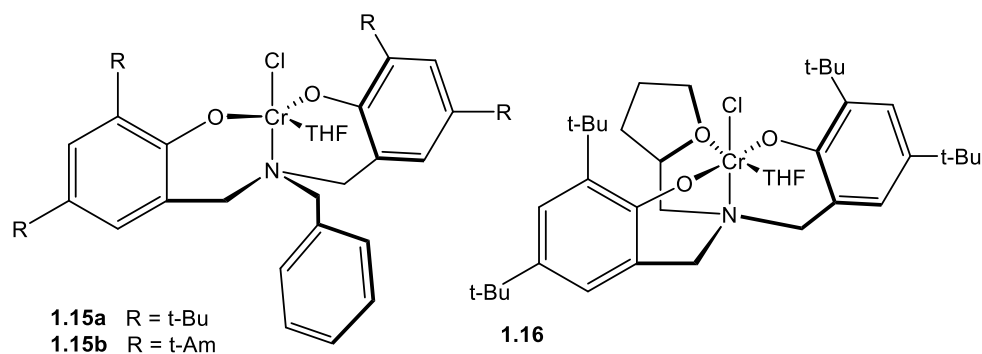


Figure 1.19: Cr(III) amino-bis(phenolate) complexes to study the effect of pendant group on activity, reference 59

Using the same conditions as Dean, the tridentate ligand systems proved to be inferior to all others at this point. A 51% conversion was reached using complex **1.15a** and PPnCl as a cocatalyst, while **1.15b** demonstrated lower activity. This is likely due to having bulky *t*-amyl groups on the phenolate rings. Complex **1.16** was able to reach an overall conversion of 76% using either PPnCl or PPnN₃ as the cocatalyst, however, the molecular weights were lower than those previously reported by Dean and had higher dispersities of 1.46.

1.4.3 Iron Complexes for the Copolymerization of CO₂ and Epoxides

In 2011, Williams and coworkers synthesized a novel di-iron species, **1.17** in Figure 1.20, which happened to be the first example of an iron catalyst capable of polycarbonate/cyclic carbonate synthesis from CO₂ and epoxides.²⁵ At 1 bar of CO₂ pressure and a 0.1 mol% catalyst loading, no cocatalyst present, a 29% conversion of CHO was noted after 48 h with 7% *trans* cyclic carbonate evident from the ¹H NMR. The polymer obtained contained 27% ether linkages with a molecular weight of 2 000 g mol⁻¹ with a relatively broad dispersity of 1.55. When the pressure was increased to 10 bar, a 70% conversion of CHO was achieved in half the time with only trace amounts of *trans* cyclic carbonate evident. The quality of the isolated polymer was also improved with less than 1% ether linkages, a molecular weight of 11 700 g mol⁻¹, and a narrower dispersity of 1.13. With the success of the second reaction noted, a lower catalyst loading of 0.01 mol% was performed under the same reaction conditions giving an overall 25% conversion of CHO with only trace *trans* cyclic carbonate product and less than 1% ether linkages. The molecular weight of the polymer increased significantly to 17 200 g mol⁻¹, and great control over polymerization was noted in the narrow dispersity, 1.03. The analysis of end-groups by MALDI-TOF MS now demonstrated a bimodal distribution at this lower catalyst loading with lower molecular weight series of approximately 8 100 g mol⁻¹ having different end groups than previously seen. The major series of peaks had all shown chlorine capped end groups, but cyclohexenyl and hydroxyl end groups were now visible as well.

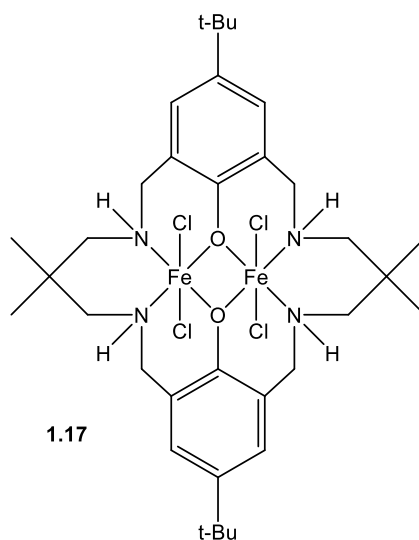
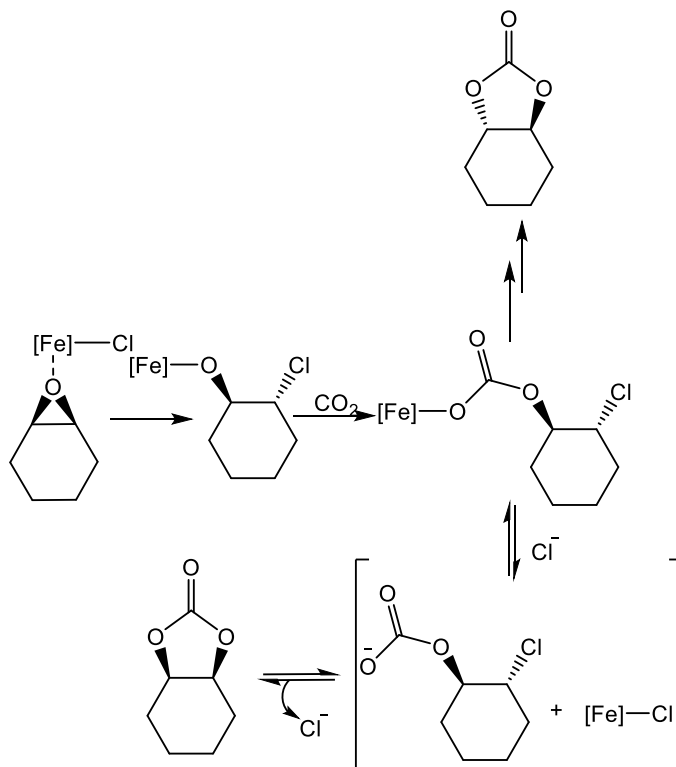


Figure 1.20: First example of an iron catalyst to copolymerize CHO and CO₂, reference 25

The same di-iron complex was also successful in for the formation of *cis* cyclohexene carbonate, *cis*-CHC. What should be noted here is the difficulty in producing *cis*-CHC as the *trans*-isomer is often favourable under thermodynamic control, formed by back biting reactions of a nucleophile. The formation of the *cis*-isomer would require a double inversion of stereochemistry; the simplified mechanism proposed by Williams is given in Scheme 1.7. Under mild conditions, with 0.1 mol% catalyst loading at 80 °C and 1 bar CO₂ pressure, cyclic product was obtained with overall conversions of 20, 33, and 41% with 1, 2, and 4 equivalents of PPNCI respectively; each reaction produced *cis* cyclic carbonate in greater than 95% selectivity. Increasing the catalyst loading to 1 mol% with 2 equivalents of PPNCI allowed for an overall conversion of 90%, almost exclusively all *cis*-CHC, after 24 h. These results demonstrate the necessity of having excess nucleophile present to favour the formation of cyclic carbonate to polycarbonate.



Scheme 1.7: Simplified mechanistic approach to produce both *cis* and *trans* cyclic carbonate. Scheme adapted from reference 25.

Kleij and coworkers in 2013 looked at three iron(III) amino-triphenolate complexes, Figure 1.21, for the coupling of CHO and CO₂, as well as the choice of cocatalyst, namely tetrabutylammonium halides (Bu₄NX) vs. bis(triphenylphosphine)iminium halides (PPNX).⁶⁰ The two main targets with this work were: i) to fine tune the selectivity towards either cyclic carbonate, utilizing high cocatalyst loadings and nucleophiles which make good leaving groups, or polycarbonate, and ii) increase the conversion of CHO by working under supercritical conditions in a solvent free system. It was shown that either salt containing a chloride anion led to the greatest selectivity for polymer formation in a 1:1 ratio with the catalyst. When comparing which salt was more effective, PPnCl demonstrated better selectivity

and activity over Bu_4NCl showing that the choice of cation is also important; the bulkier cation, PPN^+ , has less of an ion-pairing attraction towards the nucleophile.

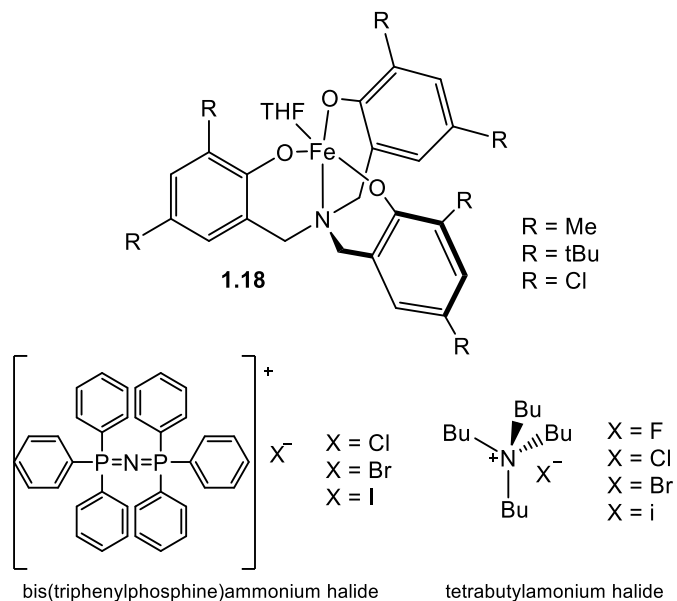


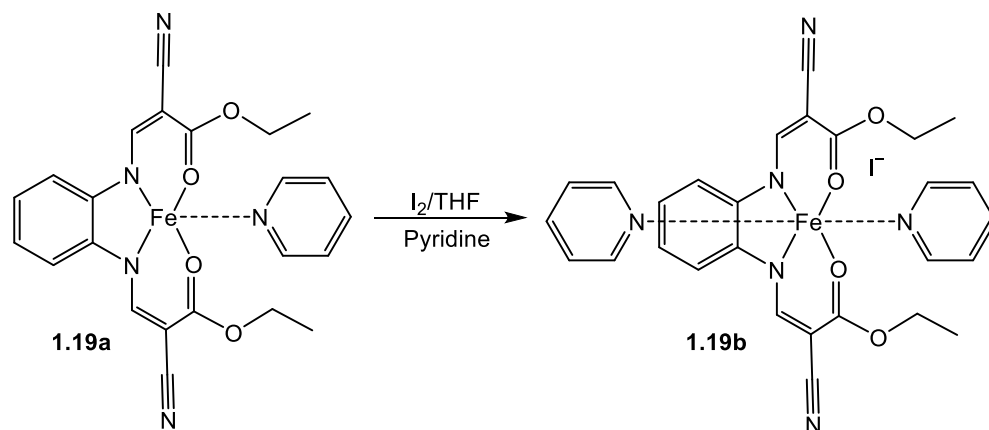
Figure 1.21: Iron amino-triphenolate complex used for the copolymerization of CO_2 with epoxides and two common cocatalysts, PPNX and Bu_4NX , reference 60

Each of the three iron complexes were then studied at a 0.1 mol% loading with one equivalent of cocatalyst (PPNCl giving optimal results), at 85 °C and 80 bar CO_2 pressure for 3 h. There was no significant difference in the results obtained from the complex with methyl substituents on the phenolate rings vs. the *t*-butyl substituted rings, indicating that steric effects do not play a large role for this reaction to occur. To demonstrate how similar the results were, the methyl substituted complex allowed for a 55% conversion, a molecular weight of 6 022 g mol^{-1} and a dispersity of 1.05, whereas the *t*-butyl substituted complex allowed for a 56% conversion, a molecular weight of 6 063 g mol^{-1} , and a dispersity of 1.06. The iron complex having chlorine substituents

did demonstrate a large decrease in activity (17% conversion), which can be associated with the poor solubility of the complex in the reaction media.

By varying the amount of cocatalyst used, the selectivity of product formed could be manipulated in favour of polymer vs. cyclic, however, the cyclic product was achieved in high conversions. With five equivalents of nucleophile added to the reaction mixture, the selectivity for cyclic product was seen to vary between 33 – 88% depending on the choice of cocatalyst demonstrating the varied selectivity. Apart from Bu₄NI, ten equivalents of nucleophile led to selectivity consistently greater than 90%. When using TBAB a 94% overall conversion was achieved with a 93% selectivity for cyclic product.

Döring and coworkers developed ionic iron(II) and iron(III) N₂O₂ ligand systems for coupling reactions involving PO and CO₂.³⁸ As shown in Scheme 1.8, complex **1.19a** can be oxidized to its iron(III) counterpart, **1.19b**, in the presence of iodine in THF and pyridine. **1.19a** required a catalyst loading of 1 mol% at 80 °C and 50 bar CO₂ pressure to achieve a 91% conversion to cyclic carbonate (5 h⁻¹) in 20 h. This reaction also required equimolar amounts of TBAB. Complex **1.19b** was able to reach a conversion of 69% (35 h⁻¹) after 20 h with a catalyst loading of 0.1 mol% at 80 °C and 35 bar CO₂ pressure; no cocatalyst was necessary. The iron(III) complex is reasoned to have higher activity as the two pyridine complexes within the coordination sphere can both act as cocatalysts, the metal centre is more Lewis acidic, favouring nucleophilic attack of the monomer, and the iodide anion may also be able to interact favourably with the epoxide.



Scheme 1.8: Oxidation of an iron(II) N_2O_2 complex to iron(III), reference 30

The only work to date to utilize only iron(II) complexes for the coupling of CO_2 and epoxides was performed by Qin and coworkers in 2014.⁶¹ Two complexes were used (**1.20a** and **1.20b**, Figure 1.22) and compared in this work. Both exhibited near quantitative results for the formation of cyclic propylene carbonate after 4 h with a catalyst loading of 0.1 mol% at 100 °C and 40 bar CO_2 pressure. Reactions employing TBAB as the cocatalyst exhibited a greater conversion over PPNC1, 99% vs. 80%, when used in a one to one molar ratio with catalyst, making it the cocatalyst of choice to further study various reaction parameters.

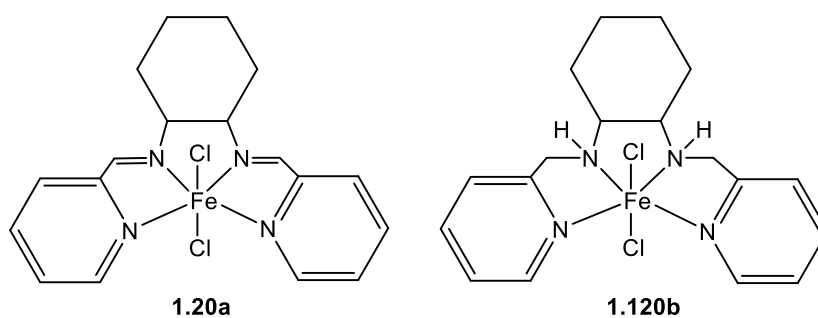


Figure 1.22: Iron(II) complexes for the copolymerization of CO_2 with epoxides, reference 61

The activity of this catalyst system was not dependant on the pressure of CO₂. Under the same conditions, 100% conversion of PO was seen when using 20 to 40 bar CO₂ pressure; increasing the pressure further to 60 bar CO₂ demonstrated a negligible decline in the results with a 98% conversion. At 70 °C, only a 42% conversion of PO was achieved, but under the same conditions at 100 and 130 °C, quantitative conversion was seen; 100 °C was chosen as the standard temperature for further reactions. With respect to time, a 91% conversion was reached after only 2 h under standard conditions. Cyclohexene oxide and epichlorohydrin were also tested to produce the cyclic product. After 4 h, the highest conversion of CHO achieved was only 6%, which increased to 47% when the catalyst loading was increased to 0.2 mol% and left to run for 12 h. Epichlorohydrin, however, gave 97% conversion to cyclic product under standard conditions after only 4 h.

In 2015, Pescarmona published work on converting CO₂ into carbonates using iron(III) pyridylamino-bis(phenolate) complexes **1.21a** and **1.21b**, Figure 1.23, as well as various cocatalysts with TBAB giving the best results.⁶² Not surprisingly, the larger radius of bromine compared to chlorine led to greater steric repulsion of the incoming epoxide to the metal centre decreasing the rate of reaction. Performing the reaction under the same conditions, but varying the cocatalyst, demonstrated the same results as found by Kleij previously. The better nucleophilic anions are those which are smaller allowing for less steric hindrance for the incoming substrate, i.e. chlorides are favourable.

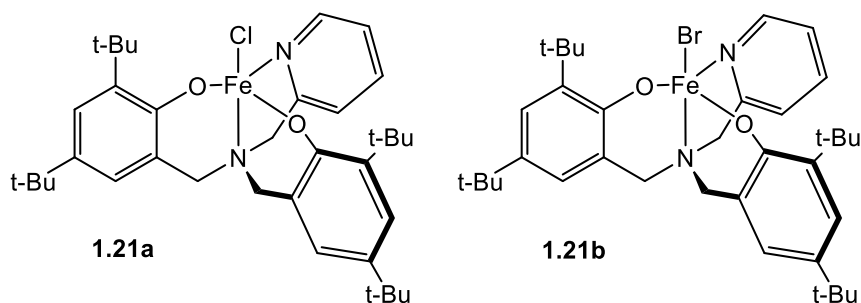


Figure 1.23: Iron(III) amino-bis(phenolate) complexes for the copolymerization of CHO and CO₂, reference 62

With a catalyst loading of 0.5 mol%, and one equivalent of TBAB, at 85 °C and 60 bar CO₂ pressure over 18 h, a 60% conversion of CHO was reached; selectivity towards polymer formation being 82%. Under the same conditions using PPnCl as the cocatalyst gave an overall conversion of 49%, selectivity for polymer formation being 81%. Higher molecular weights were seen when using TBAB compared to PPnCl, 1 418 and 704 g mol⁻¹ respectively, with the dispersity remaining the same, 1.1. Increasing the catalyst loading to 1 mol% and using PPnCl, VCHO could also be polymerized with an 84% conversion and high selectivity to polymer formation. Molecular weight was higher at 3 784 g mol⁻¹ with a broader dispersity of 1.4. To achieve selectivity for the cyclic product, ten equivalents of cocatalyst were necessary, however, the overall conversion was only increased slightly for both CHO and VCHO. Several other epoxides were also screened successfully over a 3 h period using the above conditions, with full selectivity towards to the cyclic product.

In 2016, Repo and coworkers developed novel bis(phenoxyiminato)Fe(III)-chloro complexes, Figure 1.24, which were evaluated as catalysts for the coupling of CO₂ and various epoxides.⁶³ This work focussed mainly on assessing whether or not the

catalysts would be suitable for this process before optimizing the reaction medium, cocatalyst, and reaction time parameters.

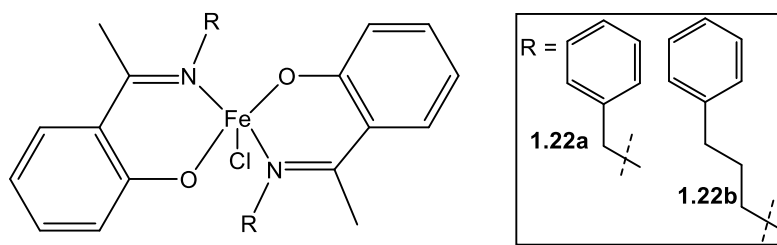


Figure 1.24: Bis(phenoxyiminato)Fe(III)-chloro complexes for the copolymerization of CO₂ and epoxides, reference 63

To assess which cocatalyst was most effective, both catalysts were used in reactions with PO as well as 1-hexene oxide, HO, under the following reaction conditions: with a 0.0125 mol% catalyst loading, 4 equivalents of cocatalyst, at 120 °C and 12.5 bar CO₂ pressure. In each case, PO led to higher conversion of cyclic product than HO, with increasing conversions seen for tetrabutylphosphonium bromide, Bu₄PBR, which was greater than DMAP, and TBAB being least active. Complex **1.22a** gave slightly higher conversions when compared to **1.22b** and was used in further screening processes. Optimal reaction times were found to be 7 h for all epoxides assessed (PO > SO > HO > CHO) although there was slight conversion achieved after only 2 h for all except CHO. DMF, toluene and 1,2-dioxane were determined to be the best reaction media for this process, with DMF suspected to be the optimal solvent as it can catalyze this reaction on its own under more harsh conditions. As it is most polar, DMF is suspected to stabilize the transition states during the ring opening and ring closure steps.⁶³ An increase in catalyst loading, 0.12 mol%, increased the amount of product seen, as did an increase in cocatalyst loading. The highest TON (1 029) was

achieved with ten equivalents of cocatalyst at the original catalyst loading, while the higher catalyst loading needed only 5 equivalents of cocatalyst to reach the highest conversion of PO of 89%.

Kerton and coworkers synthesized a series of square pyramidal iron(III) compounds supported by tetradentate amino-bis(phenolate) ligands which were effective in the production of cyclic carbonates from CO₂ and epoxides, Figure 1.25.²⁴ At 100 °C and 20 bar CO₂ pressure for 22 h, initial screening of the five complexes demonstrated that the best results arise when there are electron donating groups (chlorines) on with phenolate rings, 95% overall conversion vs. just 30% with *t*-butyl/methyl substituents. The decrease in donor ability of the chlorine atoms creates a more Lewis acidic metal centre favouring the coordination of an epoxide. Having bromine in the axial position, as opposed to chlorine, demonstrated a loss in activity as well (74% to 34%) which is speculated to be due to the larger radius of the bromine atom creating an increase in steric repulsion around the metal center for incoming nucleophiles. With respect to cocatalyst choice, there was no significant difference seen between the use of TBAB (74% conversion) vs. PPNCI (70% conversion). The use of DMAP however, almost completely halted the reaction procedure (14%), which was believed to be due to its ability to coordinate to the metal centre and compete with the incoming epoxide.

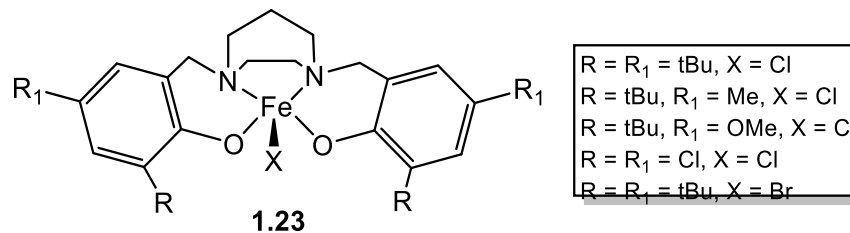


Figure 1.25: Square pyramidal iron(III) complexes for the coupling of PO and CO₂, reference 24

By studying the reaction profiles using in situ infrared spectroscopy, the cyclic carbonate carbonyl peak could be seen growing in over time at 1806 cm⁻¹. The growth of this peak was monitored over a series of temperatures ranging from 50 °C to 80 °C, which demonstrated clearly the influence temperature has on the rate of reaction; at room temperature there was no cyclic carbonate formed, at 50 °C a small linear trend was observed, whereas 80 °C gave a steep linear slope. An Arrhenius plot determined the activation barrier of the catalytic system to be 98.4 kJ mol⁻¹. Using the same reaction parameters mentioned above, various other epoxides were screened successfully as well, with higher conversions achieved when using epichlorohydrin, and very low conversion seen for others, namely 31% for styrene oxide and only 9% for CHO.

Also in 2016, Capacchione and coworkers reported thioether-triphenolate bimetallic iron(III) complexes, Figure 1.26, which were highly efficient at producing cyclic carbonates with a variety of epoxides.⁶⁴ Three of these complexes have already demonstrated their efficiency at producing cyclic carbonate when coupled with TBAB.²⁶

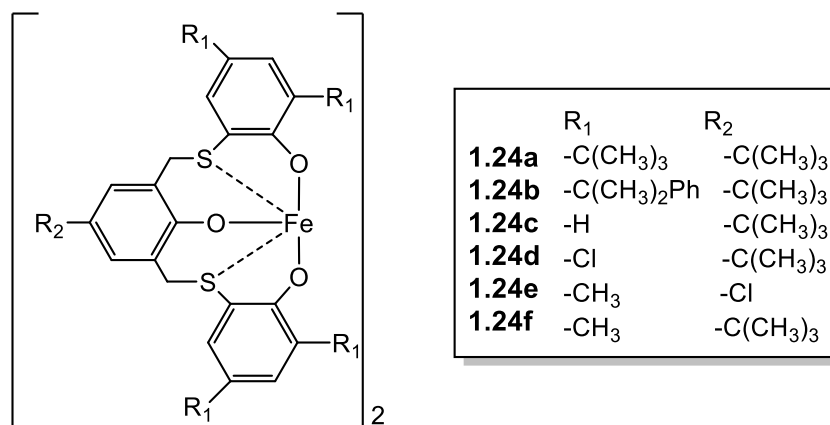


Figure 1.26: Thioether-triphenolate bimetallic iron(III) complexes for the coupling of CO₂ with various epoxides, reference 64

Screening of all complexes was carried out with a 0.01 mol% catalyst loading, 0.1 mol% TBAB at 120 °C and 20 bar CO₂ pressure for 1 h. Pressure effects were briefly investigated showing a slight decline in activity when decreasing the pressure from 20 to 5 bar CO₂, while increasing the pressure to 40 bar gave complete conversion to cyclic product. While all complexes gave relatively similar results, with conversions ranging from 36 – 52%, it was the bulkier complex, **1.24b**, and the more Lewis acidic complex, **1.24d**, which demonstrated the lowest overall activities, 36% (3 630 h⁻¹) and 336% (3 550 h⁻¹) respectively. **1.24f** demonstrated the highest overall activity, 52%, and the highest TOF for propylene carbonate formation reported to date for an iron complex, 5 200 h⁻¹. This same complex was then used to optimize several conditions, such as cocatalyst selection which is demonstrated in Figure 1.26. DMAP inhibited any carbonate formation, whereas tetrabutylammonium chloride (TBAC), PPNCI, and tetrabutylammonium iodide (TBAI) all demonstrated similar activities with a 1:2 ratio of catalyst to cocatalyst loading. Using TBAB under the same conditions demonstrated a significant increase in activity, which continued to increase with the cocatalyst loading.

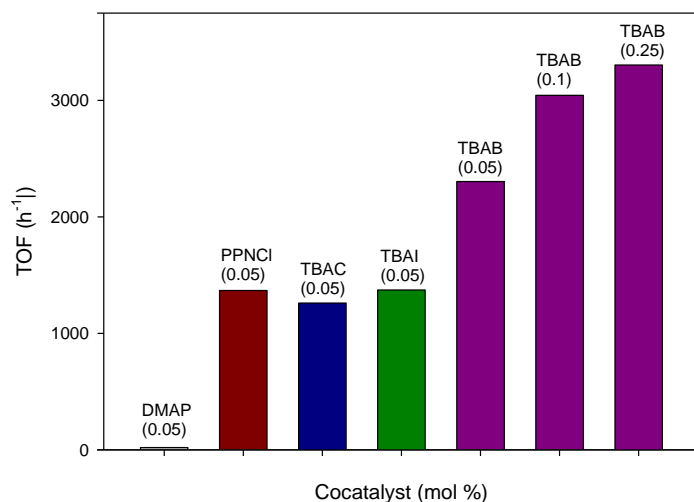


Figure 1.27: Effect of cocatalyst on the catalytic activity for the coupling of PO and CO₂ using complex **1.24f**, reference 64

1.4.3.1 Summary of Iron Catalyzed Reactions with CO₂ and Epoxides

What is highlighted in Section 1.4.3 is the deficiency of iron complexes capable of polymerizing CHO and CO₂; this work is also summarized in Table 1.3. In 2011, Charlotte Williams was the first to successfully publish work in this area with a di-iron complex, no catalyst since has been able to replicate or improve on these results.²⁵ With a modest catalyst loading, and a reaction performed at low pressure (10 bar CO₂) the resulting polymer had a high molecular weight and narrow dispersity. Two years later, Kleij published an iron tri-phenolate complex which was also successful in producing polymer. Supercritical CO₂ conditions were necessary, however, and the resultant polymer had a molecular weight which was approximately half that of Williams.⁶⁰ More recently, Pescarmona published work using an iron amine-bis(phenolate complex) which also resulted in a successful polymerization attempt, however, reaction conditions were not improved to that of previous work.⁶² The resultant polymers were produced

with lower conversions (less than 50%) and very low molecular weights (1 418 g mol⁻¹) for the few calculated.

Table 1.3: Iron catalysts used in the production of polycarbonates from CO₂ and CHO; a summary of the literature presented in Section 1.4.2

Group	Catalyst (mol %)	P (bar)	Temp. (°C)	Time (h)	Conv. (%)	Mn (g mol⁻¹)	Đ (Mn/Mw)
Williams	0.1	10	80	24	70	11 700	1.13
Kleij	0.1	80	85	3	56	6 022	1.05
Pescarmona	0.5	80	60	18	49	1 418	1.1

As summarized in Table 1.4, forming cyclic carbonates from the coupling of CHO and CO₂ is extremely rare and the conditions used have been relatively harsh, aside from Williams in 2011. At only 1 bar CO₂ pressure at 80 °C, a 41% conversion to cyclic product was achieved over 48 h.²⁶ Increasing the catalyst loading from 0.1 mol% to 1 mol% led to an increased conversion of 90% under the same conditions. Kleij,⁶⁰ Pescarmona,⁶² and coworkers were also successful in producing cyclic CHO using iron triphenolate complexes and iron amine-bis(phenolate) complexes respectively. With a catalyst loading of 0.5 mol%, Kleij was able to produce the largest TOF (55 h⁻¹) with a conversion of 82% at 85 °C and 80 bar CO₂ pressure.⁶⁰ Pescarmona was able to decrease the temperature to 60 °C, however, after 18 h the conversion only reached 56% (7 h⁻¹).

The coupling of CO₂ and PO to form cyclic carbonates, rather than using CHO, is more common for iron catalysts. This work has also been detailed in Section 1.4.3 and is summarized again in Table 1.4. Catalyst loadings have ranged from 0.01^{38,61} to 0.5 mol%²⁶ while CO₂ pressures have remained fairly low, averaging 20 bar, aside from Williams who was able to achieve high conversions with only 1 bar CO₂ pressure at room temperature. To date, Capacchione has produced the highest TOF (5 200h⁻¹),

however a large excess of cocatalyst was required, 10 equivalents.⁶⁴ Döring's work with an ionic iron(III) catalyst is the only reaction that demonstrates a good conversion to cyclic carbonate (69%) without the aid of a cocatalyst. The variety of temperatures, pressures, cocatalysts, reaction times, and loadings used previously for this reaction makes it an interesting challenge to see which parameters can be optimized the most to still achieve high conversions of TOFs of cyclic product.

Table 1.4: Iron catalysts used for the coupling of CO₂ and epoxides to produce cyclic carbonate; a summary of the literature presented in section 1.4.2

Group	Epoxide	Cat. (mol %)	P (bar)	Temp. (°C)	T (h)	Conv. (%)	TOF (h ⁻¹)
Williams	CHO	0.1	1	80	48	41	9
Williams	CHO	1	1	80	24	90	4
Kleij	CHO	0.5	80	85	3	82	55
Pescarmona	CHO	0.5	80	60	18	56	7
Williams	PO	0.5	1	25	48	91	4
Döring	PO	0.1	35	80	20	69	35
Qin	PO	0.1	40	100	4	99	248
Repo	PO	0.125	10	145	7	89	102
Kerton	PO	0.025	20	100	22	95	173
Capacchione	PO	0.01	20	120	1	52	5 200

1.5 Objectives of this Thesis

The objectives for this thesis focussed on the viability of iron(III) amino-bis(phenolate) complexes for the coupling of CO₂ with propylene oxide (and various other epoxides), as well for the copolymerization of CHO with CO₂. The catalysts proved efficient for these reactions, therefore the electronic and steric properties of the catalysts were also assessed to help determine the best catalytic system. Another aim was to optimize the parameters for each reaction. To determine more accurate reaction times, while optimizing CO₂ pressure, temperature, cocatalyst choice, and catalyst loading.

1.6 References

1. Anastas, P. T., *Tetrahedron* **2010**, *66*, 1026-1027.
2. Anastas, P. T.; Warner, J. C., *Green Chemistry: Theory and Practice*. Oxford University Press 1998.
3. Haack, J. A.; Hutchison, J. E., *ACS Sustain. Eng.* **2016**, *4*, 5889-5896.
4. Sheldon, R. A., *Green Chem.* **2017**, *19*, 18-43.
5. Anastas, P.; Eghbali, N., *Chem. Soc. Rev.* **2010**, *39*, 301-312.
6. Winterton, N., *Clean Technol. Environ.* **2016**, *18*, 991-1001.
7. Gałuszka, A.; Migaszewski, Z.; Namieśnik, J., *Trends Anal. Chem.* **2013**, *50*, 78-84.
8. Haack, J. A.; Hutchison, J. E., *Chem. Ind.* **2009**, 15.
9. McKenzie, L. C.; Huffman, L. M.; Hutchison, J. E., *Green Chem.* **2009**, 86.
10. Xin, Y.; Uyama, H., *J. Poly. Res.* **2012**, *19*, 1-7.
11. Fukuoka, S.; Fukawa, I.; Tojo, M.; Oonishi, K.; Hachiya, H.; Aminaka, M.; Hasegawa, K.; Komiya, K., *Catal. Surv. Asia* **2010**, *14*, 146-163.
12. Fukuoka, S.; Kawamura, M.; Komiya, K.; Tojo, M.; Hachiya, H.; Hasegawa, K.; Aminaka, M.; Okamoto, H.; Fukawa, I.; Konno, S., *Green Chem.* **2003**, *5*, 497-507.
13. Haba, O.; Itakura, I.; Ueda, M.; Kuze, S., *J. Polym. Sci. A* **1998**, *37*, 2087-2093.
14. vom Saal, F. S.; Hughes, C., *Environ. Health Perspect.* **2005**, *113*, 926-933.
15. Vandenberg, L. N.; Hauser, R.; Marcus, M.; Olea, N.; Welshons, W. V., *Reprod. Toxicol.* **2007**, *24*, 139-177.
16. Rubin, B. S., *J. Steroid Biochem. Mol. Biol.* **2011**, *127*, 27-34.
17. Cooper, J. E.; Kendig, E. L.; Belcher, S. M., *Chemosphere* **2011**, *85*, 943-947.
18. Kricheldorf, H. R.; Böhme, S.; Schwarz, G.; Schultz, C.-L., *J. Polym. Sci. A.* **2005**, *43*, 1248-1254.
19. Martens, J. B., A. De Kimpe, N. Jacobs, P. Marin, G. Rabaey, K. Saeys, M. Verhelst, S., *ChemSusChem* **2017**, *10*, 1039-1055.

20. Song, C., *Catal. Today* **2006**, *115*, 2-32.
21. Aresta, M.; Dibenedetto, A., *Dalton Trans.* **2007**, 2975-2992.
22. Macdowell, N. F., P. Shah, N. Maitland, G., *Nat. Clim. Change* **2017**, *7*, 243-249.
23. Inoue, S.; Koinuma, H.; Tsuruta, T., *Polym. Lett.* **1969**, *7*, 287-292.
24. Alhashmialameer, D.; Collins, J.; Hattenhauer, K.; Kerton, F. M., *Catal. Sci. Technol.* **2016**, *6*, 5364-5373.
25. Buchard, A.; Kember, M. R.; Sandeman, K. G.; Williams, C. K., *Chem. Commun.* **2011**, *47*, 212-214.
26. Buonerba, A.; De Nisi, A.; Grassi, A.; Milione, S.; Capacchione, C.; Vagin, S.; Rieger, B., *Catal. Sci. Technol.* **2015**, *5*, 118-123.
27. Darensbourg, D. J., *Chem. Rev.* **2007**, *107*, 2388-2410.
28. Devaine-Pressing, K.; Dawe, L. N.; Kozak, C. M., *Polym. Chem.* **2015**, *6*, 6305-6315.
29. Liu, Y.; Zhou, H.; Guo, J. Z.; Ren, W. M.; Lu, X. B., *Angew. Chem. Int. Ed.* **2017**, *56*, 4862-4866.
30. van Heek, J.; Arning, K.; Ziefle, M., *Energy Policy* **2017**, *105*, 53-66.
31. Cohen, C. T.; Chu, T.; Coates, G. W., *J. Am. Chem. Soc.* **2005**, *127*, 10869-10878.
32. Lu, X. B.; Darensbourg, D. J., *Chem Soc Rev* **2012**, *41*, 1462-1484.
33. Pinilla-de Dios, M.; Andrés-Iglesias, C.; Fernández, A.; Salmi, T.; Galdámez, J. R.; García-Serna, J., *Eur. Polym. J.* **2017**, *88*, 280-291.
34. von der Assen, N.; Bardow, A., *Green Chem.* **2014**, *16*, 3272-3280.
35. Fu, X.; Jing, H., *J. Catal.* **2015**, *329*, 317-324.
36. Wu, G.-P.; Wei, S.-H.; Ren, W.-M.; Lu, X.-B.; Li, B.; Zu, Y.-P.; Darensbourg, D. J., *Energy Environ. Sci.* **2011**, *4*, 5084-5092.
37. Dean, R. K.; Devaine-Pressing, K.; Dawe, L. N.; Kozak, C. M., *Dalton Trans.* **2013**, *42*, 9233-9244.

38. Fuchs, M. A.; Zevaco, T. A.; Ember, E.; Walter, O.; Held, I.; Dinjus, E.; Doring, M., *Dalton Trans.* **2013**, *42*, 5322-5329.
39. Darensbourg, D. J.; Yeung, A. D., *Polym. Chem.* **2015**, *6*, 1103-1117.
40. Bayer Annual Report 2013, <https://www.bayer.com/en/ar-2013.pdf> Accessed on October 26th 2017
41. Darensbourg, D. J.; Yarbrough, J. C.; Ortiz, C.; Fang, C. C., *J. Am. Chem. Soc.* **2003**, *125*, 7586-7591.
42. Hatazawa, M.; Nakabayashi, K.; Ohkoshi, S.; Nozaki, K., *Chem. Eur. J.* **2016**, *22*, 13677-13681.
43. Zhang, H.; Liu, B.; Ding, H.; Chen, J.; Duan, Z., *Polymer* **2017**, *129*, 5-11.
44. Darensbourg, D. J.; Holtcamp, M. W.; Struck, G. E.; Zimmer, M. S.; Niezgod, S. A.; Rainey, P.; Robertson, J. B.; Draper, J. D.; Reibenspies, J. H., *J. Am. Chem. Soc.* **1999**, *121*, 107-116.
45. Allen, S. D.; Moore, D. R.; Lobkovsky, E. B.; Coates, G. W., *J. Am. Chem. Soc.* **2002**, *124*.
46. Lee, B. Y.; Kwon, H. Y.; Lee, S. Y.; Na, S. J.; Han, S.; Yun, H.; Lee, H.; Park, Y., *J. Am. Chem. Soc.* **2005**, *127*, 3031-3037.
47. Nakano, K.; Nakamura, M.; Nozaki, K., *Macromolecules* **2009**, *42*, 6972-6980.
48. Darensbourg, D. J.; Bottarelli, P.; Andreatta, J. R., *Macromolecules* **2007**, *40*, 7727-7729.
49. Darensbourg, D. J.; Chung, W.-C.; Wilson, S. J., *ACS Catal.* **2013**, *3*, 3050-3057.
50. Darensbourg, D. J.; Fitch, S. B., *Inorg. Chem.* **2007**, *46*, 5474-5476.
51. Darensbourg, D. J.; Fitch, S. B., *Inorg. Chem.* **2008**, *47*, 11868-11878.
52. Darensbourg, D. J.; Mackiewicz, R. M., *J. Am. Chem. Soc.* **2005**, *127*, 14026-14038.
53. Darensbourg, D. J.; Mackiewicz, R. M.; Rodgers, J. L.; Fang, C. C.; Billodeaux, D. R.; Reibenspies, J. H., *Inorg. Chem.* **2004**, *43*, 6024-6034.

54. Darensbourg, D. J.; Moncada, A. I.; W., C.; Reibenspies, J. H., *J. Appl. Polym. Sci.* **2008**, *130*, 6523-6533.
55. Darensbourg, D. J.; Ulusoy, M.; Karroonnirum, O.; Poland, R. R.; Reibenspies, J. H.; Çetinkaya, B., *Macromolecules* **2009**, *42*, 6992-6998.
56. Darensbourg, D. J.; Yarbrough, J. C., *J. Am. Chem. Soc.* **2002**, *124*, 6335-6342.
57. Saunders, L. N.; Ikpo, N.; Petten, C. F.; Das, U. K.; Dawe, L. N.; Kozak, C. M.; Kerton, F. M., *Catal. Commun.* **2012**, *18*, 165-167.
58. Dean, R. K.; Dawe, L. N.; Kozak, C. M., *Inorg. Chem.* **2012**, *51*, 9095-9103.
59. Chen, H.; Dawe, L. N.; Kozak, C. M., *Catal. Sci. Technol.* **2014**, *4*, 1547-1555.
60. Taherimehr, M.; Al-Amsyar, S. M.; Whiteoak, C. J.; Kleij, A. W.; Pescarmona, P. P., *Green Chem.* **2013**, *15*, 3083-3090.
61. Sheng, X.; Qiao, L.; Qin, Y.; Wang, X.; Wang, F., *Polyhedron* **2014**, *74*, 129-133.
62. Taherimehr, M.; Serta, J.; Kleij, A. W.; Whiteoak, C. J.; Pescarmona, P. P., *ChemSusChem* **2015**, *8*, 1034-1042.
63. Al-Qaisi, F. a.; Genjang, N.; Nieger, M.; Repo, T., *Inorg. Chimi. Acta.* **2016**, *442*, 81-85.
64. Della Monica, F.; Vummaleti, S. V. C.; Buonerba, A.; Nisi, A. D.; Monari, M.; Milione, S.; Grassi, A.; Cavallo, L.; Capacchione, C., *Adv. Synth. Catal.* **2016**, *2016*, 3231-3241.

Chapter 2: Synthesis and Characterization of Iron Complexes of Diamino-bis(phenolate) Ligands

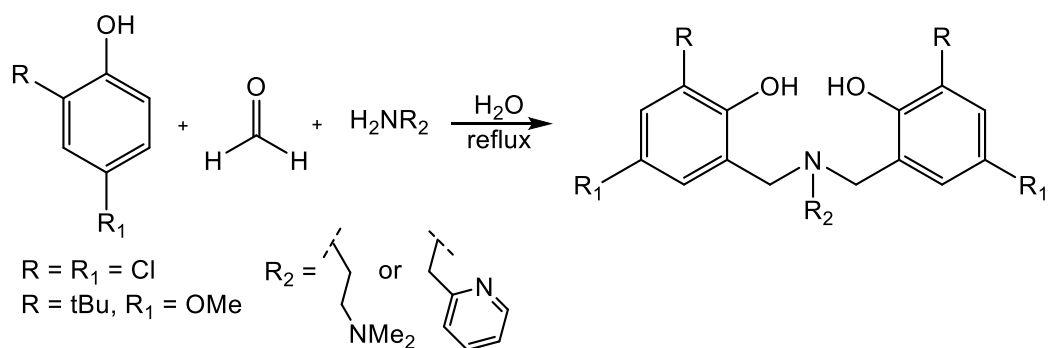
2.1 Introduction

Amino-phenolate ligands are desirable for the synthesis of transition metal complexes as they are readily prepared, as will be outlined in section 2.2, and can be modified to explore both steric and electronic effects.¹ Iron amino-phenolate complexes have been utilized in various reactions in recent years. These reactions include atom transfer radical polymerizations,²⁻⁵ hydrosilylation of ketones/aldehydes,⁶ and for the formal hydroamination of olefins.⁷ The Kozak group has utilized a variety of these complexes since 2008 for the coupling of alkyl halides,^{8,9} as well as for the cross coupling of Grignard reagents,¹⁰⁻¹³ and for the epoxidations of olefins with hydrogen peroxide.¹⁴ Additionally, they had success using these complexes for controlled radical polymerizations¹⁵ and the coupling of benzyl halides with aryl Grignard reagents.¹⁶ In 2015, work was first published on the use of iron amino-phenolate complexes for the successful copolymerization of CO₂ with cyclohexene oxide, CHO.¹⁷

2.2 Synthesis of tetradentate amino-bis(phenolate) ligands

A modified Mannich condensation was used to readily synthesize a variety of tetradentate amine-bis(phenolate) ligands, Scheme 2.1. A solution of formaldehyde, the desired 2,4-disubstituted phenol, and amine was combined in water, and the reaction mixture was brought to reflux overnight. Synthesis of these ligand systems have been previously performed in methanol¹⁸ or ethanol.¹⁹ Electron withdrawing chlorine substituents, were chosen as they will create a more Lewis acidic metal centre; this effect has proven both successful,²⁰ and unsuccessful.²¹ Kerton and coworkers noticed an increase in conversion of propylene carbonate, PC, (74% - 95%) when switching from

tert-butyl substituted phenols to dichloro substituted phenols. However, Capacchione noticed the opposite trend using the same substituents (52% - 36%). Synthesizing complexes which have electron donating groups, and others with withdrawing groups, allow for a comparative study on how electronic effects alter the performance of a catalyst.



Scheme 2.1: Synthesis of diamino-bis(phenol) ligands

Four ligands were synthesized (Figure 2.1) and used throughout the coupling and polymerization studies in Chapters 3 and 4. These ligands were chosen specifically to compare electronic effects on the phenolate rings as well as the influence of the nature of the amine pendant arm. Utilizing tetradentate ligands also allows for the formation of the 5-coordinate iron(III) species. **H₂L1** is the most broadly studied ligand of the four, demonstrating versatility and forming complexes with eight different metals. These metals include iron for radical polymerizations^{22,23} and C-C cross coupling,¹³ manganese to assess oxidase activity²⁴ as well as lactide polymerization,²⁵ vanadium for isoprene polymerization,²⁶ cobalt for the formation of organic carbonates,²⁷ aluminum for lactide polymerization,²⁸ titanium and zirconium for various polymerization studies,²⁹⁻³¹ and

tantalum for structure studies.³² For **H₂L2**, iron complexes have been the most commonly synthesized as models for catechol-bound protocatechuate 3,4-dioxygenase,³³ models for catechol bound intermediates,³⁴ and for C-C cross coupling activity. Manganese complexes for *rac*-lactide polymerization,²⁵ as well as molybdenum complexes for olefin epoxidation,³⁵ have also been synthesized.¹³ **H₂L3** has been complexed with other metals in the literature including cobalt for the copolymerization of lactone and acrylate,^{36,37} manganese,²⁴ chromium for the copolymerization of CO₂ and CHO,³⁸ and aluminum for the polymerization of caprolactone.³⁹ Various metal complexes have also been synthesized with **H₂L4** as well, such as iron,^{34,40,41} chromium,³⁸ manganese,⁴² molybdenum,⁴³ and copper.^{44,45}

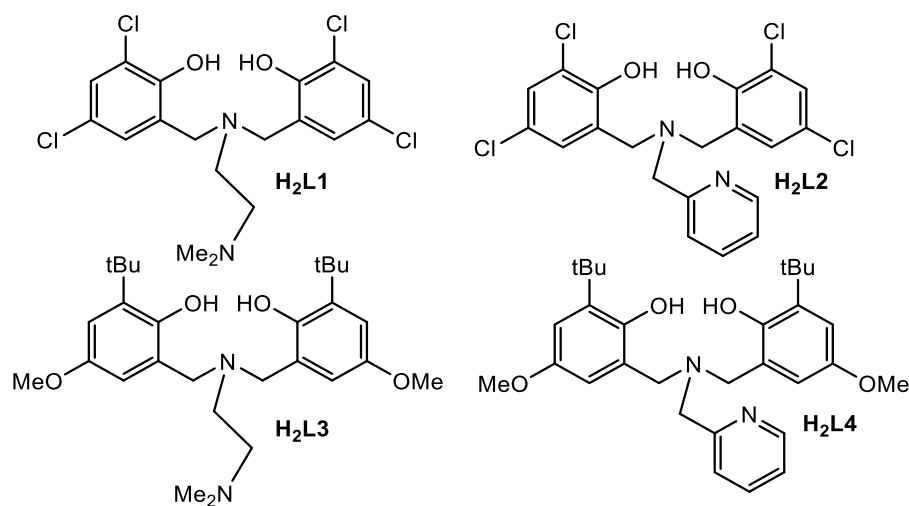
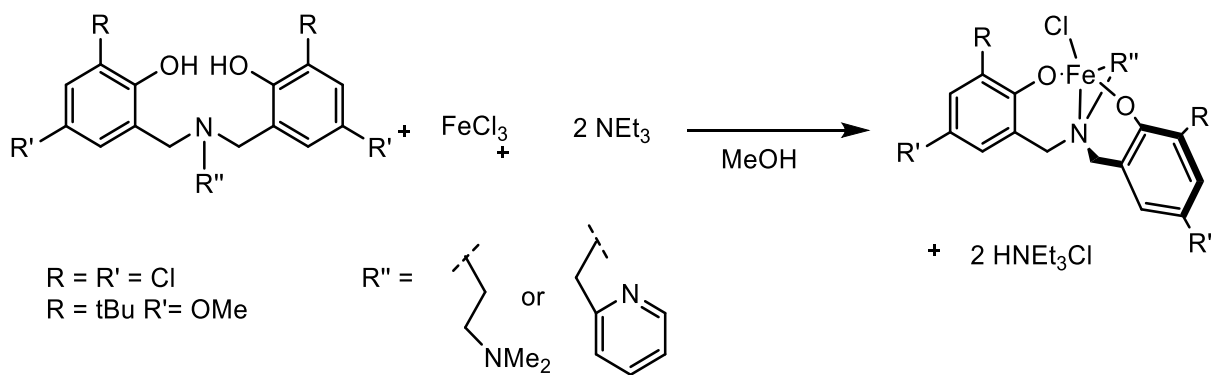


Figure 2.1: Amino-bis(phenol) ligands synthesized.

2.3 Synthesis of iron(III) complexes of tetradentate amino-bis(phenol) ligands

The procedure for the synthesis of the FeCIL complexes was performed as reported for related Fe complexes of amine-bis(phenolate) ligands, Scheme 2.2.¹⁰⁻¹⁶



Scheme 2.2: Synthesis of iron amino-bis(phenolate) complexes.

Complexes **2.1-2.4** (Figure 2.2) were obtained by adding a methanol solution of FeCl_3 to a methanol solution of H_2L . Et_3N is added to neutralize the HCl produced. Purple products **2.1-2.4** were obtained after filtration of acetone solutions and evaporation to dryness. The paramagnetic products were analytically pure by CHN elemental microanalysis.

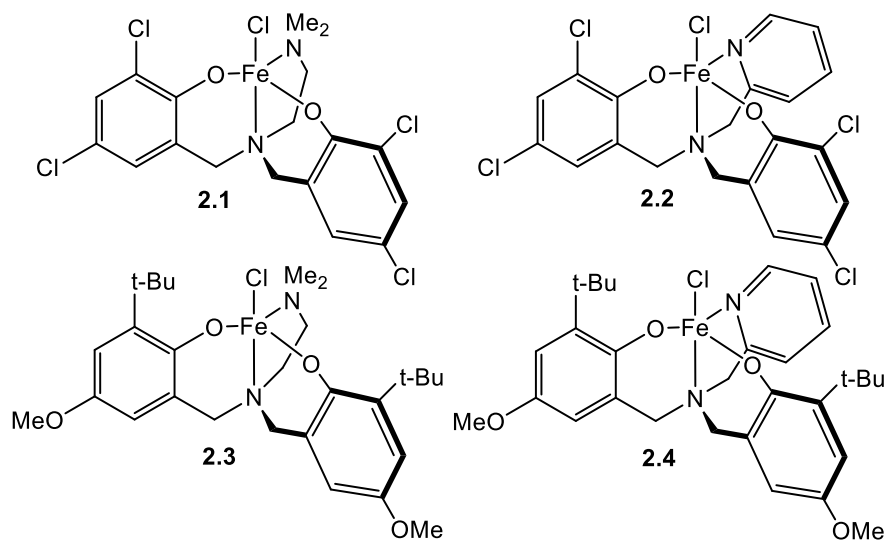


Figure 2.2: Iron amino-bis(phenolate) complexes **2.1-2.4**

2.4 Characterization

The ligands were characterized using ^1H NMR and ^{13}C NMR spectroscopy, and the spectra were compared (and matched) to literature data as they have been prepared previously.^{13,38} The iron amino-bis(phenolate) complexes were characterized using elemental analysis, MALDI TOF-MS as well as UV-visible spectroscopy. An in-depth discussion of these results can be found in this section.

2.4.1 NMR Spectroscopy

The ligands used in this work were previously reported and their spectroscopic characterization (^1H NMR and ^{13}C NMR) is consistent with that shown in the literature.^{13,38} Representative spectra are given (Figures 2.3 and 2.4) for $\text{H}_2\text{L3}$ in CDCl_3 . The ^1H NMR spectrum, Figure 2.3, contains two doublets at 6.79 and 6.38 ppm which represent the aromatic hydrogens on the phenolate rings (H_7 and H_4 respectively); these peaks are common for all ligands. The methoxy hydrogens (H_6) appear as a singlet at 3.74 ppm, while the methylene hydrogens (H_{11}) also produce a singlet at 2.60 ppm. The peak at 3.63 ppm can be attributed to methanol within the sample due to insufficient drying after recrystallization. The methyl groups are seen as a singlet at 2.24 ppm. The *t*-butyl hydrogens (H_1) are the furthest upfield producing a singlet at 1.39 ppm. As the ligand possesses C_2 symmetry, the protons on each phenolate ring are in equivalent environments. The $^{13}\text{C}\{^1\text{H}\}$ NMR spectrum, Figure 2.5, is also in agreement with literature characterization. Both spectra are summarized in Tables 2.1 and 2.2.

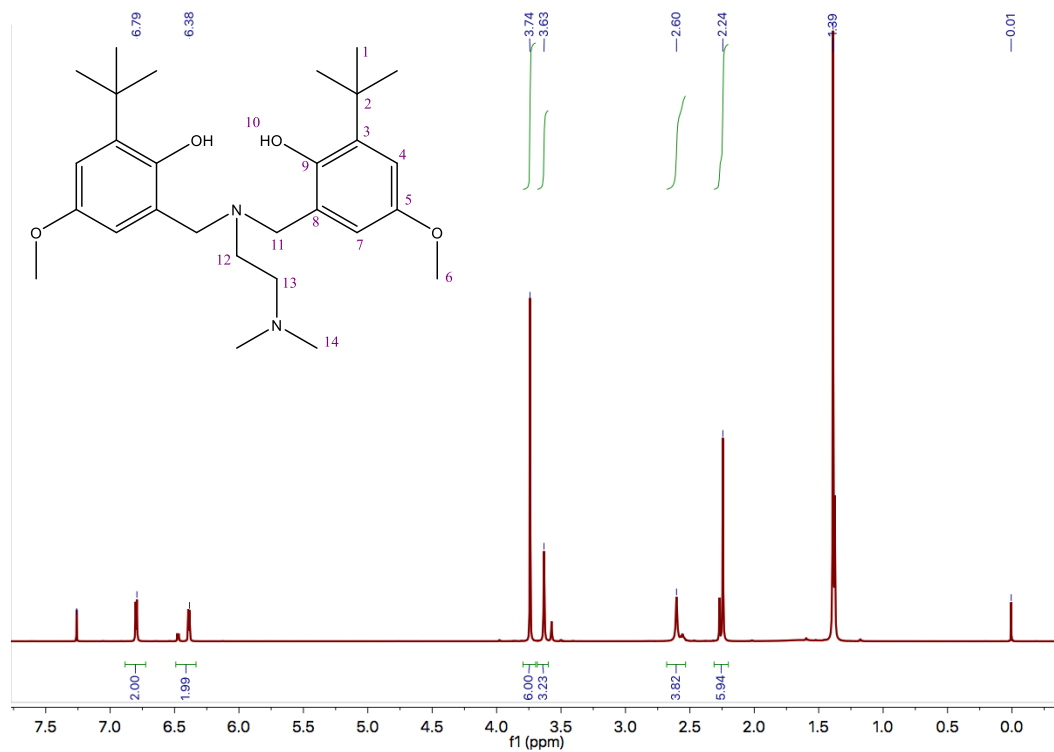


Figure 2.3: 1H NMR of H_2L3 in $CDCl_3$.

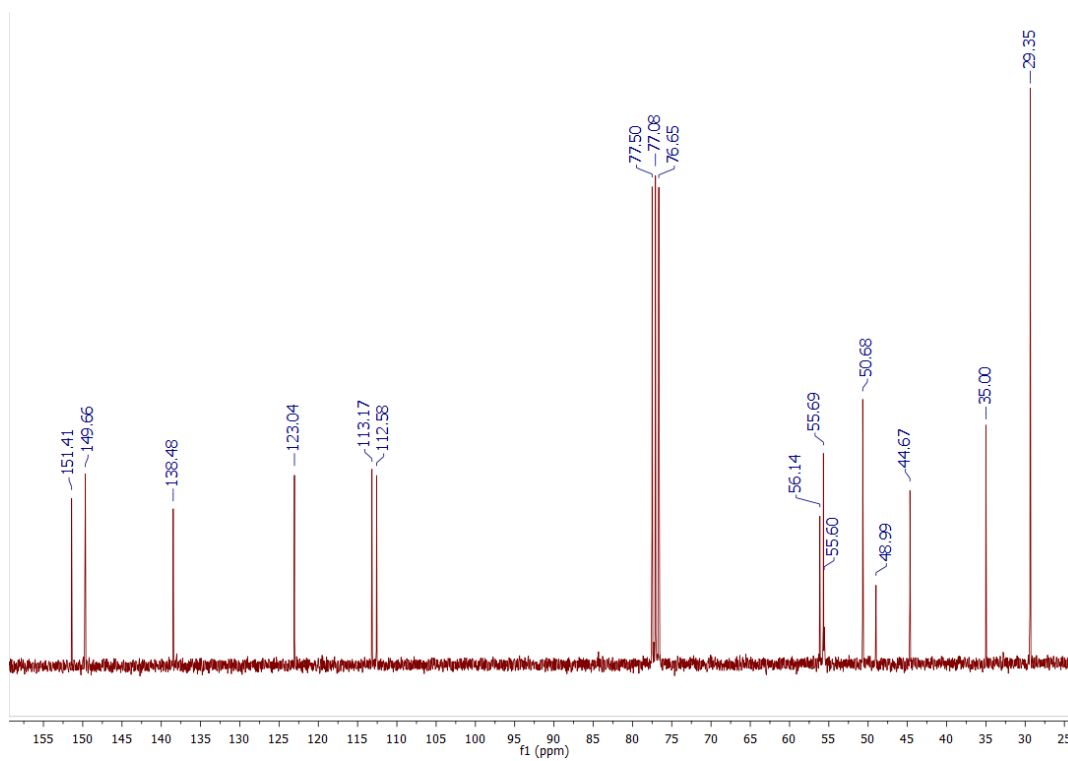


Figure 2.4: ^{13}C NMR of H_2L3 in $CDCl_3$.

Table 2.1: Assignment of resonances for H₂L3 in the ¹H NMR spectrum as seen in Figure 2.3

Protons	Chemical Shift (δ)	# Equivalent Protons	Peak	Coupling Constant
1	1.39	18	Singlet	-
4	6.38	2	Doublet	3.1 Hz
6	3.74	6	Singlet	-
7	6.79	2	Doublet	3.1 Hz
11	3.63	4	Singlet	-
12 and 13	2.60	4	Triplet	2.0 Hz
15	2.24	6	Singlet	-

Table 2.2: Assignment of resonances for H₂L3 in the ¹³C NMR spectrum as seen in Figure 2.4

Carbons	Chemical Shift (δ)	# Equivalent Carbons	Carbon Environment
1	29.35	6	C(CH ₃) ₃
2	35.00	2	C(CH ₃) ₃
3	123.04	2	Ar: CCMe ₃
4	112.58	2	Ar: CHCCMe ₃
5	138.48	2	Ar: COMe
6	55.69	2	O(CH ₃)
7	113.17	2	Ar: CHCCH ₂ N
8	149.66	2	Ar: CCH ₂ N
9	151.41	2	Ar: COH,
11	56.14	2	Ar(CH ₂)N
12	55.60	1 (CH ₂)	NCH ₂ CH ₂ NMe ₂
13	48.99	1 (CH ₂)	NCH ₂ CH ₂ NMe ₂
14	44.67	2 (CH ₃)	NCH ₂ CH ₂ NMe ₂

¹H NMR proved ineffective as a characterization technique for the iron complexes themselves as they are paramagnetic.

2.4.2 Elemental Analysis

Elemental analysis was performed on each compound after they had been purified. The compounds were dried under vacuum on a Schlenk line overnight as water has been found to coordinate to the metal centre in the past.¹³ The findings are outlined in Table 2.3.

Table 2.3: Elemental analysis data for complexes **2.1-2.4**

Compound	Carbon Theoretical % (Exp.%)	Hydrogen Theoretical % (Exp. %)	Nitrogen Theoretical % (Exp.%)
2.1 C ₁₈ H ₁₈ Cl ₅ FeN ₂ O ₂	40.99 (41.24)	3.44 (3.18)	5.31 (5.55)
2.2 C ₂₀ H ₁₄ Cl ₅ FeN ₂ O ₂	43.88 (44.15)	2.58 (2.70)	5.12 (5.31)
2.3 C ₂₈ H ₄₂ ClFeN ₂ O ₄	59.85 (59.51)	7.53 (7.50)	4.99 (5.27)
2.4 C ₃₀ H ₃₈ ClFeN ₂ O ₄	61.92 (61.64)	6.74 (6.33)	4.81 (4.44)

2.4.3 MALDI TOF-MS

Matrix assisted laser desorption/ionization mass spectrometry coupled with a time of flight detector, MALDI TOF-MS, was further used to analyze the iron complexes. All complexes could be readily dissolved in dichloromethane, CH₂Cl₂, and were thus combined with anthracene (also soluble) as a matrix in a 1:1 ratio. Anthracene is an ideal matrix for these iron complexes due largely in part to its lack of functional groups; it generates radical cations for the molecular ion of each complex through electron abstraction.⁴⁶ Therefore, for each complex a weak molecular ion peak, [M]^{•+}, can be observed, as well as an intense peak for the complex with loss of a chloride, [M-Cl]⁺, visible.

The isotopic distribution of complex **2.1** is modelled in Figure 2.5. The ligand peak, H₂L**1**, is observed at approximately *m/z* 438. An additional peak for [1-Cl]⁺ at *m/z* 489.98, which is the most intense peak in the spectrum, is also observed. The theoretical data (bottom) models the experimental data (top) well for both peaks. However, the theoretical ligand spectrum is comprised of two overlapping patterns: [H₂L**1**+H]⁺ and [H₂L**1**-H]⁻.

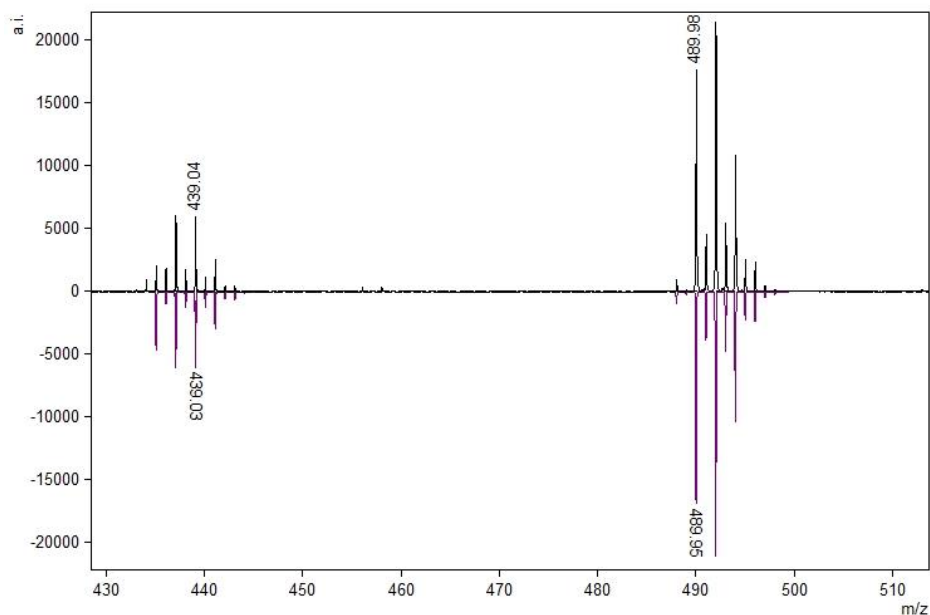


Figure 2.5: Experimental (top) and modelled (bottom) MALDI-TOF mass spectrum of **2.1**

Figure 2.6 shows two essential peaks when analyzing these iron complexes. At m/z 546.19, $[\mathbf{2.4}\text{-Cl}]^+$, is observed as the base peak. The molecular ion of **2.4** is visible as a radical cation at m/z 581.16. There is no evidence of higher mass fragments seen in this spectrum. Figure 2.7 is a magnification of the molecular ion $[\mathbf{2.4}]^{+\bullet}$ and it shows good agreement between the experimental (top) and the theoretical pattern (bottom). Figures 2.8-2.10 show the magnified area of the MALDI-TOF mass spectra of compounds **2.2-2.4** showing the experimental and calculated isotope patterns for their respective $[\text{M-Cl}]^+$ ions.

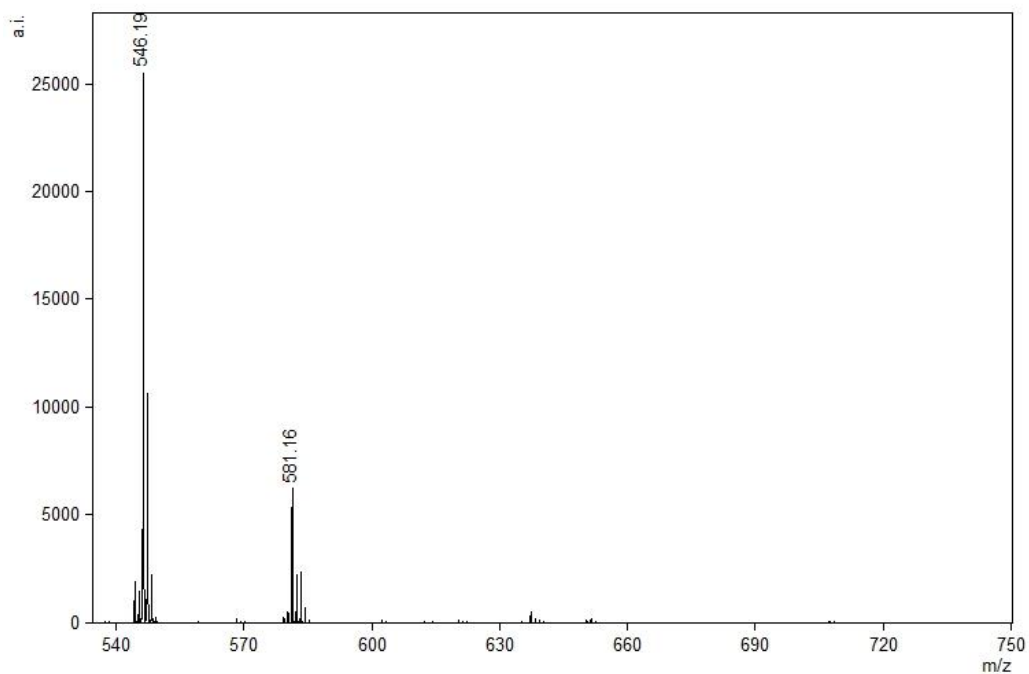


Figure 2.6: MALDI-TOF mass spectrum of **2.4**

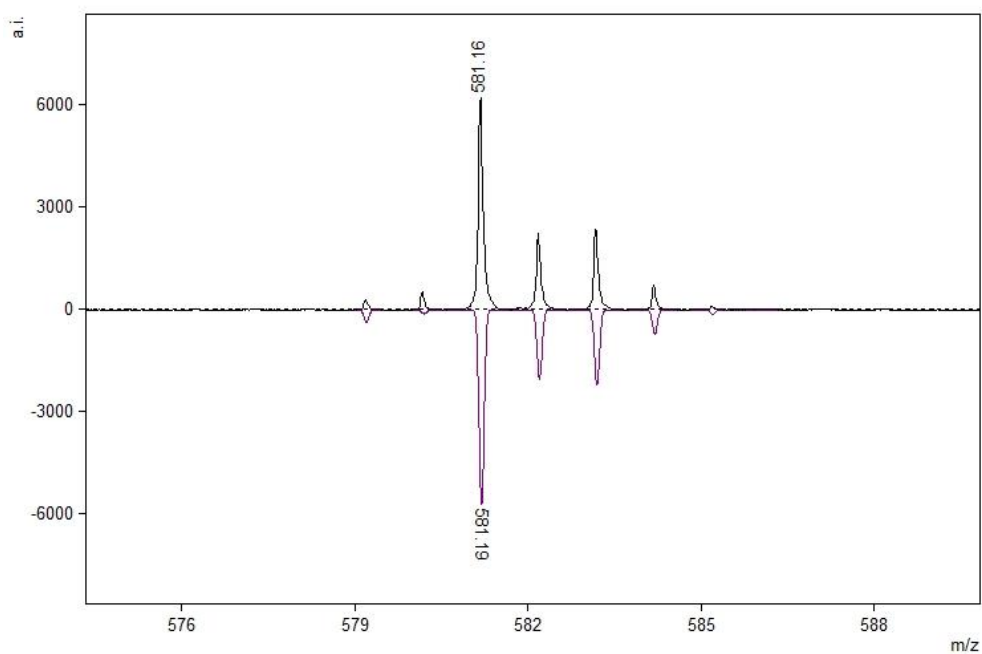


Figure 2.7: Magnification of the experimental (top) and modelled (bottom) molecular ion observed in the MALDI-TOF mass spectrum of **2.4**

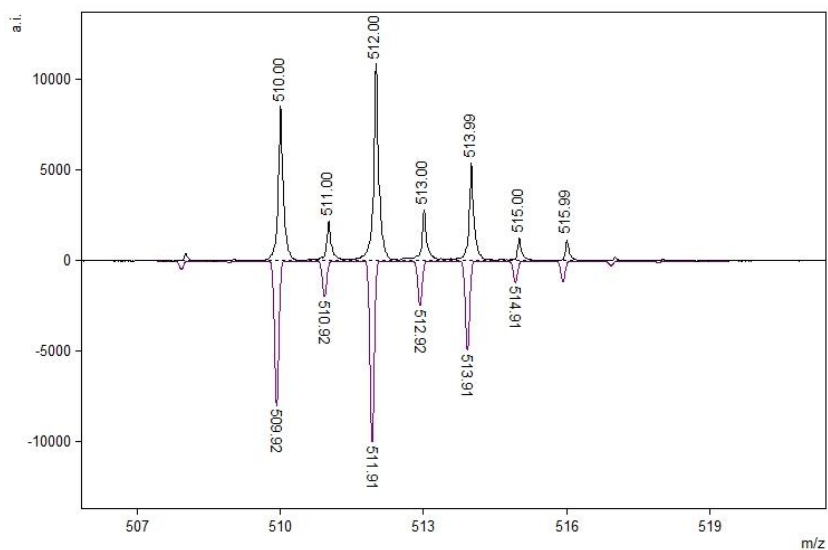


Figure 2.8: Magnification of the experimental (top) and modelled (bottom) MALDI-TOF mass spectrum of $[2.2-Cl]^+$

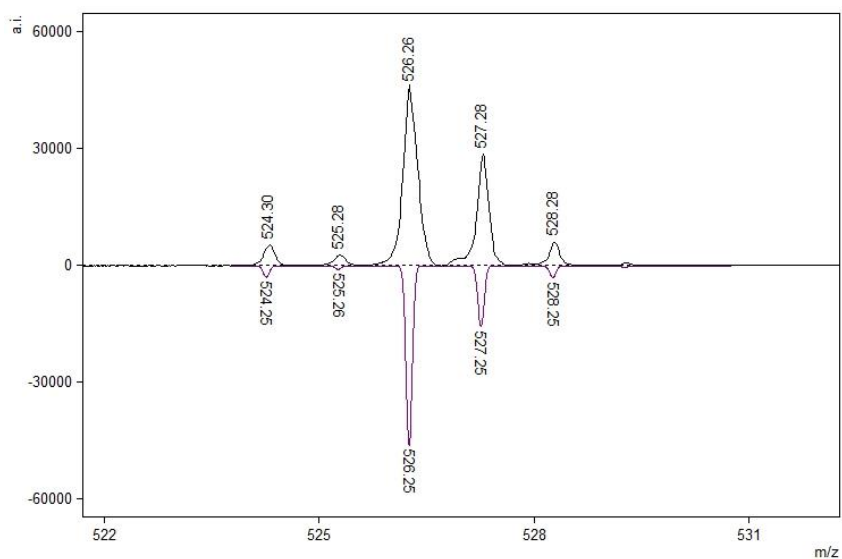


Figure 2.9: Magnification of the experimental (top) and modelled (bottom) MALDI-TOF mass spectrum of $[2.3-Cl]^+$

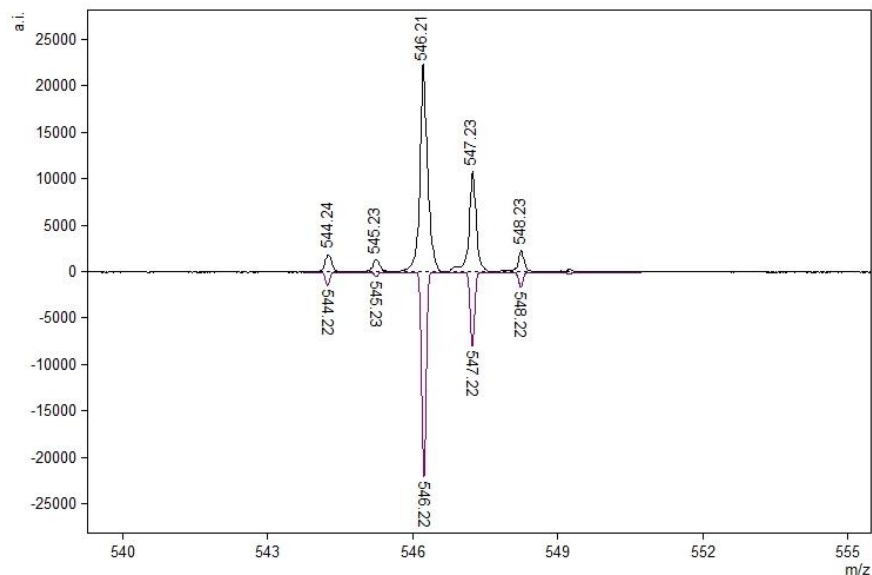


Figure 2.10: Magnification of the experimental (top) and modelled (bottom) MALDI-TOF mass spectrum of $[2.4-Cl]^+$

2.4.4 UV-visible Spectroscopy

The electronic spectra of compounds **2.1-2.4** show intense bands in both the UV and visible regions. As seen in Figure 2.11, the maximum is visible at ~ 210 nm. This can be attributed to the intense $\pi \rightarrow \pi^*$ transitions from the phenolate rings, which is common for complexes of amine-(bis)phenolate ligands, such as chromium.^{38,47,48} This strong absorbance is also visible for the non-metal containing precursors as well.⁴⁹

At 290 nm, the absorption observed is assigned to the ligand to metal ($M \leftarrow L$) charge transfer transitions. These transitions arise from the out of plane p_x orbital (the highest occupied molecular orbital, HOMO) of the phenolate oxygen to the partially filled dx^2-y^2/dz^2 orbitals of the iron(III). In the visible region, the band at 467 nm, arises from $M \leftarrow L$ charge transfer transitions from the in plane p_x orbital of the phenolate oxygen to the half filled d_{π^*} orbital of iron(III).^{13,20} The spectrum is consistent with other

similar iron amine-bis(phenolate) complexes reported, however, phenolate groups/pendant arms vary.^{10,13,15}

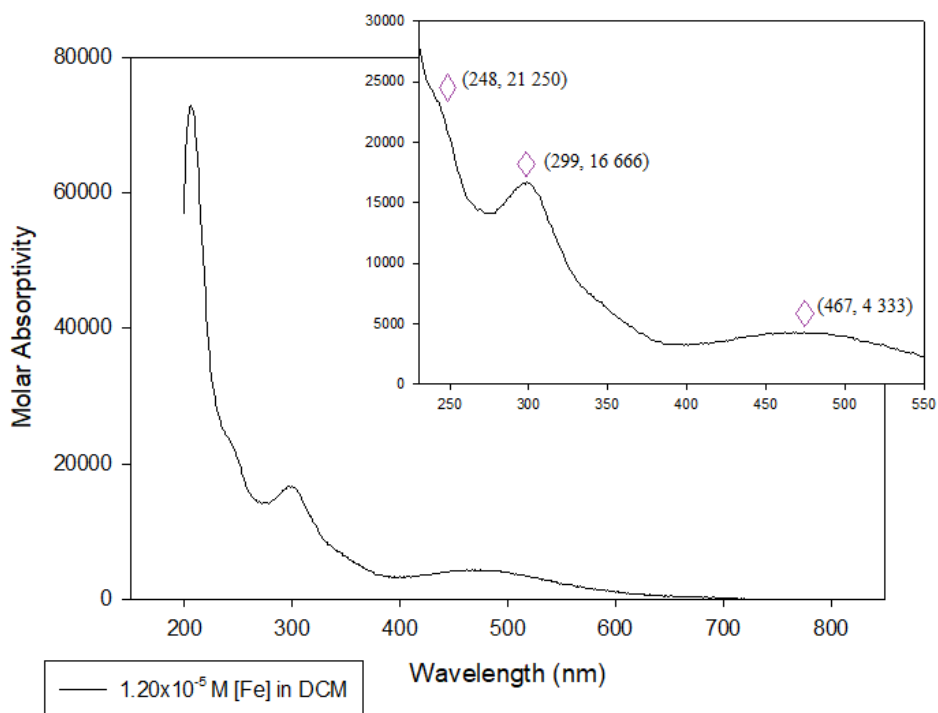


Figure 2.11: UV-vis absorption spectrum of **2.2** in CH₂Cl₂. Expansion of the mid UV to visible region shows peak wavelengths and molar extinction coefficients

2.5 Conclusions

Although complexes **2.1** and **2.2** have been previously synthesized, they have not yet been used for the work outlined in Chapters 3 and 4, while complexes **2.3** and **2.4** have been synthesized for the first time. Preparation of complexes **2.1-2.4** will allow for a thorough preliminary screening of these iron-amine(bis) phenolate complexes for the coupling of CO₂ with various epoxides, as well as the copolymerization of CO₂ and CHO. By varying the phenolate substituents, it is possible to determine whether the effect of having electron withdrawing groups will produce more effective catalysts, by

creating a more Lewis acidic metal centre. As well, varying the pendant arm will assess whether a bulkier substituent will hinder the polymerization process.

2.6 Experimental

2.6.1 General method and procedures

All manipulations/handling of ligands and iron complexes were performed on the benchtop, in the presence of air, unless otherwise stated. All reagents and solvents were purchased from either Fisher, Sigma Aldrich, or Alfa Aesar and were used without any further purification. Anhydrous FeCl_3 (97%) was purchased from Aldrich and used to synthesize complexes **2.1-2.4**.

2.6.2 Instrumentation

^1H and $^{13}\text{C}\{^1\text{H}\}$ NMR spectra were recorded on a Bruker AVANCE III instrument. MALDI-TOF MS spectra were obtained using an Applied Biosystems 4800 MALDI TOF/TOF analyzer equipped with a reflectron and a high-performance nitrogen laser operating at 355 nm. The complexes and matrix (anthracene) were dissolved separately in dichloromethane into solutions of 10 mg/mL before being combined in a 1:1 ratio and spotted onto the MALDI plate and left for several minutes as the solvent evaporated. UV-vis spectroscopy was carried out using a dual-beam Thermo ScientificTM EvolutionTM 300 UV-Vis spectrophotometer. Solutions of the complexes were made up in dichloromethane at a concentration of approximately 10^{-5} mol/L. Elemental analysis was carried out at Guelph Chemical Laboratories, Guelph, Ontario.

2.6.3 Synthesis

$\text{H}_2[\text{O}_2\text{NN}']^{\text{Cl}^{\text{ClINMe}_2}}(\text{H}_2\text{L1})$

Prepared by a previously reported method,³¹ letting it reflux for 48 h as opposed to 12 h. Yield (2.83 g, 31.1%) Spectroscopic data as previously reported.³¹

$\text{H}_2[\text{O}_2\text{NN}']^{\text{Cl}^{\text{ClPy}}}(\text{H}_2\text{L2})$

Prepared by a previously reported method giving identical spectroscopic analysis.¹³

$\text{H}_2[\text{O}_2\text{NN}']^{\text{tBuOMeNMe}_2}(\text{H}_2\text{L3})$

Prepared by a previously reported method giving identical spectroscopic data.⁵⁰
Yield (18.65 g, 64.2%)

$\text{H}_2[\text{O}_2\text{NN}']^{\text{tBuOMePy}}(\text{H}_2\text{L4})$

Prepared by a previously reported method giving identical spectroscopic data.⁵⁰
Yield (8.87 g, 73.5%)

(2.1) $\text{FeCl}[\text{L1}]$

FeClI was Prepared by a previously reported method, with modifications made to reaction time and solvent choice.¹³ A solution of anhydrous FeCl_3 (0.640 g, 3.95 mmol) in methanol was added to a stirring slurry of, recrystallized, $\text{H}_2\text{L1}$ (1.73 g, 3.95 mmol) in methanol (30 mL) resulting in an immediate vibrant purple solution. After 5 minutes, triethylamine (0.80 g, 7.91 mmol) was added to the mixture. This solution was left to stir at room temperature for 1.5 h. After stirring, the methanol was removed in vacuo leaving a thick purple oil product. The product was then dissolved into minimal amounts of acetone and gravity filtered through fluted filter paper three times. The acetone was then removed and the crystalline purple product was left to dry on the

Schlenk line under vacuum before being collected. Yield 1.88 g, 86.5%. Analysis calculated for $C_{18}H_{18}Cl_5FeN_2O_2$: C, 40.99; H, 3.44; N, 5.31. Found: C, 41.24; H, 3.18; N, 5.55. MALDI-TOF m/z (ion): 524.9 ($[M]^{+}$), 490.9 ($[M-Cl]^{+}$), 436.0 ($[H_2L1]^{+}$ and). UV-vis λ_{max} , nm (ϵ): 484 (2741), 290 (9257), 227 (13136)

(2.2) FeCl[L2]

Prepared by a previously reported method, with modifications made to reaction time and solvent choice.¹³ A solution of anhydrous $FeCl_3$ (1.30 g, 8.01 mmol) in methanol was added to a stirring slurry of, recrystallized, H_2L2 (3.66 g, 8.00 mmol) in methanol (30 mL) resulting in an immediate vibrant purple solution. After 5 minutes, triethylamine (1.62 g, 16.01 mmol) was added to the mixture creating a thicker solution upon addition. This solution was left to stir at room temperature for 1.5 h. After stirring, the methanol was removed in vacuo leaving a thick oil purple product. The product was then dissolved into minimal amounts of acetone and gravity filtered through fluted filter paper three times. The acetone was then removed, and the crystalline purple product was left to dry on the Schlenk line under vacuum before being collected. Yield 4.19 g, 95.9%. Analysis calculated for $C_{20}H_{14}Cl_5FeN_2O_2$: C, 43.88; H, 2.58; N, 5.12. Found: C, 44.15; H, 2.70; N, 5.31. MALDI-TOF m/z (ion): 544.8 ($[M]^{+}$), 509.9 ($[M-Cl]^{+}$), 456.0 ($[M-FeCl]^{+}$). UV-vis λ_{max} , nm (ϵ): 467 (4333), 299 (16666), 206 (72900)

(2.3) FeCl[L3]

In the glovebox, NaH (0.490 g, 20.4 mmol) and H_2L3 (2.41 g, 5.09 mmol) were weighed into a Schlenk flask. To this flask was added ~40 mL of dry THF via cannula on a Schlenk line. After stirring for 30 minutes, the ligand solution was transferred via filter cannula to another Schlenk flask. To a Schlenk flask containing $FeCl_3$ (0.83g, 5.11

mmol) the ligand solution was slowly transferred via cannula producing an instantaneous deep purple solution at room temperature. Once transferred completely, and rinsed with dry THF, the solution was left to stir for 1.5 h. The vibrant purple solution was then filtered through celite into a round bottom flask, the solution was then removed in vacuo leaving a thick oil purple product. The product was then extracted into minimal amounts of toluene and gravity filtered through fluted filter paper three times. The toluene was then removed under vacuum affording a fine powdered purple product that was left to dry on the Schlenk line under vacuum before being collected. Yield 4.19 g, 95.9%. Analysis calculated for $C_{28}H_{42}ClFeN_2O_4$: C, 59.85; H, 7.53; N, 4.99. Found: C, 59.51; H, 7.50; N, 5.27. MALDI-TOF m/z (ion): 561.2 ($[M]^+$), 526.3 ($[M-Cl]^+$), 472.3 ($[M-FeCl]^+$). UV-vis λ_{max} , nm (ϵ): 512 (3751), 292 (14470), 227 (13248).

(2.4) $FeCl[L4]$

A solution of anhydrous $FeCl_3$ (0.74 g, 4.56 mmol) in methanol was added to a stirring slurry of, recrystallized, H_2L4 (2.24 g, 4.55 mmol) in methanol (30 mL) resulting in an immediate vibrant purple solution. After 5 min, triethylamine (0.92 g, 9.03 mmol) was added to the mixture creating a thicker solution upon addition. This solution was left to stir at room temperature for 1.5 h. After stirring, the methanol was removed using the rotovap leaving a thick purple product. The product was then extracted into minimal amounts of acetone and gravity filtered through fluted filter paper twice. The acetone was then removed and the fine powdered purple product was left to dry on the Schlenk line under vacuum before being collected. Yield 2.62 g, 93.9%. Analysis calculated for $C_{30}H_{38}ClFeN_2O_4$: C, 61.92; H, 6.74; N, 4.81. Found: C, 61.64; H, 6.33; N, 4.44.

MALDI-TOF m/z (ion): 581.2 ($[M]^+$), 546.2 ($[M-Cl]^+$), 492.3 ($[M-FeCl]^+$). UV-vis λ_{\max} ,
nm (ϵ): 520 (3595), 293 (13152), 275(13209), 263 (13295), 230 (43395).

2.7 References

1. Wichmann, O.; Sillanpää, R.; Lehtonen, A., *Coord. Chem. Rev.* **2012**, *256*, 371-392.
2. Allan, L. E. N.; MacDonald, J. P.; Nichol, G. S.; Shaver, M. P., *Macromolecules* **2014**, *47*, 1249-1257.
3. Coward, D. L.; Lake, B. R. M.; Shaver, M. P., *Organometallics* **2017**, *36*, 3322-3328.
4. Schroeder, H.; Buback, M.; Shaver, M. P., *Macromolecules* **2015**, *48*, 6114-6120.
5. Schroeder, H.; Lake, B. R. M.; Demeshko, S.; Shaver, M. P.; Buback, M., *Macromolecules* **2015**, *48*, 4329-4338.
6. Zhu, K.; Shaver, M. P.; Thomas, S. P., *Eur. J. Org. Chem.* **2015**, *2015*, 2119-2123.
7. Zhu, K.; Shaver, M. P.; Thomas, S. P., *Chem. Asian J.* **2016**, *11*, 977-980.
8. Chowdhury, R. R.; Crane, A. K.; Fowler, C.; Kwong, P.; Kozak, C. M., *Chem. Commun.* **2008**, 94-96.
9. Hasan, K.; Fowler, C.; Kwong, P.; Crane, A. K.; Collins, J. L.; Kozak, C. M., *Dalton Trans.* **2008**, 2991-2998.
10. Hasan, K.; Dawe, L. N.; Kozak, C. M., *Eur. J. Inorg. Chem.* **2011**, *2011*, 4610-4621.
11. Kozak, C.; Qian, X., *Synlett.* **2011**, *2011*, 852-856.
12. Qian, X.; Dawe, L. N.; Kozak, C. M., *Dalton Trans.* **2011**, *40*, 933-943.
13. Reckling, A. M.; Martin, D.; Dawe, L. N.; Decken, A.; Kozak, C. M., *J. Organomet. Chem.* **2011**, *696*, 787-794.
14. Hasan, K.; Brown, N.; Kozak, C. M., *Green Chem.* **2011**, *13*, 1230.
15. Allan, L. E.; MacDonald, J. P.; Reckling, A. M.; Kozak, C. M.; Shaver, M. P., *Macromol. Rapid Commun.* **2012**, *33*, 414-418.
16. Chard, E. F.; Dawe, L. N.; Kozak, C. M., *J. Organomet. Chem.* **2013**, *737*, 32-39.

17. Taherimehr, M.; Serta, J.; Kleij, A. W.; Whiteoak, C. J.; Pescarmona, P. P., *ChemSusChem*. **2015**, *8*, 1034-1042.
18. Sarazin, Y.; Howard, R. H.; Hughes, D. L.; Humphrey, S. M.; Bochmann, M., *Dalton Trans.* **2006**, 340-350.
19. Toupance, T.; Dubberley, S. R.; Rees, N. H.; Tyrrell, B. R.; Mountford, P., *Organometallics* **2002**, *21*, 1367-1382.
20. Alhashmialameer, D.; Collins, J.; Hattenhauer, K.; Kerton, F. M., *Catal. Sci. Technol.* **2016**, *6*, 5364-5373.
21. Vummaleti, S. V. C.; Buonerba, A.; De Nisi, A.; Monari, M.; Della Monica, F.; Nisi, A. D.; Milione, S.; Grassi, A.; Cavallo, L.; Capacchione, C., *Adv. Synth. Catal.* **2016**, *358*, 3231-3243.
22. Allan, L. E. N.; MacDonald, J. P.; Nichol, G. S.; Shaver, M. P., *Macromolecules* **2014**, *47*, 1249-1257.
23. Schroeder, H.; Lake, B. R. M.; Demeshko, S.; Shaver, M. P.; Buback, M., *Macromolecules* **2015**, *48*, 4329-4338.
24. Mondal, D.; Kundu, S.; Majee, M. C.; Rana, A.; Endo, A.; Chaudhury, M., *Inorg. Chem.* **2017**, *56*, 9448-9460.
25. Daneshmand, P.; Schaper, F., *Dalton Trans.* **2015**, *44*, 20449-20458.
26. Phuphuak, Y.; Bonnet, F.; Vendier, L.; Lorber, C.; Zinck, P., *Dalton Trans.* **2016**, *45*, 12069-12077.
27. Reiter, M.; Altenbuchner, P. T.; Kissling, S.; Herdtweck, E.; Rieger, B., *Eur. J. Inorg. Chem.* **2015**, *2015*, 1766-1774.
28. Tang, Z.; Gibson, V. C., *Eur. Polym. J.* **2006**, *43*, 150-155.
29. Gendler, S.; Groysman, S.; Goldschmidt, Z.; Shuster, M.; Kol, M., *J. Polym. Sci., Part A: Polym. Chem.* **2006**, *44*, 1136-1146.
30. Gendler, S.; Segal, S.; Goldberg, I.; Goldschmidt, Z.; Kol, M., *Inorg. Chem.* **2006**, *45*, 4783-4790.
31. Groysman, S.; Tshuva, E. Y.; Goldberg, I.; Kol, M.; Goldschmidt, Z.; Shuster, M., *Organometallics* **2004**, *23*, 5291-5299.
32. Groysman, S.; Goldberg, I.; Kol, M.; Genizi, E.; Goldschmidt, Z., *Organometallics* **2004**, *23*, 1880-1890.

33. Safaei, E.; Heidari, S.; Wojtczak, A.; Cotic, P.; Kozakiewicz, A., *J. Mol. Struct.* **2016**, *1106*, 30-36.
34. Heidari, S.; Safaei, E.; Wojtczak, A.; Cotic, P.; Kozakiewicz, A., *Polyhedron* **2013**, *55*, 109-116.
35. Lei, X.; Chelamalla, N., *Polyhedron* **2013**, *49*, 244-251.
36. Wang, L.; Cao, Z.; Sun, J.; Zhang, Y.; Zhang, J. (2017) *CN106633019A* Application of cobalt complex in active polymerization and copolymerization of lactone and acrylate.
37. Zhang, J.; Wang, B.; Wang, L.; Sun, J.; Zhang, Y.; Cao, Z.; Wu, Z., *Appl. Organomet. Chem.* **2018**, *32* (2), e4077
38. Devaine-Pressing, K.; Dawe, L. N.; Kozak, C. M., *Polym. Chem.* **2015**, *6*, 6305-6315.
39. Alcazar-Roman, L. M.; O'Keefe, B. J.; Hillmyer, M. A.; Tolman, W. B., *Dalton Trans.* **2003**, 3082-3087.
40. Heidari, S.; Safaei, E.; Wojtczak, A.; Cotic, P., *Inorg. Chim. Acta.* **2013**, *405*, 134-139.
41. Tang, L.-Z.; Lin, C.-N.; Zhan, S.-Z., *Polyhedron* **2016**, *110*, 247-253.
42. Devaine-Pressing, K.; Lehr, J. H.; Pratt, M. E.; Dawe, L. N.; Sarjeant, A. A.; Kozak, C. M., *Dalton Trans.* **2015**, *44*, 12365-12375.
43. Cao, J.-P.; Zhou, L.-L.; Fu, L.-Z.; Zhao, J.-X.; Lu, H.-X.; Zhan, S.-Z., *Catal. Commun.* **2014**, *57*, 1-4.
44. Michel, F.; Thomas, F.; Hamman, S.; Saint-Aman, E.; Bucher, C.; Pierre, J.-L., *Chem. Eur. J.* **2004**, *10*, 4115-4125.
45. Philibert, A.; Thomas, F.; Philouze, C.; Hamman, S.; Saint-Aman, E.; Pierre, J.-L., *Chem. Eur. J.* **2003**, *9*, 3803-3812.
46. Bailey, G. A.; Fogg, D. E., *ACS Catal.* **2016**, *6*, 4962-4971.
47. Chen, H.; Dawe, L. N.; Kozak, C. M., *Catal. Sci. Technol.* **2014**, *4*, 1547-1555.
48. Dean, R. K.; Dawe, L. N.; Kozak, C. M., *Inorg. Chem.* **2012**, *51*, 9095-9103.
49. Dean, R. K.; Granville, S. L.; Dawe, L. N.; Decken, A.; Hattenhauer, K.; Kozak, C. M., *Dalton Trans.* **2010**, *39*, 548-559.

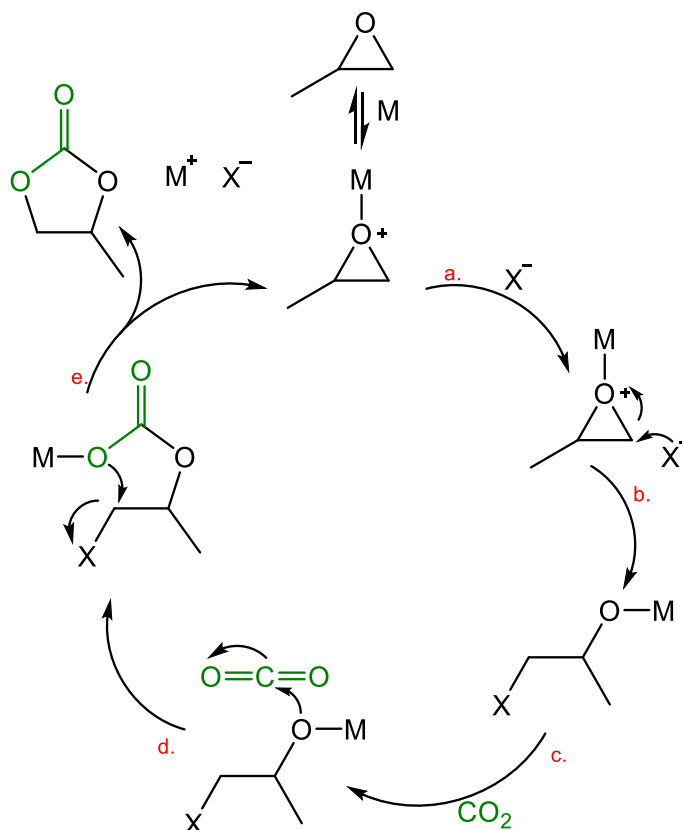
50. Devaine-Pressing, K.; Lehr, J. H.; Pratt, M. E.; Dawe, L. N.; Sarjeant, A. A.; Kozak, C. M., *Dalton Trans.* **2015**, *44*, 12365-13375.

Chapter 3: Iron amino-bis(phenolate) Complexes for the Coupling of CO₂ with Propylene Oxide

3.1 Introduction

As outlined in Chapter 1, finding efficient methods to utilize CO₂ can be a challenge. However, its coupling with epoxides has shown to be a promising reaction and way to develop polymeric materials.¹⁻⁸ Not only is this process important for activating thermodynamically stable CO₂, but using CO₂ as a C1 feedstock has several advantages as well; it is abundant, inexpensive, and non-toxic.⁹⁻¹² With respect to epoxide selection, propylene oxide is common for many catalytic systems.^{9-11,13-15} Propylene oxide tends to favor formation of cyclic product (vs. polymeric), and these cyclic carbonates have been found useful in several applications to date, including non-toxic high boiling point solvents, degreasers, and reactive intermediates for ring opening polymerizations as well fine chemical production.^{10,16}

As demonstrated by several examples of iron-catalyzed reactions of CO₂ with propylene oxide in Section 1.4, exclusive selectivity for the cyclic product was observed with no evidence of polymer formation. Williams achieved a 91% conversion (TOF 4 h⁻¹) after 48 h with a 0.5 mol% catalyst loading.² Dropping the catalyst loading to 0.025 mol%, Kerton achieved near quantitative conversion after 22 h (TOF 173 h⁻¹).¹ Capacchione and coworkers used 0.01 mol% of catalyst, achieving a 52% conversion to cyclic product in only 1 h demonstrating the highest TOF reported to date, 5 200 h⁻¹.¹⁷



Scheme 3.1: A simplified mechanistic cycle for the formation of propylene carbonate

Scheme 3.1 demonstrates a simplified mechanism for the formation of cyclic propylene carbonate. Propylene oxide can coordinate to a sufficiently Lewis acidic metal centre, represented by 'M', before a nucleophile, 'X⁻', can attack to ring open the epoxide as shown in step b. This nucleophile may have been previously coordinated to the metal as part of the catalyst or introduced into the system as the anion of the cocatalyst. In step c, carbon dioxide inserts into the metal-alkoxide bond, followed by ring closing and ejection of the nucleophile, X⁻ (step d). The nucleophile is released as a free anion, or to potentially re-coordinate to the metal centre. Where this is a base catalyzed ring opening of an epoxide, nucleophilic attack is expected to occur at the least substituted carbon via an S_N2 reaction. Therefore, the nucleophile, X⁻, as shown in step

b, will always attack at the methylene carbon for these reactions as opposed to the methine.

In this chapter, the initial goal was to examine how varying the Lewis acidity at the Fe(III) centre of the catalyst influences CO₂/epoxide coupling or copolymerization. This was approached by using chlorine as electron withdrawing substituents on the phenolate rings. For comparison, electron donating groups were used in two derivatives. In these, methoxy and *t*-butyl groups were used ortho to the phenolic -OH, Figure 3.1. A coordinating pendant arm was chosen to achieve 5-coordinate trigonal bipyramidal iron(III) complexes in this work; similar complexes have already been used for various other reactions within the group.¹⁸⁻²³ Nitrogen donors (amino ethyl and pyridyl groups) were found to be more effective at CO₂/epoxide copolymerization than O-donor groups²⁴ hence the nitrogen donors were used in this project.

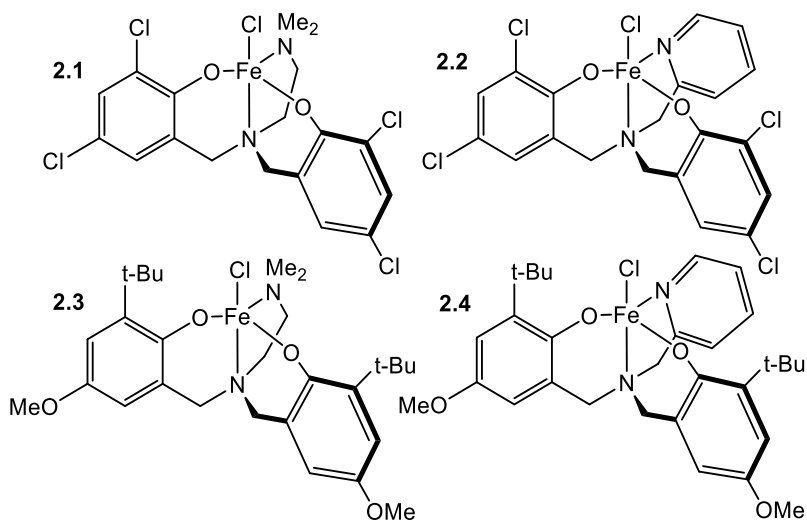


Figure 3.1: Iron amino-bis(phenolate) complexes **2.1-2.4** used in this study for the coupling of PO with CO₂

3.2 Results and Discussion

3.2.1 Catalyst Screening and Parameter Optimization

The coupling of PO and CO₂ was initially investigated using complexes **2.1** – **2.4**. Parameters were chosen based on recent literature to gain comparative results of similar complexes.¹ The initial conditions used were a catalyst loading of 0.025 mol%, 0.1 mol% cocatalyst, for 22 h at 100 °C and 20 bar CO₂ pressure, as summarized in Table 3.1. PPnCl was chosen initially as the cocatalyst as it is common in the literature, and it is speculated that the bulky cation exhibits low ion pairing to the chlorine atom making it a better nucleophile for initiation processes.^{1,3,17,25,26} Complexes **2.1**, **2.2**, and **2.4** demonstrated very similar activity, with complex **2.3** demonstrating a slight decrease in activity but still achieving a conversion of 79%. Complexes **2.2**, **2.3**, and **2.4** were run in duplicate to ensure reproducibility, as well as in different pressure vessels; no significant changes were seen. Using a different pressure vessel can change the surface area of which the reaction takes place, it could be speculated that a larger surface area will allow for increased CO₂ incorporation into the product, however, results remained consistent.

Table 3.1: Catalyst screening for the formation of propylene carbonate

Catalyst	Conv. ^a (%)	TON ^b	TOF ^c (h ⁻¹)
2.1	92	3 698	168
2.2	98 – 99	3 968	180
2.3	77-79	3 177	144
2.4	92 - 93	3 649	168

Reaction conditions unless otherwise stated: PO (5.0 × 10⁻² mol), catalyst (1.73 × 10⁻⁵ mol, 0.025 mol%), PPnCl (5.2 × 10⁻⁵ mol, 0.1 mol%), 100 °C, 22 h, 20 bar CO₂. ^aDetermined by ¹H NMR spectroscopy. ^bOverall turnover number (mol_{converted epoxide}/mol_{catalyst}). ^cOverall turnover frequency (TON/reaction time).

There was no evidence for polypropylene carbonate formation by ^1H NMR spectroscopy. Therefore these catalysts are selective for cyclic propylene carbonate under the given conditions. In Figure 3.2, it is evident that there is negligible propylene oxide remaining in the product. The complexes having dichloro-substituted phenolate rings were expected to be the most active as the iron centre would be more Lewis acidic than the methoxy/*t*-Bu substituted analogues; increasing the Lewis acidity makes the iron centre more electropositive and susceptible to nucleophilic attack. With the exception of complex **2.3**, it appears that the substituents on the phenolate rings did not play a significant role in the coupling process. As complex **2.2** demonstrated the overall highest conversion (as well as TON/TOF) it was utilized to determine optimum reaction conditions.

temperature allowed for 76% conversion after 4 h (entry 10). A further decrease in reaction time to 2 h at 100 °C and 20 bar CO₂, resulted in only 62% conversion but also the highest TOF achieved yet, 1 252 h⁻¹ (entry 11). The catalyst loading was decreased to 0.0125 mol% and after 4 h at the same temperature and pressure, a 47% conversion was achieved (entry 12), which could be increased to 91% if the reaction is left for 22 h.

Table 3.2: Optimization of parameters for cyclic carbonate formation

Entry	[Fe]:[PO]: [PPNCl]	Time (h)	T (°C)	Pressure (bar)	Conv. ^a (%)	TON ^b	TOF ^c (h ⁻¹)
1	1:4000:0	22	100	20	12	482	22
2	0:4000:4	22	100	20	26	261	12
3	1:4000:4	22	100	20	99	3 968	180
4	1:4000:4	22	80	20	98	3 921	178
5	1:4000:4	22	60	20	37	1 489	68
6	1:4000:4	22	25	20	<1	n/a	n/a
7 ^d	1:500:4	22	25	20	8	40	1.8
8	1:4000:4	6	100	20	91	3 673	612
9	1:4000:4	4	100	20	91	3 665	916
10	1:4000:4	4	100	10	76	3 042	761
11	1:4000:4	2	100	20	62	2 504	1 252
12	1:8000:4	4	100	20	47	3 790	948
13	1:8000:4	22	100	20	91	7 370	335

Reaction conditions unless otherwise stated: PO (5.0×10^{-2} mol), catalyst **2.2** (1.73×10^{-5} mol, 0.025 mol%), PPNCl (5.2×10^{-5} mol, 0.1 mol%). ^aDetermined by ¹H NMR spectroscopy. ^bOverall turnover number (mol_{converted epoxide}/mol_{catalyst}). ^cOverall turnover frequency (TON/reaction time). ^dCatalyst loading increased to 0.20 mol%

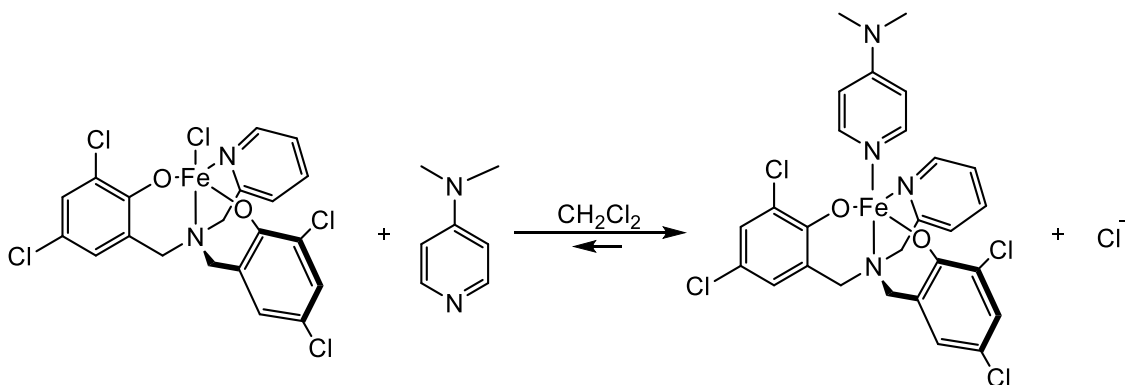
Other cocatalysts were investigated which showed PPNCl was superior. The literature has shown tetrabutylammonium bromide, TBAB, to be a slightly superior as a cocatalyst when compared to PPNCl.^{1,17} However the results shown in Table 3.3 demonstrate PPNCl having the better results, entry 2, with a 74% conversion after only 2 h when compared to a 64% conversion using TBAB as the cocatalyst.

Table 3.3: Cocatalyst effects on the formation of propylene carbonate

Entry	Cocatalyst	[Fe]:[PO]: [Cocatalyst]	Conv. (%)	TON	TOF (h ⁻¹)
1	PPNCl	1:4000:4	91	3 665	916
2	PPNCl	1:4000:2	74	3 016	751
3	DMAP	1:4000:2	26	1 043	261
4	TBAB	1:4000:2	64	2 565	641

Reaction conditions unless otherwise stated: PO (5.0×10^{-2} mol), catalyst **2.2** (1.73×10^{-5} mol, 0.025 mol%), 100 °C, 4 h, 20 bar CO₂. ^a Determined by ¹H NMR spectroscopy. ^b Overall turnover number (mol_{converted epoxide}/mol_{catalyst}). ^c Overall turnover frequency (TON/reaction time).

4-Dimethylaminopyridine, DMAP, is suspected to coordinate to the metal centre which would decrease the activity of the catalytic system by hindering coordination of the epoxide. While this is true for all nucleophiles present, DMAP appears to have the strongest binding affinity to the metal centre when compared to chloride and bromide ions, Scheme 3.2, and within this thesis, mass spectrometric data supports this.

**Scheme 3.2:** Coordination of DMAP to **2.2**

MALDI-TOF MS was also used to show that DMAP will bind to iron replacing the chloride. Figure 3.3 compares spectra collected from complex **2.2** (top), **2.2** with one equivalent of DMAP (middle), and **2.2** with two equivalents of DMAP (bottom). A 5 coordinate iron species with DMAP coordinated is visible at m/z 634 when there is one equivalent of DMAP present with respect to iron; the isotopic modelling is shown in

Figure 3.4. This peak almost doubles in intensity when there are two equivalents of DMAP added. The peaks at m/z 456 correspond to the ligand, H_2L_2 , which also decreases in intensity with the addition of DMAP. $[2.2-Cl]^+$ is represented by m/z 511, while the peak at m/z 615 is not easily identifiable, however, it could correspond to $[2.2-Cl]^+$ with a fragmented pyridyl peak; this peak is not seen in spectra for the other complexes.

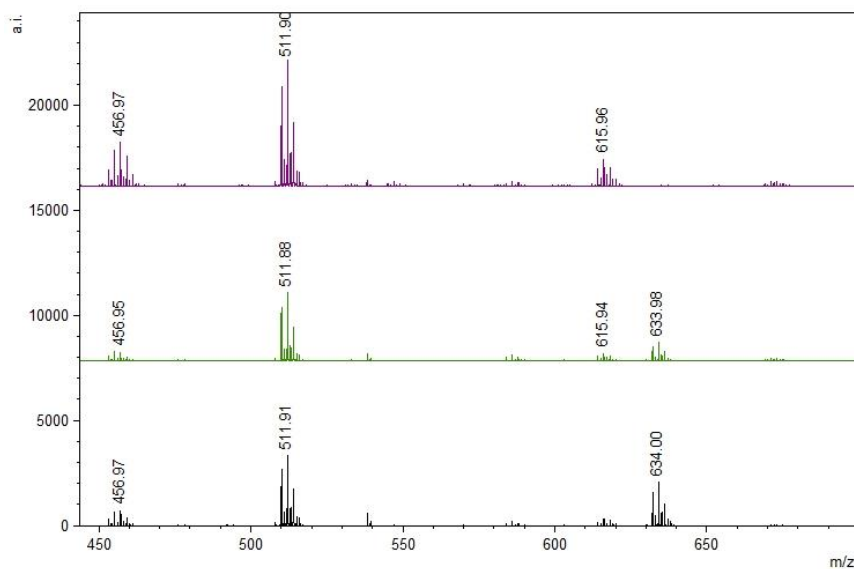


Figure 3.3: MALDI-TOF mass spectra of **2.2** (top) with one equivalent of DMAP (middle) and two equivalents of DMAP (bottom)

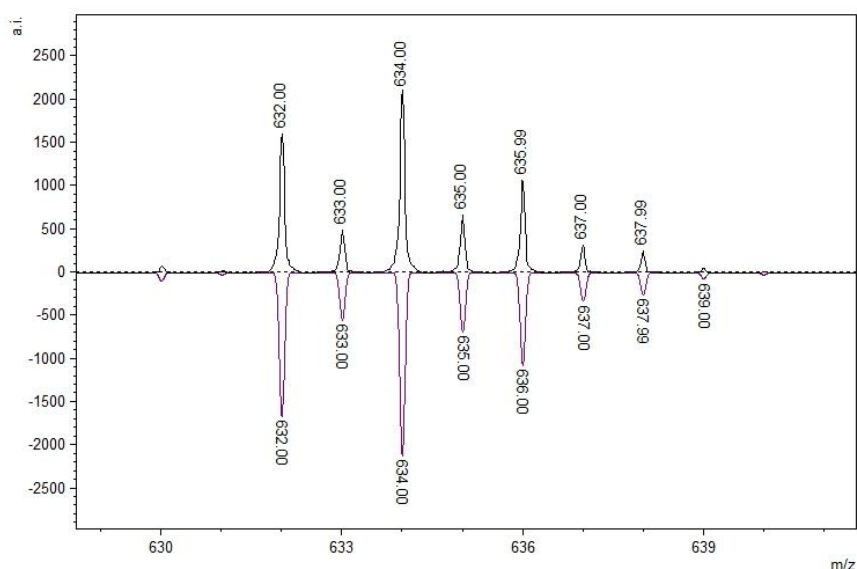


Figure 3.4: MALDI TOF mass spectrum of $[2.2\text{-CH-DMAP}]^+$. Experimental shown on top, isotopic modelling on bottom

Reaction rate data were obtained using in situ FTIR spectroscopy. The pressure vessel was equipped with an ATR sensor connected to a Mettler Toledo ReactIR 15 unit through a DS silver-halide fibre optic conduit. The ν_{CO} absorbance at 1810 cm^{-1} was measured over time (Figure 3.5) using three cocatalysts and varying the loading of PPNCl. For the first 6 minutes, the growth of the ν_{CO} peak appears to increase at similar rates, as the temperature rises from room temperature to $100\text{ }^{\circ}\text{C}$, but when the reaction reaches $100\text{ }^{\circ}\text{C}$ (approximately 7 minutes in) faster reaction propagation is observed, with different rates for each set of cocatalyst conditions. When using TBAB, the sensor reaches signal saturation within 10 minutes with propylene carbonate production, demonstrating the steepest slope and fastest initial observed rate of reaction. When using DMAP as a cocatalyst, there is a steep increase in rate as well during those initial 10 minutes.

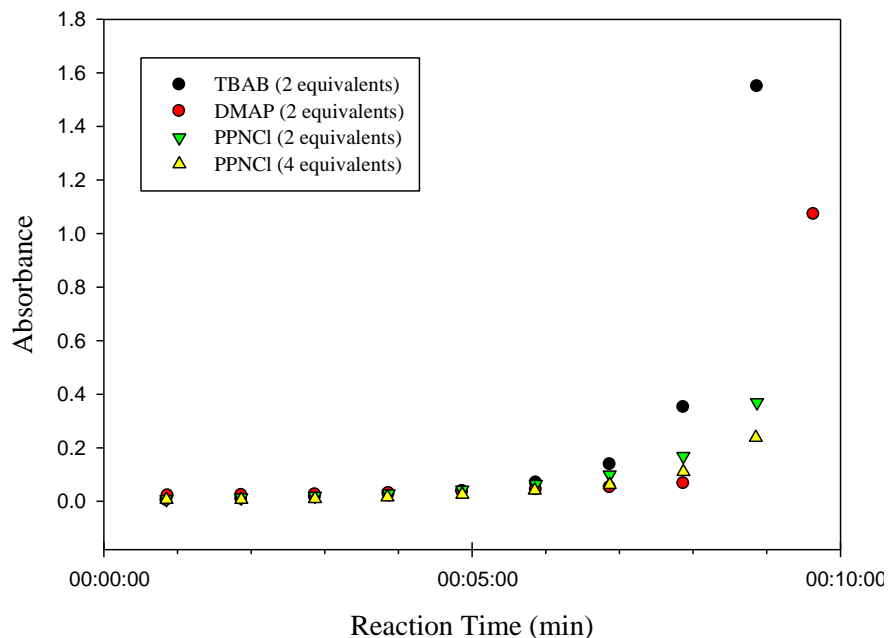


Figure 3.5: Effect of cocatalyst on absorbance vs. time for $\nu_{\text{CO}} = 1810 \text{ cm}^{-1}$ corresponding to cyclic propylene carbonate formation

By using in situ IR, it is possible to collect information about initial rates of reaction for each experiment run. Initially, reactions were started by heating the vessel to 100 °C and then pressurizing to 20 bar CO₂. There was concern that this could affect results, even slightly, as PO is quite volatile, having a boiling point of 34 °C. Therefore, the reactions were pressurized to 10 bar CO₂ before heating, then upon reaching the desired temperature, the pressure increased to approximately 20 bar (or the final pressure slightly adjusted to achieve the desired pressure). Reactions were not pressurized to 20 bar initially before being heated as the pressure would then rise to 28-30 bar CO₂ with the rise in temperature.

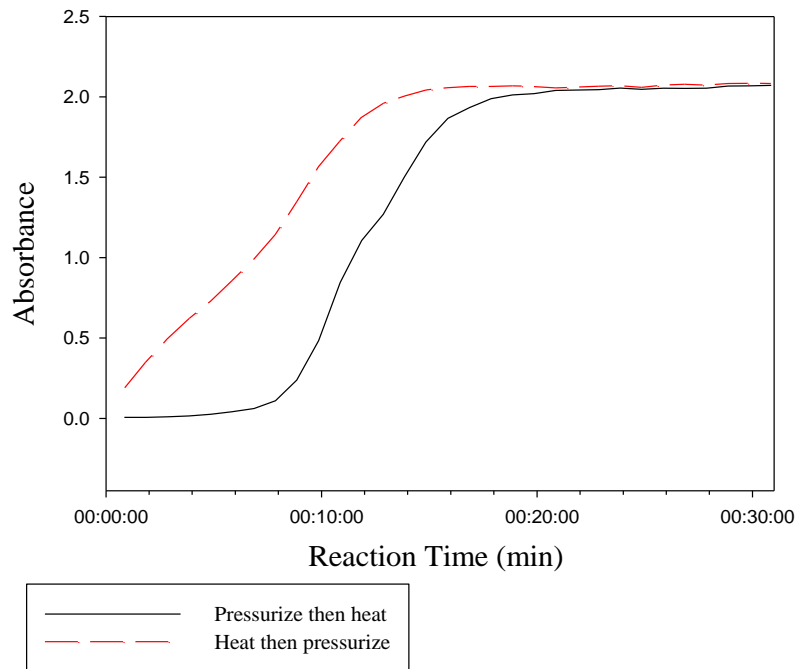


Figure 3.6: Initial rates of reaction comparing method of data collection

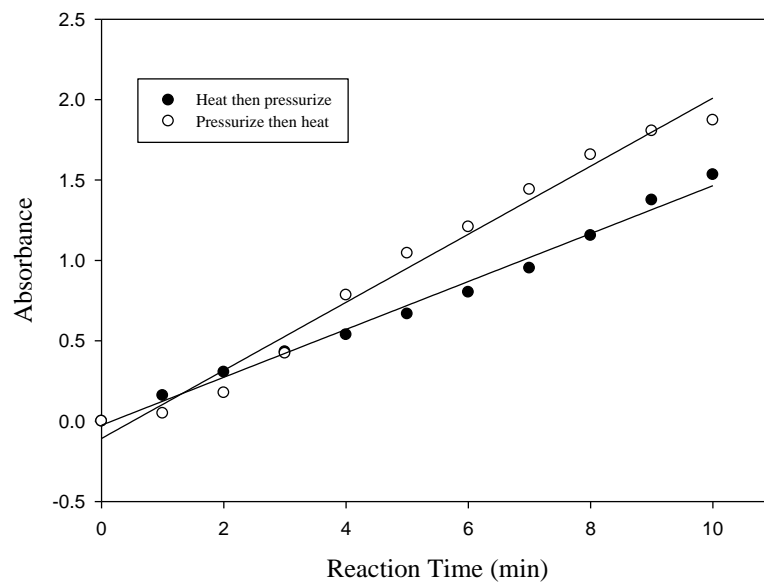


Figure 3.7: Normalized data demonstrating initial rates of reaction comparing methods of data collection

As can be seen from Figures 3.6 and 3.7, there is a difference in the most linear portion for each reaction. Figure 3.7 has been normalized demonstrating these linear regions. From this it becomes apparent that when the reaction is pressurized before it is heated, the initial observed rate of reaction is significantly faster than when the reaction is heated to the desired temperature before any pressure is applied (Table 3.4). It should be noted, however, that the CO₂ is cold when added, and therefore the temperature will be lowered upon addition of CO₂ and there will be a slight equilibration period.

Table 3.4: Observed reaction rates for different methods of achieving the desired temperature and pressure conditions

Data Collection Method	Observed Reaction Rate $r_{\text{obs}} (\times 10^{-2} \text{ min}^{-1})$	R²
Heat First	1.44 ± 0.05	0.990
Pressurize First	2.19 ± 0.10	0.983

As was also demonstrated in Table 3.2, temperature plays a large role in the overall conversion of propylene oxide, and it is evident from the initial rates of reaction that at temperatures below 80 °C, the reaction slows down significantly. At both 80 °C and 100 °C, very similar trends can be seen throughout the ten minutes of each reaction (Figure 3.8). Even when the reaction temperature is increased to 60 °C the rate of reaction is only increased a slight amount, but when going from 60 to 80 °C the rate is increased by a factor of 10. At room temperature, there is no evidence of propylene carbonate formation as no absorbance at 1810 cm⁻¹ is visible, this is confirmed by the overall conversion being less than 1% at that temperature.

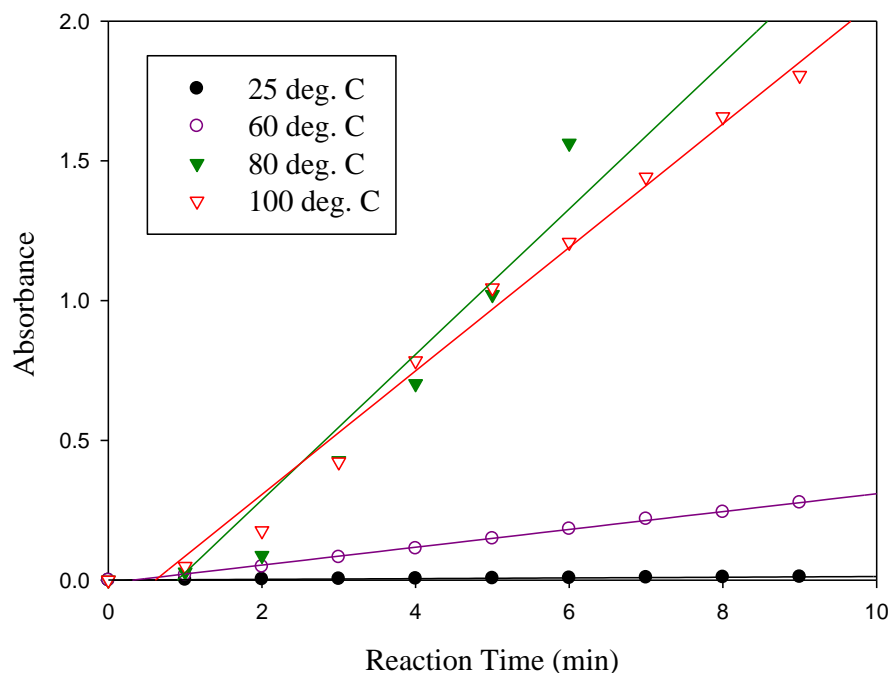


Figure 3.8: Initial rates of reaction for cyclic propylene carbonate formation at various temperatures

Table 3.5: Observed reaction rates for various temperatures

Temperature (°C)	Observed Reaction Rate $r_{\text{obs}} (\times 10^{-2} \text{ min}^{-1})$	R^2
25	2.46×10^{-4}	0.998
60	3.20×10^{-2}	0.997
80	2.60×10^{-1}	0.914
100	2.21×10^{-1}	0.986

3.2.2 Use of an Internal Standard

As PO is a volatile organic compound, having a boiling point of only 34 °C, it is possible to overestimate the overall conversion of product, due to starting material evaporating. This is attributed to the conversion being calculated by comparing the methyl protons on propylene oxide to those on propylene carbonate; if propylene oxide has evaporated the conversion will be increased artificially. The use of an internal

standard allows the results to be better quantified by $^1\text{H NMR}$ and ensures more accurate results.

Mesitylene was chosen as the internal standard for these reactions as it has been used previously in the literature,^{3,25} has a high boiling point (163 – 166 °C) which eliminates the concern of evaporation, and is chemically inert under these conditions. To ensure reactions are kept as similar as possible, mesitylene was added to the reaction mixture prior to being placed in the reaction vessel. An NMR spectrum using mesitylene is shown in Figure 3.9, the protons used for comparison and are found at approximately 1.3 ppm (propylene oxide), 1.5 ppm (propylene carbonate), and 2.3 ppm (mesitylene).

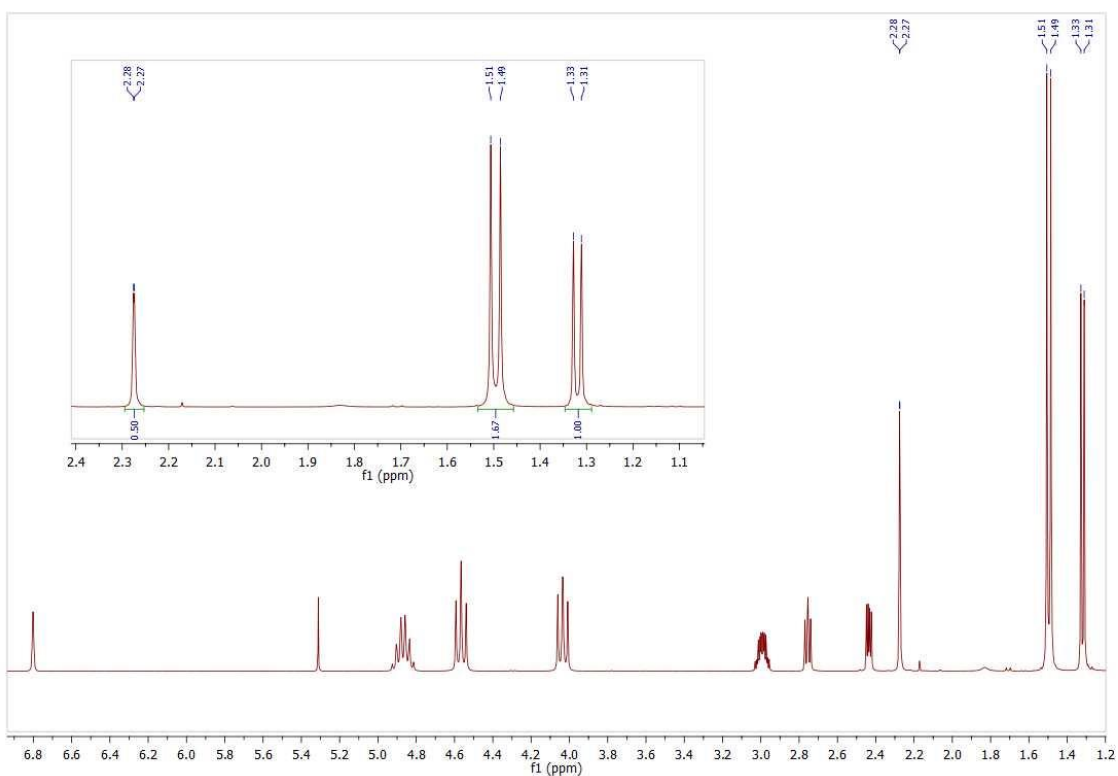


Figure 3.9: $^1\text{H NMR}$ spectrum of cyclic propylene carbonate using mesitylene as an internal standard. Insert showing the 3 peaks analyzed: PO at 1.3ppm, PC at 1.5ppm, and mesitylene at 2.8 ppm

Table 3.6: Various reactions of propylene carbonate formation, using mesitylene as an internal standard to determine yields

Entry	[Fe]:[PO]: [PPNCl]	Time (h)	T (°C)	Conv. ^a (%)	Yield ^b (%)
5	1:4000:4	22	60	37	41
7	1:500:4	22	25	8	5
8	1:4000:4	6	100	91	91
9	1:4000:4	4	100	91	89
11	1:4000:4	2	100	62	59
12	1:8000:4	4	100	47	43

Reaction conditions unless otherwise stated: PO (5.0×10^{-2} mol), catalyst **2.2** (1.73×10^{-5} mol, 0.025 mol%), PPNCl (5.2×10^{-5} mol, 0.1 mol%). P CO₂ 20 bar ^aDetermined by ¹H NMR spectroscopy. ^bSpectroscopic yield calculated by ¹H NMR using mesitylene

The reactions in which mesitylene was used are outlined in Table 3.6. Yields were found to be within $\pm 4\%$ of the conversion, both calculated by ¹H NMR, which is in agreement to what has been reported in recent literature.¹ Therefore, if the reaction is stopped and worked up efficiently there should be no concern surrounding the volatility of PO. Every reaction is cooled to room temperature (roughly 25 – 26 °C) before the CO₂ is vented slowly out of the vessel. Once the vessel has been opened to view/collect the product, a sample is taken immediately for NMR and sealed. Through these precautions, it is seen that the conversion is in very close agreement to spectroscopic yields, through use of mesitylene as an internal standard, without isolating product.

3.2.3 Temperature Dependence and Kinetics

The reaction activation energy was obtained by measuring the rate of increase of the ν_{CO} band at 1810 cm⁻¹ at temperatures between 40 and 60 °C using in situ FTIR spectroscopy (Figure 3.10 and Table 3.7). The reaction mixture used a 0.025 mol% loading for **2.2** and 0.1 mol% PPNCl cocatalyst under 20 bar CO₂ pressure. Upon achieving the desired temperatures, data was collected for 10 minutes, Figure 3.10. An Arrhenius plot was constructed using these data, Figure 3.11, giving an activation energy

of 49.6 kJ mol⁻¹. The only other activation energy reported for an iron complex was found to be 98.4 kJ mol⁻¹ under the same reaction conditions, however, TBAB was used as the cocatalyst.¹ The linearity at 60 °C is noticeably decreased compared to the other temperatures in Figure 3.10. This is due to a significant increase in the rate of propylenecarbonate formation, thus the sensor is beginning to become saturated and the absorbance will begin to plateau at this temperature.

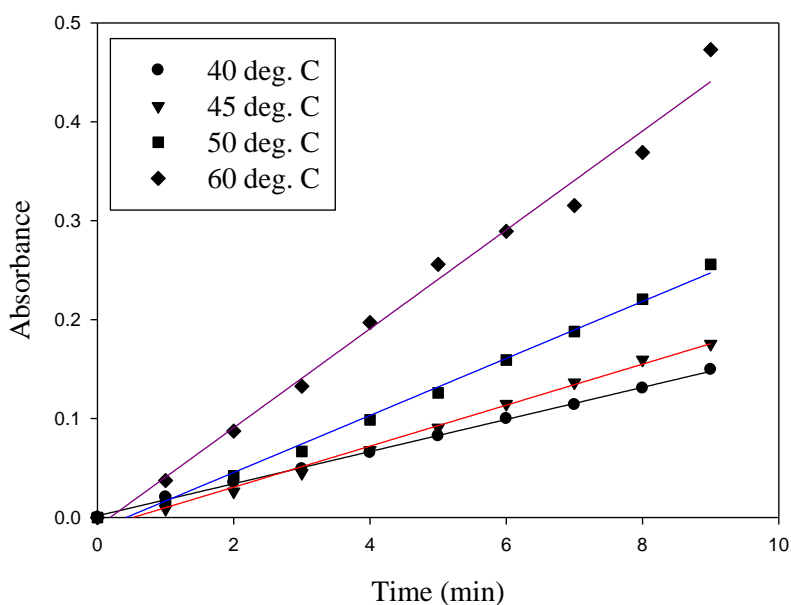


Figure 3.10: Normalized data demonstrating observed initial rates of reaction for propylene carbonate formation at various temperatures

Table 3.7: Observed rates of reaction for propylene carbonate formation

Temperature	Observed Reaction Rate $r_{\text{obs}}(\times 10^{-2} \text{ min}^{-1})$	R^2
40	1.62 ± 0.0179	0.999
45	2.07 ± 0.0589	0.994
50	2.88 ± 0.0739	0.995
60	5.00 ± 0.0020	0.988

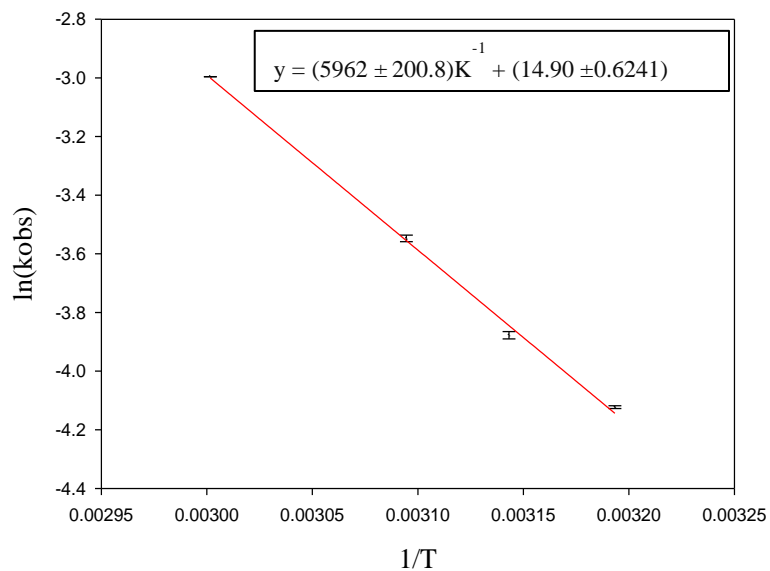


Figure 3.11: Arrhenius plot for the formation of propylene carbonate to determine the activation energy for the **2.2/PPNCl** system

An Eyring plot was also constructed, Figure 3.12, to determine the entropy, ΔS , and enthalpy, ΔH , of the reaction. Each were found to be $-124 \text{ J K}^{-1} \text{ mol}^{-1}$ and 47.9 kJ mol^{-1} respectively. This gives a ΔG value of 88.0 kJ mol^{-1} for this particular reaction at $50 \text{ }^\circ\text{C}$, indicating that the formation of propylene carbonate, under these conditions, is a non-spontaneous process.

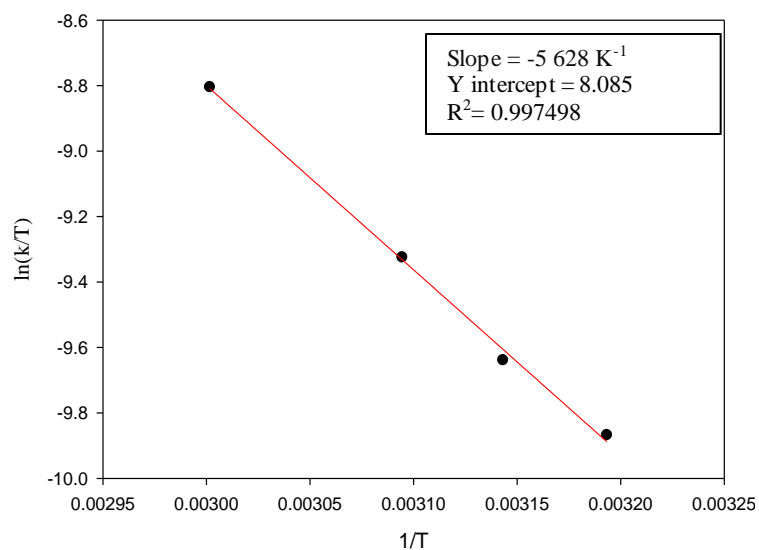


Figure 3.12: Eyring plot for the formation of propylene carbonate to determine Gibbs free energy for the **2.2**/PPNCl system

3.2.4 Epoxide Screening

The conditions that gave optimal results for propylene carbonate formation, from section 3.2.1 were applied to other epoxides: 100 °C, 4 h, 20 bar CO₂. The main goal of this study was to see if the cyclic product could be formed efficiently, and to then compare the activities, along with reaction rates, for each epoxide. Using **2.2**, results for four new epoxides, Figure 3.13, as well as PO, are outlined in Table 3.8. Epichlorohydrin has an increased activity over PO, whereas the other epoxides only reach a maximum conversion of 62% (entry 4).

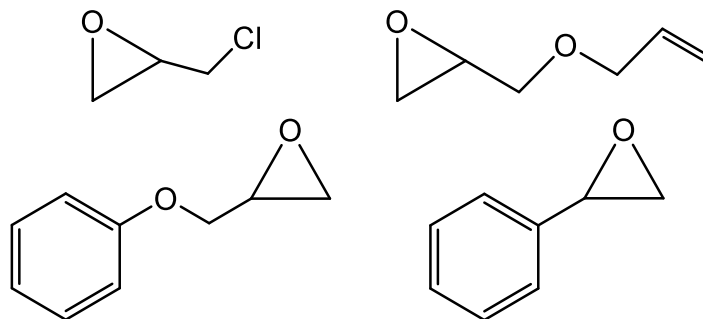


Figure 3.13: Various epoxides studied. Top: epichlorohydrin (left) and allyl glycidyl ether (right). Bottom: phenyl glycidyl ether(left) and styrene oxide (right)

Table 3.8: Cyclic carbonate formation using various epoxides

Entry	Substrate	Conversion ^a (%)	TON ^b	TOF ^c (h ⁻¹)
1	Propylene oxide	91	3 665	916
2	Epichlorohydrin	98	3 972	993
3	Allyl glycidyl ether	46	1 860	465
4	Phenyl glycidyl ether	62	2 508	627
5	Styrene oxide	42	1 688	422

Reaction conditions: Epoxide (3.0×10^{-2} mol), catalyst **2.2** (7.6×10^{-6} , 0.025 mol%), PPNCI (1.5×10^{-5} mol, 0.1 mol%), [Fe]:[Epoxide]:[PPNCI] = 1:4000:4, 20 bar, 100 °C, 4 hours. ^aDetermined by ¹H NMR spectroscopy. ^bOverall turnover number ($\text{mol}_{\text{converted epoxide}}/\text{mol}_{\text{catalyst}}$). ^cOverall turnover frequency (TON/reaction time)

It has been speculated that epichlorohydrin would be more reactive than PO due to the electron withdrawing chloro-substituent,^{1,3,16,17,28} and it was in this case under the conditions mentioned in Table 3.8 (entry 2). As the above reactions were monitored in situ, data were collected by following the carbonyl stretch, ν_{CO} 1810 cm^{-1} , allowing for the initial rates of reaction for each epoxide to be determined. Epichlorohydrin and propylene oxide demonstrate similar initial reaction rates (Figure 3.14), both also level off quickly as the detector becomes saturated with propylene carbonate formation. Allyl glycidyl ether, phenyl glycidyl ether, and styrene oxide all exhibit very similar trends with respect to activity. After ten minutes, the observed rate of propylene carbonate formation increases slightly but begins to level off after 30 minutes.

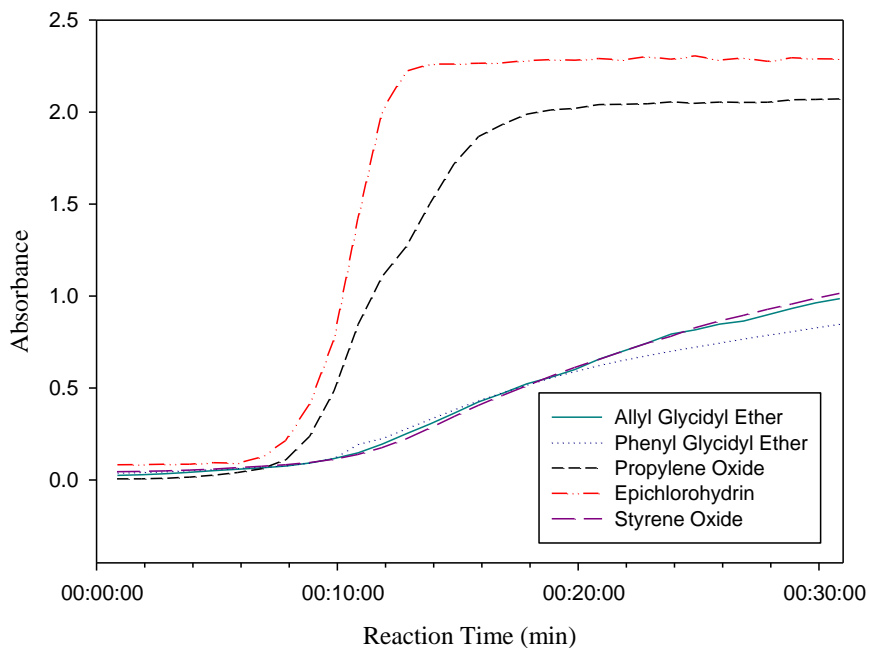


Figure 3.14: Initial rates of reaction for cyclic carbonate formation using various epoxides

It is possible to zoom in on the linear regions for each reaction to obtain a slope, representing the observed initial rate of reaction, r_{obs} . With respect to both propylene oxide and epichlorohydrin, there is a poor linearity to the slopes. This is due to the reactions proceeding at a fast rate under these conditions, and the sensor becoming saturated quickly. Looking at the initial rates of reaction in Figures 3.15 and 3.16, it can be seen clearly that epichlorohydrin proceeds at a much faster rate than PO, while the other epoxides are still relatively active at the same rate. Phenyl glycidyl ether does appear to be leveling off after 20 minutes, indicating that reaction may in fact be completed after only four hours.

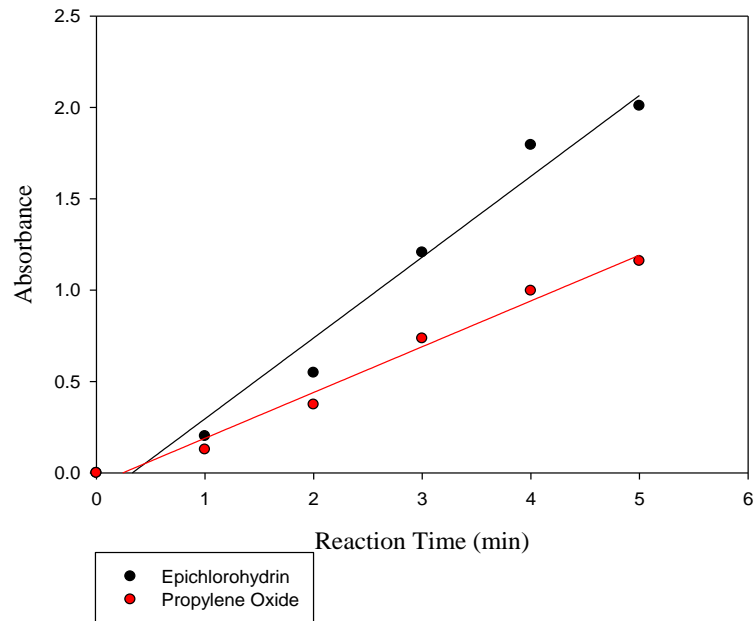


Figure 3.15: Normalized data for the observed rates of reaction of cyclic carbonate formation for epichlorohydrin and propylene oxide

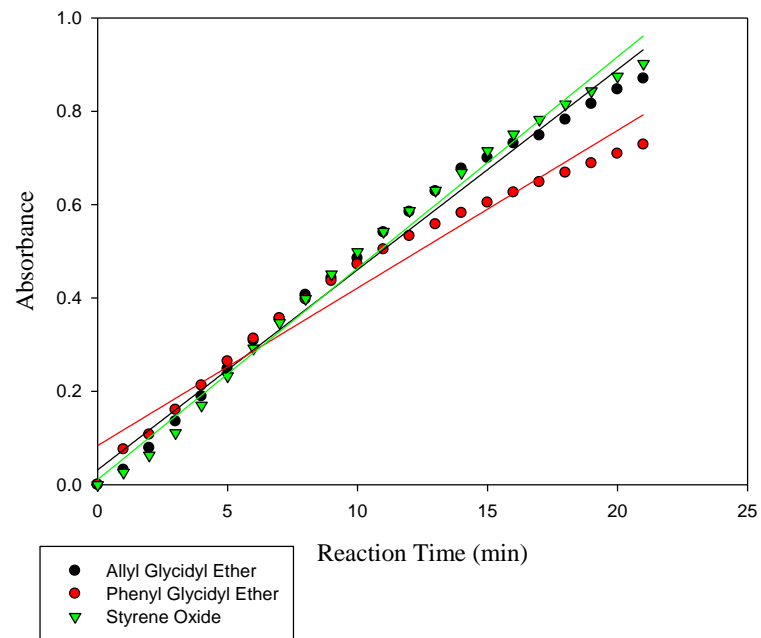


Figure 3.16: Normalized data for the observed rates of reaction of cyclic carbonate formation for allyl glycidyl ether, phenyl glycidyl ether, and styrene oxide

Table 3.9 summarizes the maximum observed rates for the carbonate formation from the selected epoxides. Epichlorohydrin reacts at a rate almost double that of propylene oxide, which is over 5 times faster than the other epoxides. The increased steric effects of allyl glycidyl ether, phenyl glycidyl ether, and styrene oxide, specifically with respect to the phenyl groups, may be a reason for the decreased conversions and reaction rates. Epichlorohydrin has an electron withdrawing substituent which will therefore make the epoxide slightly more electropositive, favoring nucleophile attack and ring opening; this may be why the reaction with epichlorohydrin proceeds twice as fast as with propylene oxide.

Table 3.9: Observed reaction rates for cyclic carbonate formation using various epoxides

Epoxide	Observed Reaction Rate $r_{\text{obs}} (\times 10^{-2} \text{ min}^{-1})$	R^2
Epichlorohydrin	44.2 ± 7.8	0.972
Propylene oxide	24.5 ± 1.9	0.989
Styrene oxide	4.53 ± 0.10	0.990
Allyl glycidyl ether	4.29 ± 0.11	0.986
Glycidyl phenol ether	3.38 ± 0.14	0.966

3.3 Conclusions

Complexes **2.1-2.4** have proven effective for the coupling of CO₂ and PO under various conditions, giving comparable results to the other iron(III) complexes used in literature;^{1-3,17,25,27} Reaction parameters were optimized with respect to reaction time (4 h), catalyst loading (0.025 mol%), temperature (80 °C), and CO₂ pressure (20 bar). While certain conditions could certainly be lowered while still achieving conversion of propylene oxide, the overall production of propylene carbonate would decrease as well as the turnover numbers and frequencies. Although PPnCl appeared to give optimal

results when used as a cocatalyst, DMAP and TBAB were assessed as well. Under identical conditions, using PPNCI allowed for higher conversion over TBAB (74% vs. 64% respectively), which is an opposite trend to that previously reported.^{1, 3, 17} DMAP resulted in the lowest conversion as it is speculated to coordinate to iron more strongly than the other nucleophiles, hindering the epoxide coordination step. To prove this theory, it would be beneficial to have a crystal structure demonstrating the coordinated DMAP molecule, this has been accomplished and studied extensively by a former group member using chromium catalysts.²⁹

Temperature plays a large role throughout this reaction process, as no conversion at all is seen at room temperature, and the rate of reaction only starts to increase drastically when the temperature is raised above 60 °C. This is also common for iron catalysts in this area, as most reactions are performed between 80 and 100 °C.^{1-3, 16, 17} By following the initial rates of reaction at lower temperatures however, the activation energy for **2.2**/PPNCI towards propylene carbonate formation was found to be 49.6 kJ mol⁻¹.

The reaction conditions used throughout the PO work were also applied to four other epoxides. Styrene oxide, phenyl glycidyl ether, and allyl glycidyl ether all gave greater than 50% conversions after 4 h. These are comparable to previous reports.^{1, 17} The highest conversion of any epoxide was using epichlorohydrin, which agrees with the literature findings.^{1, 3, 16, 17}

3.4 Experimental

3.4.1 General Method and Procedures

Unless otherwise stated, all reactions were performed on the benchtop. Propylene oxide, purchased from Fisher Scientific, was dried over CaH_2 and distilled prior to use. All other reagents and solvents were purchased from Sigma Aldrich, Fisher, and Alfa Aesar, and used without further purification.

3.4.2 Instrumentation

^1H and $^{13}\text{C}\{^1\text{H}\}$ NMR spectra were recorded on a Bruker AVANCE III instrument. MALDI-TOF MS for the DMAP coordinated iron complex were obtained using an Applied Biosystems 4800 MALDI TOF/TOF analyzer equipped with a reflectron and a high-performance nitrogen laser operating at 355 nm. The complex (with increasing DMAP ratio added) and anthracene matrix were dissolved separately in dichloromethane into solutions of 10 mg/mL before being combined in a 1:1 ratio and spotted onto the MALDI plate and dried.

3.4.3 Preparation of a 2-component Catalyst System for CO_2 -Epoxide Coupling Reactions

A stock solution of the desired iron complex in dichloromethane was made using a 25.00 mL volumetric flask to a concentration of 7.04×10^{-4} mg/mL. A 10 mL aliquot of stock solution was pipetted into a 20 mL scintillation vial containing 298 mg (5.19×10^{-2} mmol) of PPNCl . Minimal dichloromethane was added to dissolve both compounds, after which the dark purple solution was transferred to a 100 mL round bottom flask. The solvent was removed under reduced pressure leaving a very thick, oily

purple substance. 3.00 g (5.17×10^{-2} mol) PO was added directly to the round bottom and stoppered immediately; the purple oil dissolved to form a clear orange solution.

3.4.4 In situ monitoring of the coupling reactions by IR spectroscopy

A 100 mL stainless steel pressure vessel (Parr Instruments) was equipped with a silicon sensor (SiComp), a motorized mechanical stirrer, and a heating ring. To monitor the reaction in situ, the silicon sensor was connected to a ReactIR 15 unit through a DS silver-halide Fiber-to-sentinel conduit. Prior to any reaction, the vessel was cleaned and left to bake at 100 °C overnight under vacuum. Once cooled to room temperature, the reaction mixture, prepared as above in Section 3.3.4, was added to the vessel by pipette, sealed tightly, and pressurized with 10 bar CO₂. Heating and stirring (250 rpm) were then started and the reaction was monitored for the desired time. Note, once heated to 100 °C the operating pressure would be 20 bar CO₂.

3.5 References

1. Alhashmialameer, D.; Collins, J.; Hattenhauer, K.; Kerton, F. M., *Catal. Sci. Technol.* **2016**, *6*, 5364-5373.
2. Buchard, A.; Kember, M. R.; Sandeman, K. G.; Williams, C. K., *Chem. Commun.* **2011**, *47*, 212-214.
3. Buonerba, A.; De Nisi, A.; Grassi, A.; Milione, S.; Capacchione, C.; Vagin, S.; Rieger, B., *Catal. Sci. Technol.* **2015**, *5*, 118-123.
4. Darensbourg, D. J., *Chem. Rev.* **2007**, *107*, 2388-2410.
5. Devaine-Pressing, K.; Dawe, L. N.; Kozak, C. M., *Polym. Chem.* **2015**, *6*, 6305-6315.
6. Fukuoka, S.; Fukawa, I.; Tojo, M.; Oonishi, K.; Hachiya, H.; Aminaka, M.; Hasegawa, K.; Komiya, K., *Catal. Surv. Asia* **2010**, *14*, 146-163.
7. Liu, Y.; Zhou, H.; Guo, J. Z.; Ren, W. M.; Lu, X. B., *Angew. Chem. Int. Ed.* **2017**, *56*, 4862-4866.
8. van Heek, J.; Arning, K.; Ziefle, M., *Energy Policy* **2017**, *105*, 53-66.
9. Cohen, C. T.; Chu, T.; Coates, G. W., *J. Am. Chem. Soc.* **2005**, *127*, 10869-10878.
10. Lu, X. B.; Darensbourg, D. J., *Chem Soc. Rev.* **2012**, *41*, 1462-1484.
11. Pinilla-de Dios, M.; Andrés-Iglesias, C.; Fernández, A.; Salmi, T.; Galdámez, J. R.; García-Serna, J., *Eur. Polym. J.* **2017**, *88*, 280-291.
12. von der Assen, N.; Bardow, A., *Green Chem.* **2014**, *16*, 3272-3280.
13. Fu, X.; Jing, H., *J. Catal.* **2015**, *329*, 317-324.
14. Wu, G.-P.; Wei, S.-H.; Ren, W.-M.; Lu, X.-B.; Li, B.; Zu, Y.-P.; Darensbourg, D. J., *Energy Environ. Sci.* **2011**, *4*, 5084-5092.
15. Dean, R. K.; Devaine-Pressing, K.; Dawe, L. N.; Kozak, C. M., *Dalton Trans.* **2013**, *42*, 9233-9244.
16. Fuchs, M. A.; Zevaco, T. A.; Ember, E.; Walter, O.; Held, I.; Dinjus, E.; Doring, M., *Dalton Trans.* **2013**, *42*, 5322-5329.

17. Vummaleti, S. V. C.; Buonerba, A.; De Nisi, A.; Monari, M.; Della Monica, F.; Nisi, A. D.; Milione, S.; Grassi, A.; Cavallo, L.; Capacchione, C., *Adv. Synth. Catal.* **2016**, 358, 3231-3243.
18. Allan, L. E.; MacDonald, J. P.; Reckling, A. M.; Kozak, C. M.; Shaver, M. P., *Macromol. Rapid Commun.* **2012**, 33, 414-418.
19. Chard, E. F.; Dawe, L. N.; Kozak, C. M., *J. Organomet. Chem.* **2013**, 737, 32-39.
20. Hasan, K.; Brown, N.; Kozak, C. M., *Green Chem.* **2011**, 13, 1230.
21. Hasan, K.; Dawe, L. N.; Kozak, C. M., *Eur. J. Inorg. Chem.* **2011**, 2011, 4610-4621.
22. Qian, X.; Dawe, L. N.; Kozak, C. M., *Dalton Trans.* **2011**, 40, 933-943.
23. Reckling, A. M.; Martin, D.; Dawe, L. N.; Decken, A.; Kozak, C. M., *J. Organomet. Chem.* **2011**, 696, 787-794.
24. Chen, H.; Dawe, L. N.; Kozak, C. M., *Catal. Sci. Technol.* **2014**, 4, 1547-1555.
25. Taherimehr, M.; Al-Amsyar, S. M.; Whiteoak, C. J.; Kleij, A. W.; Pescarmona, P. P., *Green Chem.* **2013**, 15, 3083-3090.
26. Taherimehr, M.; Serta, J.; Kleij, A. W.; Whiteoak, C. J.; Pescarmona, P. P., *ChemSusChem.* **2015**, 8, 1034-1042.
27. Al-Qaisi, F. a.; Genjang, N.; Nieger, M.; Repo, T., *Inorg. Chim. Acta.* **2016**, 442, 81-85.
28. Adolph, M.; Zevaco, T. A.; Altesleben, C.; Walter, O.; Dinjus, E., *Dalton Trans.* **2014**, 43, 3285-3296.
29. Devaine-Pressing, K.; Kozak, C. M., *ChemSusChem.* **2017**, 10, 1266-1273.

4. Iron Amino-bis(phenolate) Complexes for the Copolymerization of CO₂ and Cyclohexene Oxide

4.1 Introduction

In Chapter 3, the focus was on cyclic carbonate formation from the coupling of propylene oxide and CO₂. Cyclic carbonate was demonstrated to be the only product formed under several conditions, which was expected as i) the literature demonstrated 100% selectivity for the cyclic product when using iron catalysts,¹⁻⁵ and ii) the activation barrier between polymer and cyclic products is low.⁶

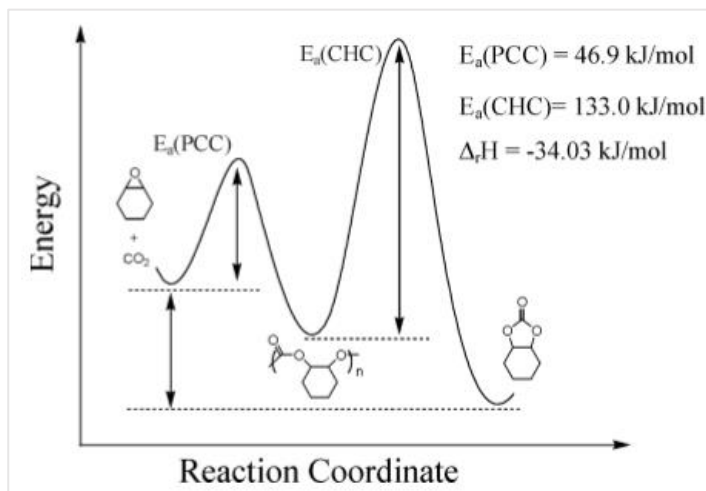
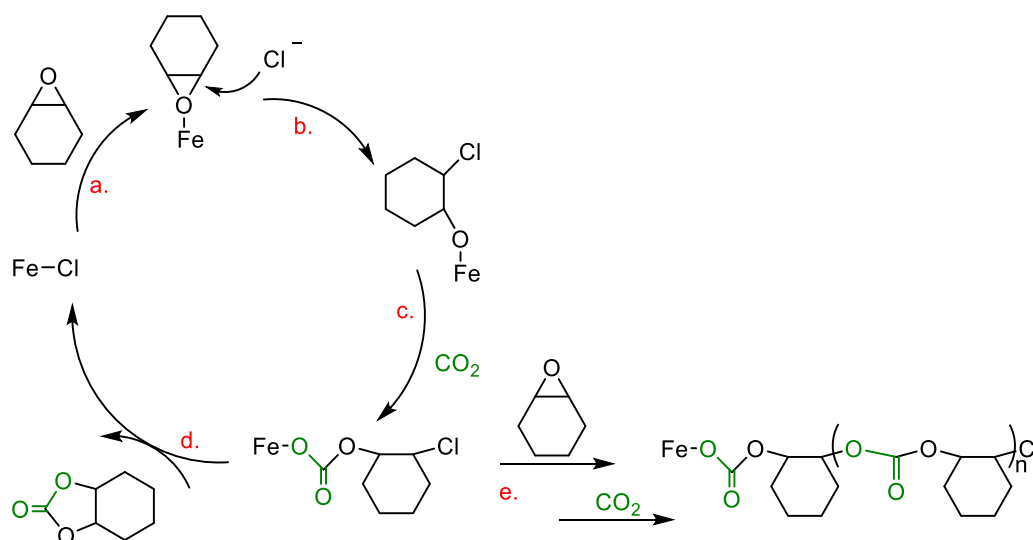


Figure 4.1: Activation energy diagram for the copolymerization of CHO and CO₂, image taken with permission from reference 6

Figure 4.1, demonstrates how the cyclic cyclohexene oxide product is harder to achieve thermodynamically. The activation barrier between the polymer and cyclic product is now 86.1 kJ mol⁻¹, compared with propylene oxide with a difference of only ~ 30 kJ mol⁻¹, therefore the reaction favors polycarbonate formation.⁶ The iron complexes used in literature for the polymerization of CHO and CO₂ are highly selective

for polycarbonate formation, unless there are 5-10 equivalents of cocatalyst present to force backbiting reactions.⁷⁻⁹



Scheme 4.1: A simplified mechanistic cycle for the copolymerization/coupling of CHO and CO₂

Scheme 4.1 demonstrates a simplified mechanism for the formation of polycarbonate from cyclohexene oxide and CO₂ using iron as the catalyst. Cyclohexene oxide can coordinate to the iron as it is sufficiently Lewis acidic center, before a nucleophile, such as chloride, can attack to ring open the epoxide as shown in steps a and b. In this mechanism, the nucleophile was previously coordinated to the metal as part of the catalyst, however, it can be introduced into the system as the anion of the cocatalyst. In step c, carbon dioxide inserts into the metal-alkoxide bond, which may be followed by ring closing and ejection of the nucleophile to produce cyclic cyclohexene carbonate in step d. Step e is most likely to occur where there is a repeated addition of epoxide followed by CO₂ insertion until the reaction is terminated, producing polycarbonate.

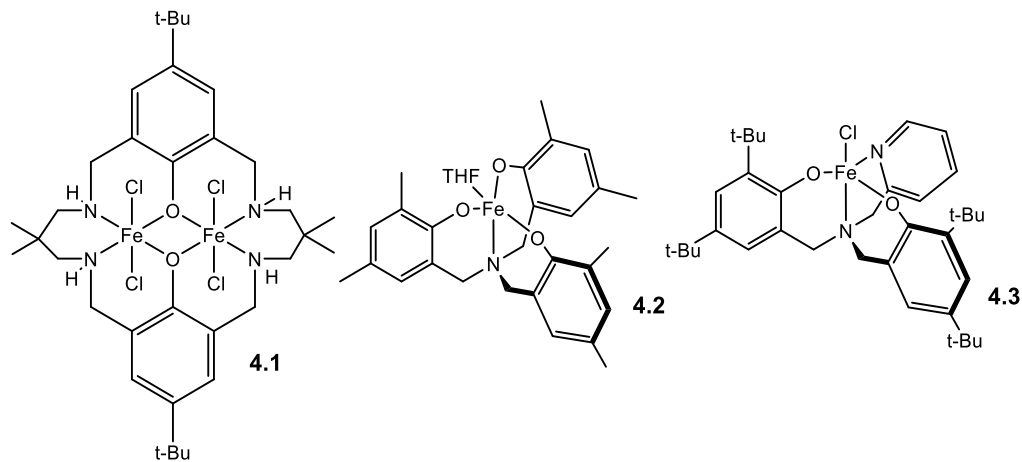


Figure 4.2: Iron catalysts in the literature used for the copolymerization of CHO and CO₂

There are few examples in the literature for iron-catalyzed polymerization reactions of CO₂ with CHO. Figure 4.2 shows three of the catalysts that have been successful in synthesizing polycarbonate with high carbonate linkages, while controlling the selectivity of polymer to cyclic product. In 2011 Williams published the first example of iron performing this type of chemistry with a di-iron complex, **4.1**.⁷ With a 0.1 mol % catalyst loading, at 80 °C and only 10 bar CO₂ pressure, a 70% conversion of polycarbonate was achieved after 24 h without the use of a cocatalyst; the polymer had high molecular weight (11 700 g mol⁻¹) and narrow dispersity, 1.13. Two years later Kleij and Pescarmona achieved a 56% conversion to polycarbonate using the same catalyst loading with complex **4.2** and TBAB as the cocatalyst, but this time under supercritical conditions, 80 bar CO₂ and 85 °C. The polymer produced demonstrated a narrower dispersity (1.05) but lower molecular weights (6 020 g mol⁻¹).⁸ In 2015, Pescarmona published work in which the catalyst loading of **4.3** was increased to

0.5 mol % using TBAB as the cocatalyst, with the reaction still relying upon supercritical CO₂; polymer molecular weight was decreased (1 420 g mol⁻¹) while maintaining a narrow dispersity (1.1).⁹ Pescarmona's catalyst is near identical to complexes first reported by the Kozak group which have been extensively characterized and used in various reactions such as cross-coupling and radical polymerizations.¹⁰⁻¹⁸ As such, our complexes make this a great opportunity.

4.2 Results and Discussion

4.2.1 Catalyst Screening and Parameter Optimization

Iron complexes **2.1-2.4** were assessed for the copolymerization of CO₂ and CHO. Initial parameters were 0.5 mol % Fe with 0.5 mol % PPNCI at 60 °C and 60 bar CO₂ for 22 h. Parameters were chosen based on successful reactions in the group which have been able to produce polymer efficiently with Cr complexes,¹⁹ as well as the cyclic product with Co complexes, which is currently unpublished. It was interesting to see if the reaction could work well using iron complexes, and if the polymer or cyclic product would be favoured. All four complexes demonstrated high selectivity towards polycarbonate formation, with **2.4**, Figure 4.3, achieving a near quantitative conversion after 22 h (Table 4.1). Temperature, time, and pressure dependence were all studied to determine which factors have the greatest influence on polymer formation, as well as the polymeric properties. End group analysis was carried out using MALDI-TOF MS demonstrating that chain transfer appears to be evident throughout the reactions, with polymers having dichloro and dihydroxy end groups.

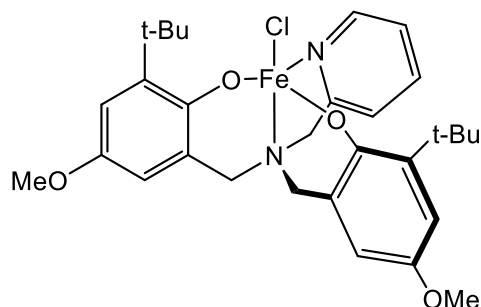


Figure 4.3: Iron complex **2.4**

It was interesting to find that the iron(III) complexes behave similar to the chromium complexes in our group,¹⁹ as iron(III) is slightly more labile/Lewis acidic. It has been shown, however, that the iron complexes can potentially form 6 coordinate systems identical to chromium, when mixed with PPnCl. As both systems could readily lose a nucleophilic ligand, chloride, it would allow for coordination of CHO to the metal center followed by ring opening allowing these reactions to proceed. Kelij and Pescarmona's catalyst, **4.2**, was able to selectively produce both polymer and cyclic product by changing the amount of cocatalyst present in the reaction.⁸

Table 4.1: Catalyst screening for the formation of polycarbonate

Catalyst	Conversion ^a	M _n (g mol ⁻¹) ^b	Đ ^c
2.1	90	7 460	1.09
2.2	89	8 120	1.09
2.2^d	96	5 380	1.05
2.3	30	3 580	1.02
2.4	99	9 190	1.14
2.4^e	39	4 710	1.02

Reaction conditions unless otherwise stated: CHO (3.1×10^{-2} mol), catalyst (1.5×10^{-4} mol, 0.5 mol%), PPnCl (1.5×10^{-4} mol, 0.5 mol%), 60 °C, 22 h, 60 bar CO₂. ^a Determined by ¹H NMR spectroscopy. ^b Determined by GPC analysis ^c Determined by GPC analysis ^d Catalyst loading increased to 1 mol% ^e Catalyst loading decreased to 0.2 mol%

No cyclic product was observed by ^1H NMR spectroscopy, or near negligible amounts, making polycarbonate the selective product for each reaction. After 22 h, at 60 bar CO_2 pressure and 60 $^\circ\text{C}$, complexes **2.1**, **2.2** and **2.4** gave high conversions to polycarbonate ranging from 89 – 99%. **2.4** led to near quantitative results and demonstrated slightly the highest molecular weight (9 190 g mol^{-1}) but also demonstrated slightly higher dispersity (1.14). PPNCI was the only cocatalyst used throughout these studies, however, there was an attempt to utilize complex **2.4** without purification, i.e. not removing the triethylammonium chloride to determine if it could act sufficiently as the cocatalyst or external nucleophile for ring opening. This reaction showed no conversion of epoxide. Figure 4.4 is an NMR spectrum of crude polycarbonate taken at the end of a reaction. Typical peaks are assigned below. H_a and H_b represent the hydrogens on the terminal cyclohexene ring, H_a representing the hydrogen next to a hydroxy end group. H_c and H_c' are represented by the broad peak at 4.6 ppm, the hydrogens on the repeating unit of the polycarbonate. Conversions are found by comparing the integration of H_c/H_c' with CHO at 3.12 ppm. Both peaks represent two hydrogen atoms, however, the polymer peak is much more broad and larger as there can be several different molecular weight polymer chains present in the sample.

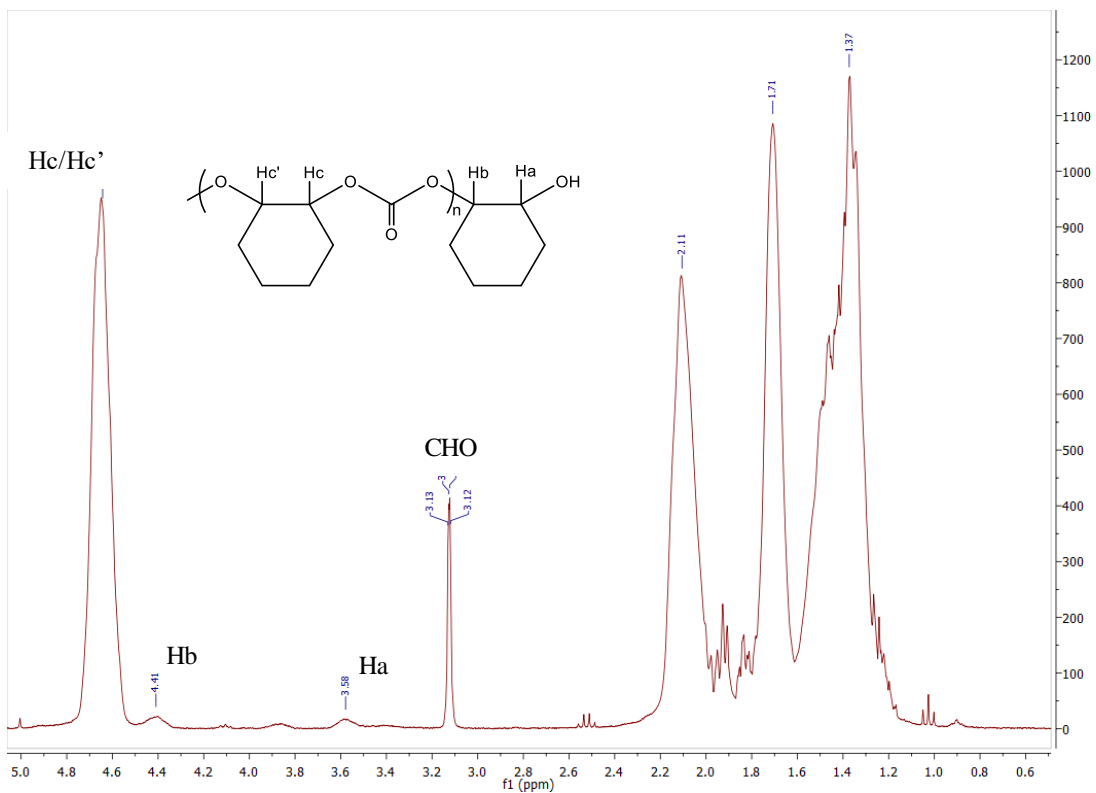


Figure 4.4: ^1H NMR spectrum in CDCl_3 of polycarbonate obtained according to the conditions in Table 4.1, entry 3

The polymers produced have a very high percentage of carbonate linkages, > 98%, as seen by ^1H NMR spectroscopy. As a control to assess whether or not this catalyst system could homopolymerize cyclohexene oxide to produce polyether in the absence of CO_2 . Mixtures of **2.2** and **2.4**, at a 0.5 mol % catalyst and cocatalyst loading, in 1 g CHO were placed in scintillation vials and stirred at room temperature for 24 h. A small aliquot was removed from each and analyzed by ^1H NMR. Reactions were also stirred at 40, 60, and 80 °C each for 24 h, no evidence of polyether was observed under these conditions.

4.2.2 Temperature, Pressure, and Time Effects

Although the conditions used to screen the complexes were desirable as they did not exceed supercritical conditions as seen in the literature,^{8,9} the effects of temperature and pressure were still assessed, Table 4.2. Looking at temperature effects first using complex **2.4**. At room temperature (entry 1), the reaction is halted completely, but at 40 °C (entry 2) 89% conversion was achieved with almost full selectivity towards polycarbonate formation. No evidence of polycarbonate or cyclic carbonate is seen at 25 °C.

Table 4.2: Temperature and pressure effects on the formation of polycarbonate

Entry	Temperature (°C)	Pressure (bar)	Conv. ^a (bar)	Mn ^b (g mol ⁻¹)	Đ ^c	TOF (h ⁻¹)
1	25	60	0	-	-	-
2	40	60	89	5 710	1.06	8.1
3	60	60	99	9 190	1.14	9
4	60	40	88	5 410	1.05	8
5	60	20	77	6 350	1.13	7
6	60	10	63	4 980	1.04	5.7
7	60	7 ± 1	56	5 150	1.09	5.1

Reaction conditions unless otherwise stated: CHO (3.1×10^{-2} mol), catalyst **2.4** (1.5×10^{-4} mol, 0.5 mol%), PPnCl (1.5×10^{-4} mol, 0.5 mol%), 22 h. ^a Determined by ¹H NMR spectroscopy. ^b Determined by GPC analysis ^c Determined by GPC analysis

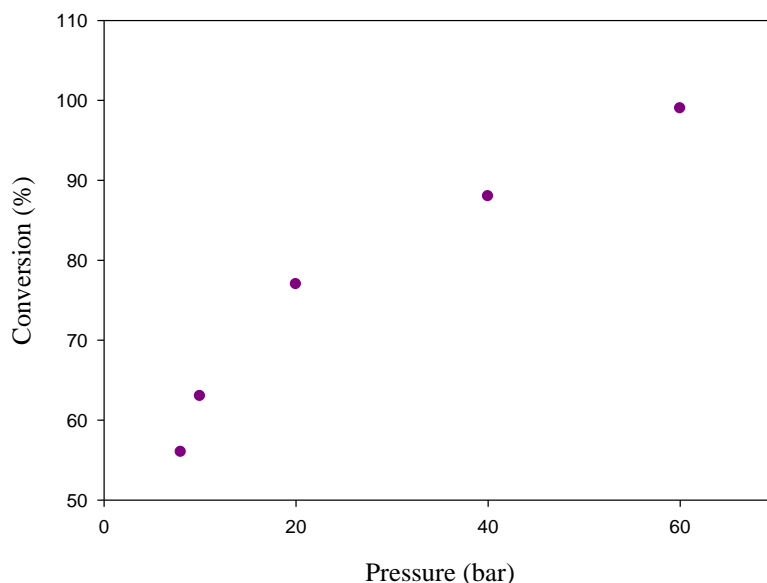


Figure 4.5: The effect of pressure on overall conversion to polycarbonate

The effect of pressure on the reaction showed an interesting trend. As the pressure of CO₂ was decreased, so was the conversion of polycarbonate formation before it reaches a maximum at 99% conversion. At 40 bar CO₂, the conversion dropped to 88% (entry 4), and again to 77% with only 20 bar CO₂ (entry 5). This was an unexpected result as there is limited literature published for this reaction using an iron catalyst, and they do not report reactions at pressures lower than 60 bar. Only Williams has been able to achieve results with pressure lower than 60 bar, and in fact, only 1 bar CO₂ pressure was necessary for the reaction to proceed.⁷ This demonstrated that the catalytic system using **4.1**, was not entirely dependant on CO₂ concentration. However, it is not zero order with respect to CO₂ as there is an increase in conversion (29% - 70%) when the pressure of CO₂ is increased from 1 to 10 bar.⁷ Other pressures were not looked into to gain further insight on CO₂ dependency in throughout that work.⁷ Entry 7 demonstrated

some uncertainty with CO₂ pressure of the system, starting at roughly 6 bar and fluctuating to 8 bar by the end of the reaction. Figure 4.5 demonstrates the relationship between overall conversion of CHO with increasing pressure.

Figure 4.6 relates the effect of CO₂ pressure on TOF which appears to be similar to the work by published by Darensbourg in 2005.²⁰ As is shown in Figure 4.7, Darensbourg was able to identify that his reaction, utilizing a Cr salen complex and N-methylimidazole as a cocatalyst, is highly selective for copolymer production. As well, in the range up to 15 bar CO₂ pressure where Henry's law is applicable it is apparent that the rate of copolymer production is first order in [CO₂].²⁰ This is not the case for the work presented in Figure 4.6 as the data does not go through the origin if extrapolated, like it does in Figure 4.7. Rieger and coworkers published an extensive study on the dependence of CO₂ concentration using a Zn complex, and determined that for their particular system the reaction was first order with respect to CO₂ between 5 and 25 bar, however, at pressures greater than 25 bar the rate changed to zero order.²¹ This demonstrates how each system may be dependant on CO₂ pressure, but only up until a certain point.

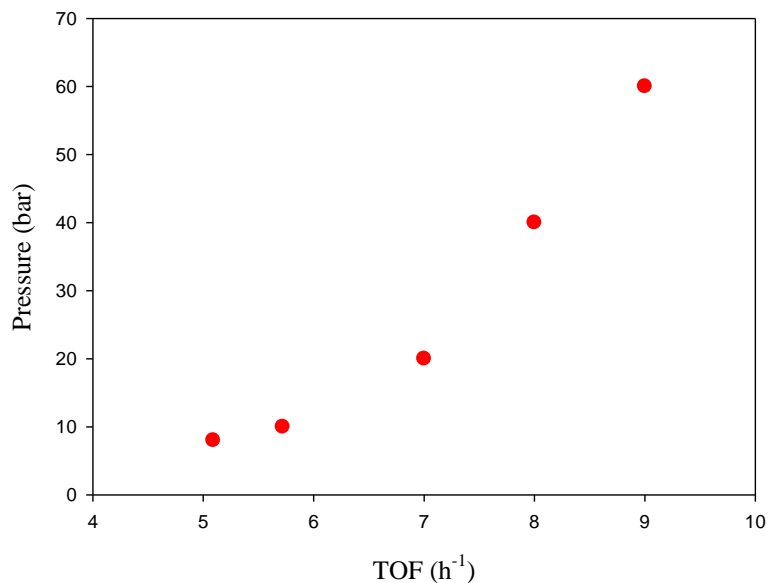


Figure 4.6: Relationship between the pressure of CO₂ and TOF for the production of polycarbonate

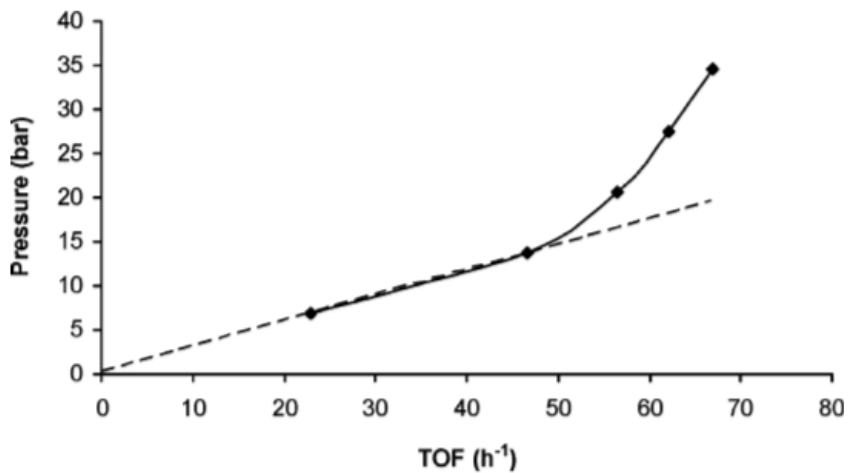


Figure 4.7: Relationship between the pressure of CO₂ and TOF to produce polycarbonate using a Cr salen complex, image taken with permission from ref. 20

In a study by Beckman and coworkers the phase behaviour of CO₂ and CHO are thoroughly studied in which it is shown that they will form a one phase system under a variety of conditions;²² this explains the increase of copolymerization from low

pressures to high pressures as demonstrated in this work as well in Darensbourg's.²⁰ If, however, the pressure is too high, it has been shown to be detrimental to copolymerization due to dilution of the catalyst and epoxide. There is great volumetric expansion of the liquid phase.²⁰

Reaction time was looked into, and, as the length of reaction increased, the conversion of CHO, as well as molecular weights of polycarbonate, was increased. After only 4 h using complex **2.2**, a 41% conversion to polycarbonate was achieved with a molecular weight of 3 620 g mol⁻¹. Increasing the time to 8 h allowed for higher conversion (41 %) and molecular weights (4 930 g mol⁻¹). Very narrow dispersities of 1.03 and 1.01, respectively, were seen for both reactions. Increasing the reaction time to 22 h led to near quantitative conversion with the highest molecular polycarbonate produced, 9 190 g mol⁻¹. The dispersity, however, broadened to 1.14 suggesting that the longer reaction time leads to more chain transfer events.

Table 4.3: Reaction time effects on the formation of polycarbonate

Entry	Time (h)	Conversion ^a (%)	Mn ^b (g mol ⁻¹)	Đ ^c
1	4	41	3 620	1.03
2	8	66	4 930	1.01
3	22	99	9 190	1.14

Reaction conditions unless otherwise stated: CHO (3.1 × 10⁻² mol), catalyst **2.4** (1.5 × 10⁻⁴ mol, 0.5 mol%), PPNCI (1.5 × 10⁻⁴ mol, 0.5 mol%), 60 bar CO₂, 60 °C ^aDetermined by ¹H NMR spectroscopy. ^bDetermined by GPC analysis ^cDetermined by GPC analysis

4.2.3 Method of Polymer Isolation

Cyclohexene oxide is not very volatile, therefore the conversions calculated by ¹H NMR are reliable, and no internal standard was used. It was previously demonstrated in Chapter 3, however, that even for a volatile compound like PO, results obtained by

^1H NMR spectroscopy were reliable as well. The conversions are calculated by using the crude polymer taken from the pressure vessel immediately upon reaction completion. There are a few ways in which the amount of isolated polycarbonate can be found: precipitation with acidified methanol, precipitation with acidified methanol and isolating layers, or drying of crude product for ~ 24 h.

The first method is straightforward as the polymer product is simply collected, dissolved in a minimal amount of dichloromethane, before a solution of acidified methanol is added slowly. Once the polymer has precipitated out of solution, the flask can be placed in the freezer for a short length of time before removing the solution and repeating the process of dissolving/precipitating polymer.

Precipitating the polymer with acidified methanol is effective, however it results in much lower yields than the conversions calculated using ^1H NMR data. This can be explained due to loss of polymer in the discarded solutions between each washing step. To increase isolated polymer yields, the discarded washing layers can once again be placed into a freezer and left for extended periods of time. Visibly crystalline polymer has been seen to precipitate out of these washings. In other instances, the solutions which have been left for long periods, could be concentrated down to reveal polymer product as well. This is especially true when low molecular weight polymers are obtained, which are inherently more soluble in the solvent mixtures used for polymer purification.

Table 4.4: The effect of polymer isolation and increasing yield through various precipitation steps

Entry	Conversion ^a (%)	Washing ^b	Yield ^c (%)	Mn ^d (g mol ⁻¹)	Đ
1	96	Initial	59	5 380	1.05
		Wash 2	63	3 830	1.02
		Wash 3	66	3 510	1.02
2	90	Initial	63	7 460	1.09
		Wash 3	66	5 150	1.02

^aOverall conversion of polycarbonate determined by ¹H NMR spectroscopy. ^bPolymer isolated in each precipitation step ^cCumulative yield of polymer ^dDetermined by GPC analysis, representative only of polymer isolated in each step ^eDetermined by GPC analysis, representative only of polymer isolate in each step

What can be seen in Table 4.4 is that the polymer isolated from the subsequent washings decreases in molecular weight as well as dispersity. This is to be expected as the lower molecular weight polymer chains will not precipitate out of an excess of solution and are often discarded when trying to isolate bulk polymer, thus explaining the lower yields of polymer when compared to conversions obtained from NMR data.

To avoid several washing/precipitation steps, the yield of isolated polymer can be calculated by simply drying the crude product. The crude polymer can be collected and dissolved in dichloromethane. Once the solvent has been removed, the product can be further dried on a Schlenk line, a method which has been utilized previously in the literature.⁷ All solvent should be removed using this method, as well as the cyclohexene oxide starting material, and any cyclic carbonate that may have been formed. More accurate yields can therefore be accounted for when taking into account of the catalyst, however, pure polymer is not obtained.

4.2.4 Characterization of Polymers by MALDI-TOF MS

End group analysis was carried out using MALDI-TOF MS in linear mode, as shown in Figure 4.8. The spectrum exhibits a bimodal distribution with higher molecular weight polymer visible around m/z 10 000, but a distribution of more intense signals in the lower mass region at m/z 5 500. This is not in agreement with the molecular weight determined through gel permeation chromatography, GPC, of $7\,460\text{ g mol}^{-1}$. The higher molecular weight polymer possesses only chloro end groups, consistent with a chain transfer mechanism, Figure 4.8. Two end groups are present in the lower molecular weight polymer region, chloro and hydroxy, Figure 4.9. Theoretically, we would expect to see chloro and hydroxy end groups on each polymer chain. Chlorine is the only nucleophile present (with exception of the epoxide) and it is expected to ring open CHO in the initiation step. The reaction is quenched with acidified methanol protonating the terminal alkoxide releasing metal from the polymer.

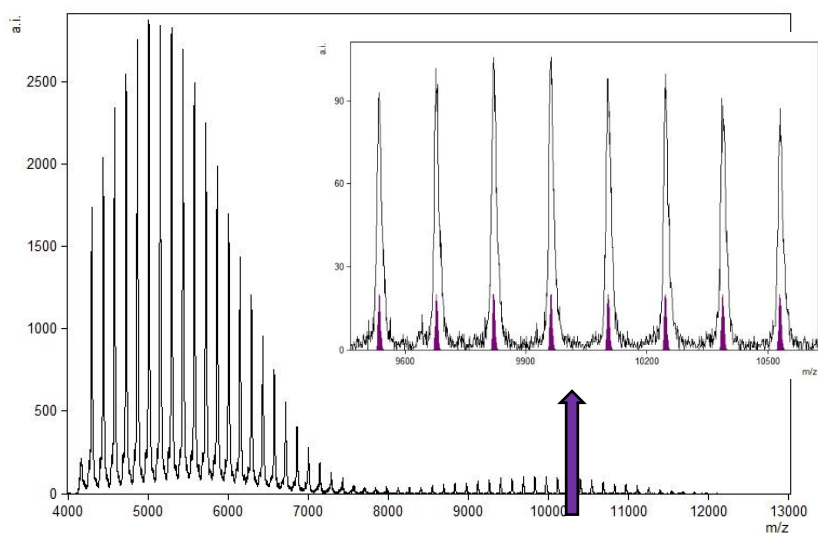


Figure 4.8: MALDI-TOF spectrum of polycarbonate, insert demonstrating pattern at high molecular weights with only one end group present

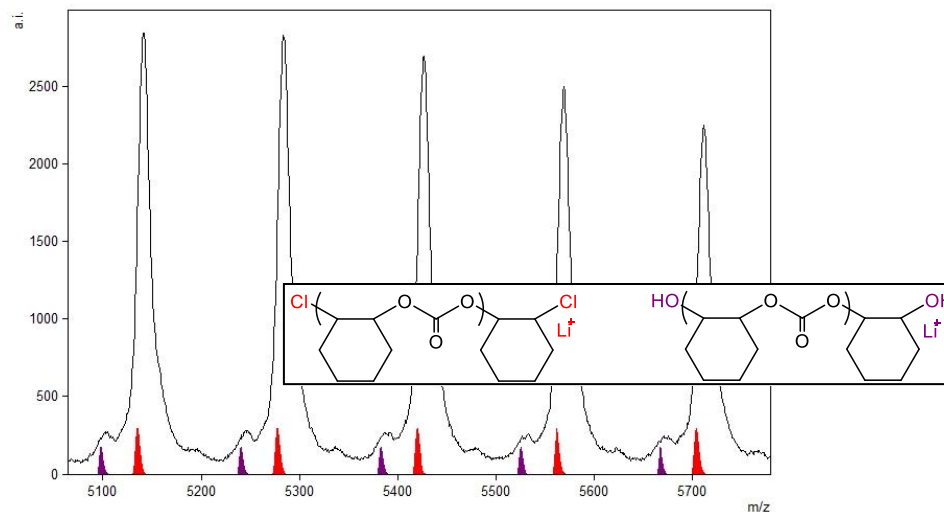


Figure 4.9: Magnified MALDI-TOF spectra from Figure 4.8 demonstrating two potential end groups

4.3 Conclusions

Complexes **2.1-2.4** were effective in copolymerization reactions with CO₂ and CHO, and were capable of producing polycarbonate at lower pressures and temperatures than is seen in recent literature.^{8, 9} Selectivity for polycarbonate product vs. cyclic was greater than 95% in all reactions, and reaction parameters were assessed with respect to pressure, temperature and time. As demonstrated in Chapter 3, temperature once again plays a large role in this reaction process, as there is only a slight drop in conversion from 60 – 40 °C; the reaction is halted completely at 25 °C. After only 4 h at 60 °C and 60 bar CO₂, 41% conversion of CHO is achieved, and at only 7 bar CO₂ pressure at 60 °C, there is greater than 50% conversion after 22 h. This is the first iron complex to use low pressures of CO₂ since 2011 when Williams first published work on iron catalyzed copolymerization of CO₂ and epoxides.⁷ End group analysis demonstrated dichloro capped polymers, as well as dihydroxy capped polymers, indicating the presence of chain transfer reactions readily occurring.

4.4 Experimental

4.4.1 General Method and Procedures

Unless otherwise stated, all chemistry in this chapter was performed on the benchtop. Cyclohexene oxide, purchased from Fisher Scientific, was distilled over CaH₂ under vacuum prior to use. All other reagents and solvents were purchased from Sigma Aldrich, Fisher, and Alfa Aesar, and used without further purification.

4.4.2 Instrumentation

¹H and ¹³C{¹H} NMR spectra were recorded on a Bruker AVANCE III instrument. MALDI-TOF MS spectra were obtained using an Applied Biosystems 4800 MALDI TOF/TOF analyzer equipped with a reflectron and a high-performance nitrogen laser operating at 355 nm. The isolated polymer was dissolved in THF(10 mg/mL), while the matrix, 2,5-dihydroxybenzoic acid, was dissolved separately in THF (15 mg/mL). The polymer and matrix solutions were mixed together in a 1:4 ratio respectively and spotted onto the MALDI plate; the plate was left for 10-15 minutes to allow the solution to evaporate fully from the plate. Gel permeation chromatography (GPC) was carried out on an Agilent Triple Detector, at 35 °C. Polymer samples were prepared using THF from the GPC system, at a concentration of 2 mg/mL. These samples were left to equilibrate briefly before being filtered through 0.2 μm syringe filters prior to analysis. The flow rate was set to 0.30 mL/min with an injection volume of 100 μL.

4.4.3 Copolymerization Procedure

The appropriate amount of iron and cocatalyst were weighed out separately into scintillation vials. Each was dissolved into minimal amounts of dichloromethane prior to mixing in a round bottom flask. The purple solution was placed on the rotovap to

remove the dichloromethane, leaving behind a very thick purple oil. Cyclohexene oxide was then added, to create a dark red solution which was pipetted into the pressure vessel which had been dried under vacuum at 100 °C for a minimum of 4 hours prior to use. The vessel was then heated to the desired temperature before being charged with CO₂ and left to stir. Once the reaction was completed, the stirring was stopped, and the vessel was placed into an ice bath until it cooled to room temperature then vented into a fumehood. A small amount of crude product was taken for NMR analysis. The polymer was then isolated through extraction into dichloromethane and precipitation with cold acidified methanol.

4.5 References

1. Alhashmialameer, D.; Collins, J.; Hattenhauer, K.; Kerton, F. M., *Catal. Sci. Technol.* **2016**, *6*, 5364-5373.
2. Al-Qaisi, F. a.; Genjang, N.; Nieger, M.; Repo, T., *Inorganica Chim. Acta.* **2016**, *442*, 81-85.
3. Buonerba, A.; De Nisi, A.; Grassi, A.; Milione, S.; Capacchione, C.; Vagin, S.; Rieger, B., *Catal. Sci. Tech.* **2015**, *5*, 118-123.
4. Fuchs, M. A.; Zevaco, T. A.; Ember, E.; Walter, O.; Held, I.; Dinjus, E.; Doring, M., *Dalton Trans.* **2013**, *42*, 5322-5329.
5. Vummaleti, S. V. C.; Buonerba, A.; De Nisi, A.; Monari, M.; Della Monica, F.; Nisi, A. D.; Milione, S.; Grassi, A.; Cavallo, L.; Capacchione, C., *Adv. Synth. Catal.* **2016**, *358*, 3231-3243.
6. Darensbourg, D. J.; Yarbrough, J. C.; Ortiz, C.; Fang, C. C., *J. Am. Chem. Soc.* **2003**, *125*, 7586-7591.
7. Buchard, A.; Kember, M. R.; Sandeman, K. G.; Williams, C. K., *Chem. Commun.* **2011**, *47*, 212-214.
8. Taherimehr, M.; Al-Amsyar, S. M.; Whiteoak, C. J.; Kleij, A. W.; Pescarmona, P. P., *Green Chem.* **2013**, *15*, 3083-3090.
9. Taherimehr, M.; Serta, J.; Kleij, A. W.; Whiteoak, C. J.; Pescarmona, P. P., *ChemSusChem.* **2015**, *8*, 1034-1042.
10. Allan, L. E.; MacDonald, J. P.; Reckling, A. M.; Kozak, C. M.; Shaver, M. P., *Macromol. Rapid. Commun.* **2012**, *33*, 414-418.
11. Chard, E. F.; Dawe, L. N.; Kozak, C. M., *J. Organomet. Chem.* **2013**, *737*, 32-39.
12. Chowdhury, R. R.; Crane, A. K.; Fowler, C.; Kwong, P.; Kozak, C. M., *Chem. Commun.* **2008**, 94-96.
13. Hasan, K.; Brown, N.; Kozak, C. M., *Green Chem.* **2011**, *13*, 1230-1237.
14. Hasan, K.; Dawe, L. N.; Kozak, C. M., *Eur. J. Inorg. Chem.* **2011**, *2011*, 4610-4621.
15. Hasan, K.; Fowler, C.; Kwong, P.; Crane, A. K.; Collins, J. L.; Kozak, C. M., *Dalton Trans.* **2008**, 2991-2998.

16. Kozak, C.; Qian, X., *Synlett* **2011**, 2011, 852-856.
17. Qian, X.; Dawe, L. N.; Kozak, C. M., *Dalton Trans.* **2011**, 40, 933-943.
18. Reckling, A. M.; Martin, D.; Dawe, L. N.; Decken, A.; Kozak, C. M., *J. Organomet. Chem.* **2011**, 696, 787-794.
19. Devaine-Pressing, K.; Dawe, L. N.; Kozak, C. M., *Polym. Chem.* **2015**, 6, 6305-6315.
20. Darensbourg, D. J.; Mackiewicz, R. M.; Billodeaux, D. R., *Organometallics* **2005**, 24, 144-148.
21. Lehenmeier, M. W.; Kissling, S.; Altenbuchner, P. T.; Bruckmeier, C.; Deglmann, P.; Brym, A. K.; Rieger, B., *Angew. Chem. Int. Ed.* **2013**, 52, 9821-9826.
22. Super, M. S.; Enick, R. M.; Beckman, E. J., *J. Chem. Eng. Data* **1997**, 42, 664-667.

5. Conclusions and Future Work

Four iron(III) iron amino-(bis) phenolate complexes (**2.1** - **2.4**) have been synthesized and were characterized through elemental analysis, MALDI-TOF MS, and UV-vis spectroscopy. Preparation of complexes **2.1** - **2.4** allowed for catalytic studies of their behaviour in the coupling of CO₂ with various epoxides, as well as the copolymerization of CO₂ and CHO. All four complexes were successful throughout these reactions. However, **2.3** demonstrated the lowest activity in all cases. This can be attributed to the combination of steric and electronic effects; something worth investigating further in the future. Although the other catalysts worked well in all reactions, it appeared that having a more Lewis acidic metal centre, achieved by placing electron withdrawing substituents on the phenolate rings, was beneficial to produce cyclic carbonates. Electron donating substituents created a less Lewis acid iron centre and led to optimal results for the copolymerization of CO₂ and CHO.

Reaction parameters were optimized in the coupling of CO₂ and PO by completing several reactions and changing only one parameter at a time. These parameters included: catalyst choice, reaction time, catalyst loading, temperature, cocatalyst choice, and CO₂ pressure. While conversions may have decreased, reaction time could be lowered to just 2 h and the production of PPC was still achieved. PPNCI demonstrated the best results as a cocatalyst, and only 2 equivalents were necessary to achieve near quantitative results after 22 h. While TBAB demonstrated to be an efficient cocatalyst for this reaction also, the use of DMAP nearly halted the reaction process completely. It would be beneficial in the future to obtain a crystal of **2.2** with DMAP

(**2.2•DMAP**) to support the theory this particular nucleophile coordinates strongly to the metal centre, therefore hindering the possibility of epoxide coordination.

Temperature was very important for the coupling of CO₂ and PO as well. Observed reaction rates, by following $\nu_{\text{CO}} = 1810 \text{ cm}^{-1}$, demonstrated a large increase in conversion only after the temperature reaches 60 °C. No PPC is formed at room temperature, even after 22 h. To achieve the E_a of this reaction, 49.6 kJ mol⁻¹, initial reaction rates were followed by in situ IR at lower temperatures (40 – 60 °C) using **2.2/PPNCl**. The entropy and enthalpy were also determined to be -124 J K⁻¹ mol⁻¹ and 47.9 kJ mol⁻¹ respectively.

Applying optimized reaction conditions (4 h, 100 °C, 20 bar CO₂ pressure) using **2.2** with 2 equivalents PPNCl, other epoxides were assessed as well and successfully formed cyclic carbonates. As outlined in Chapter 3, a few of these epoxides (styrene oxide, allyl glycidyl ether, and phenyl glycidyl ether) could be left to run longer and potentially achieve higher conversions. The same optimization and testing that was completed with PO could be applied to these epoxides as well.

Copolymerization for CO₂ and CHO was successful as well using complexes **2.1-2.4**, demonstrating a selectivity for polycarbonate product vs. cyclic of greater than 95% in all reactions. For these reactions, only pressure dependence, time, and temperature were thoroughly looked into to optimize parameters. Similar to the PO work, no activity is seen when performing the reaction at room temperature. However, at 40 °C very high conversion of CHO was observed after 22 h. Reaction time could be decreased to only 4 h and still produce polycarbonate indicating that the length of reactions could be greatly improved upon in the future by performing reactions between

10 h and 22 h to determine when the reaction has come to completion. Information can be gained from such reactions by determining molecular weights of each polymer obtained at different times, as it appears that using the **2.4**/PPNCl system could indicate a living polymerization looking at the results from 4 h and 8 h. Polycarbonate synthesis also proved successful at pressures as low as 7 bar CO₂. Developing methods to perform this reaction at pressures as low as 1 bar CO₂ reliably would be well worth attempting in the future, along with thorough kinetic and rate law studies. Fine tuning the reaction parameters in an attempt to form cyclic cyclohexene carbonate would also be an interesting future endeavor.

6. Appendix

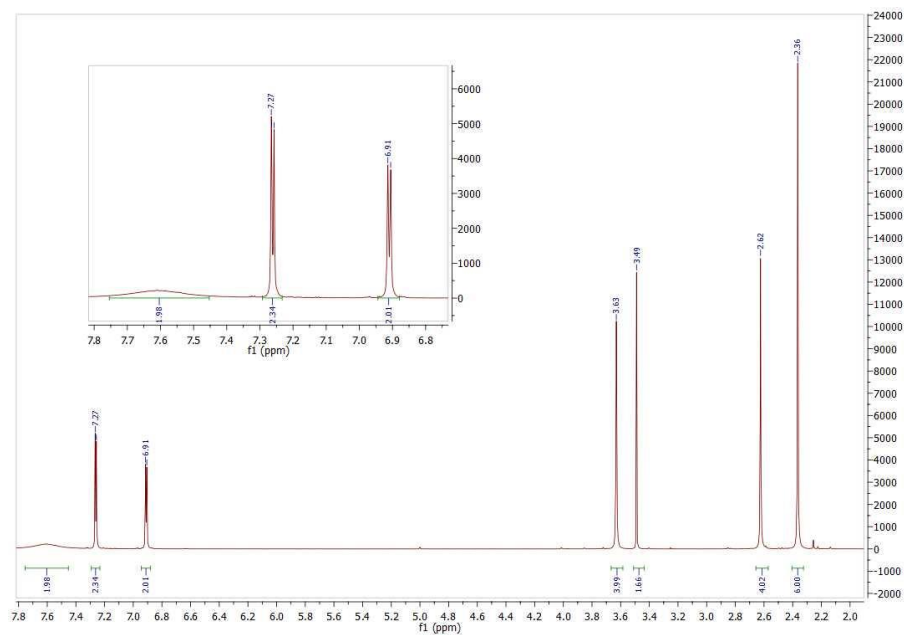


Figure 6.1: ^1H NMR spectrum of $\text{H}_2\text{L1}$ in CDCl_3

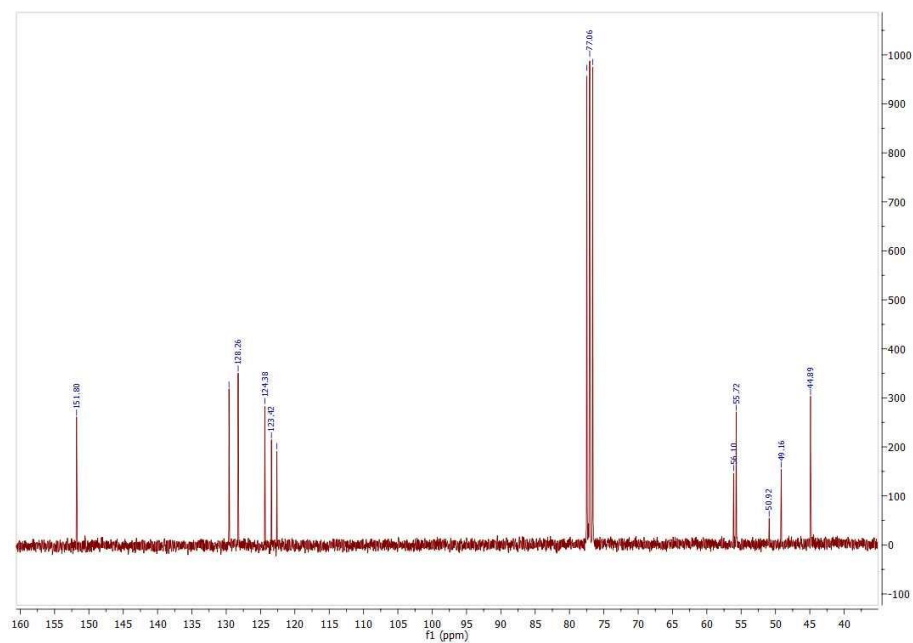


Figure 6.2: $^{13}\text{C}\{^1\text{H}\}$ NMR spectrum of $\text{H}_2\text{L1}$ in CDCl_3

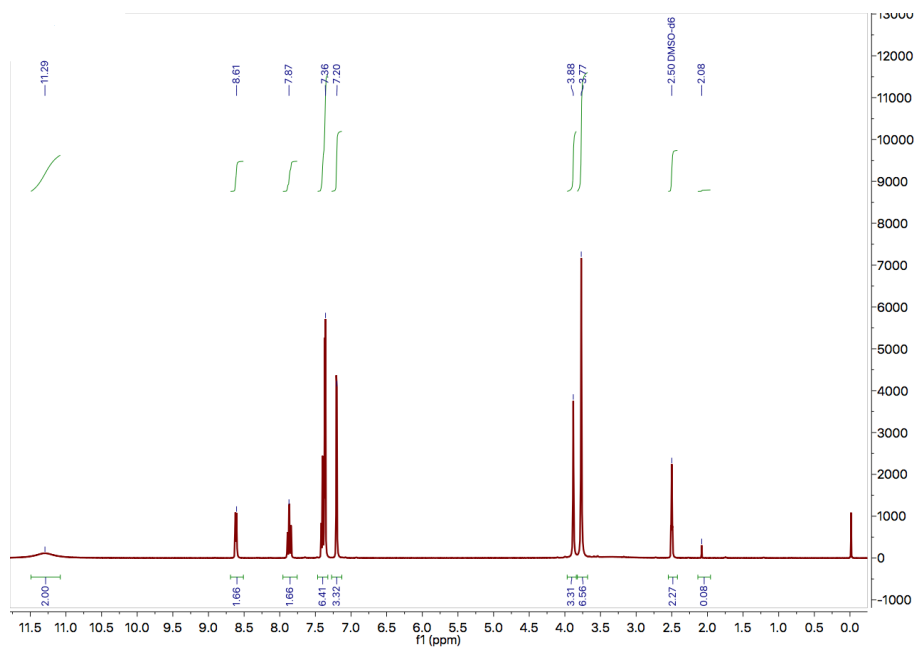


Figure 6.3: ^1H NMR spectrum of H_2L_2 in DMSO

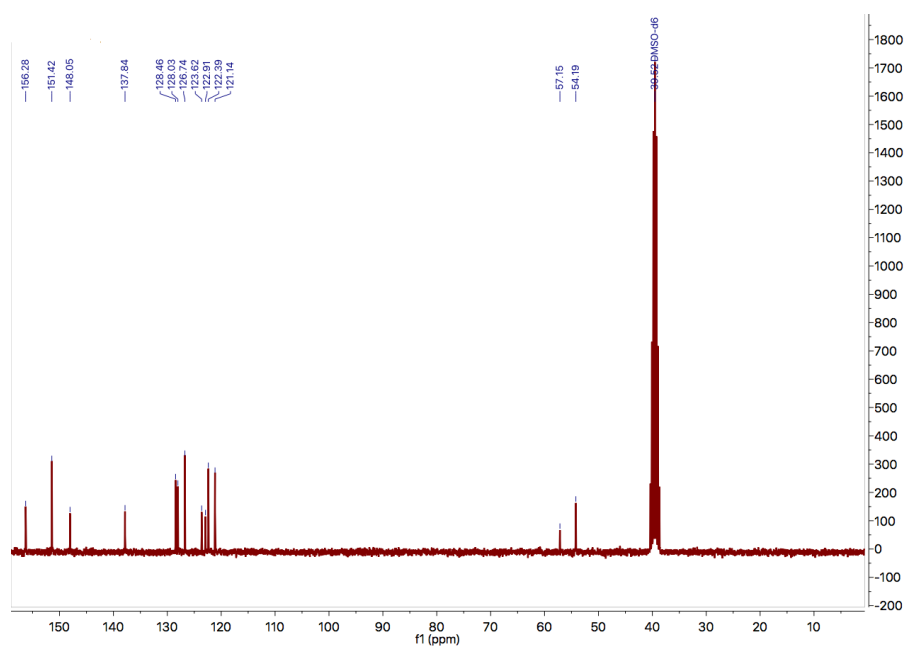


Figure 6.4: $^{13}\text{C}\{^1\text{H}\}$ NMR spectrum of H_2L_2 in DMSO

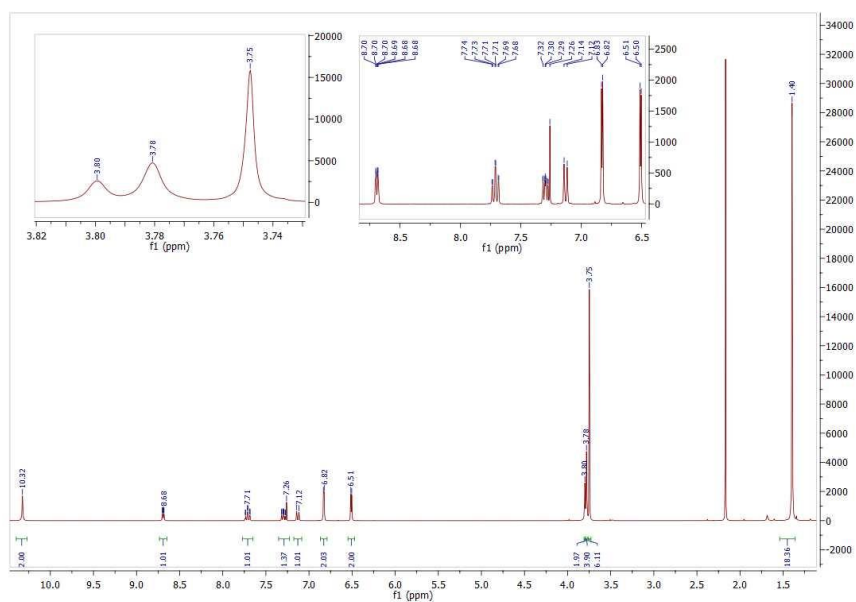


Figure 6.5: ^1H NMR spectrum of $\text{H}_2\text{L4}$ in CDCl_3

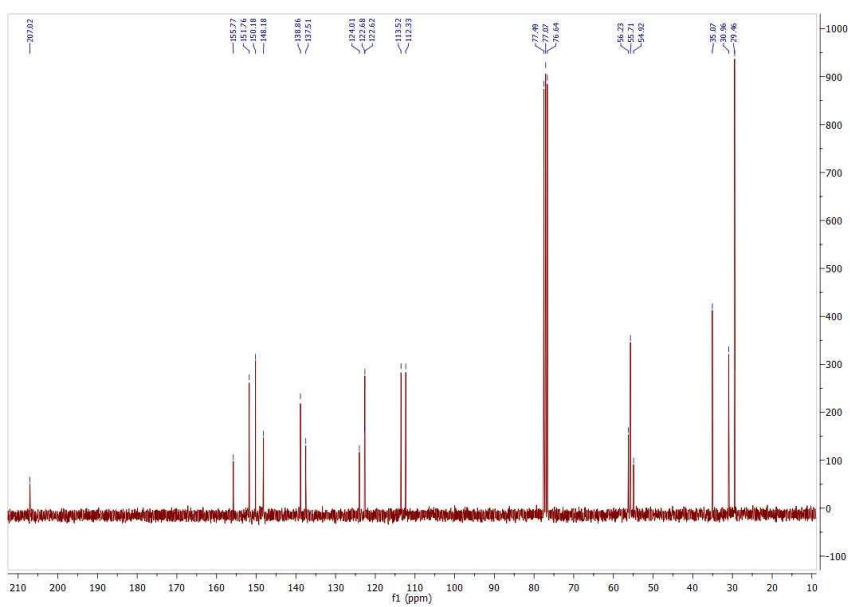


Figure 6.6: $^{13}\text{C}\{^1\text{H}\}$ NMR spectrum of $\text{H}_2\text{L4}$ in CDCl_3

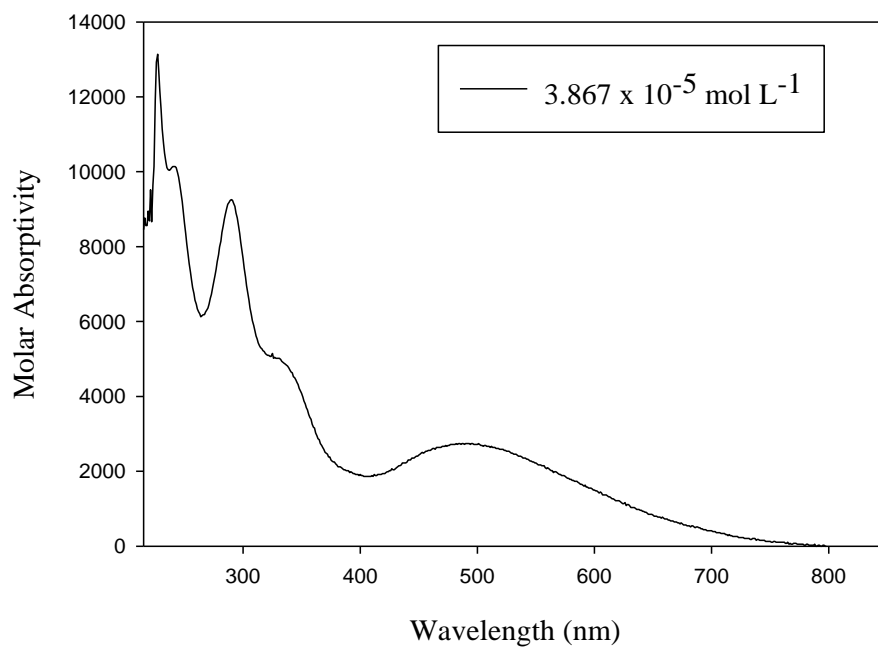


Figure 6.7: UV-vis spectrum of **2.1** in CH_2Cl_2

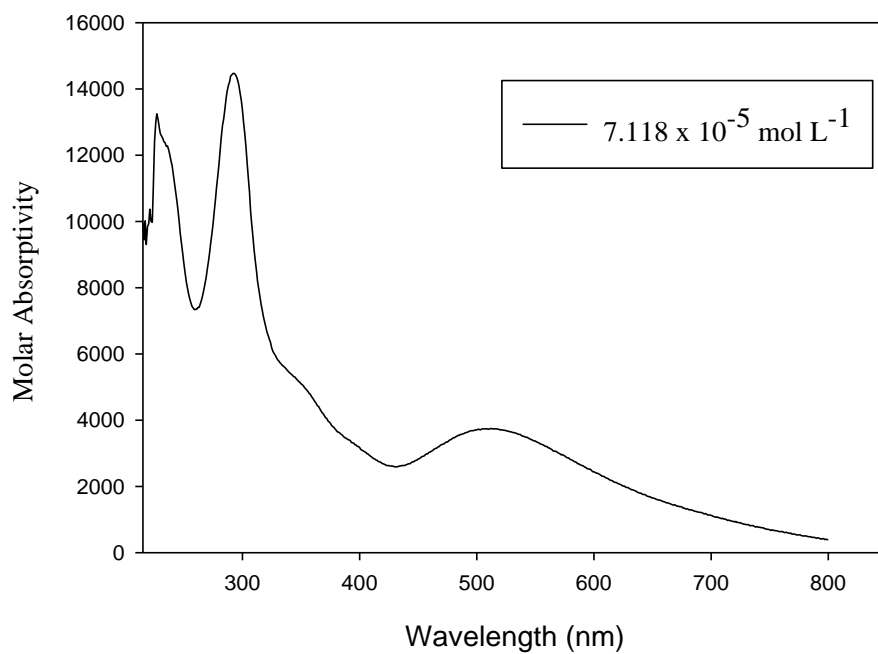


Figure 6.8: UV-vis spectrum of **2.3** in CH_2Cl_2

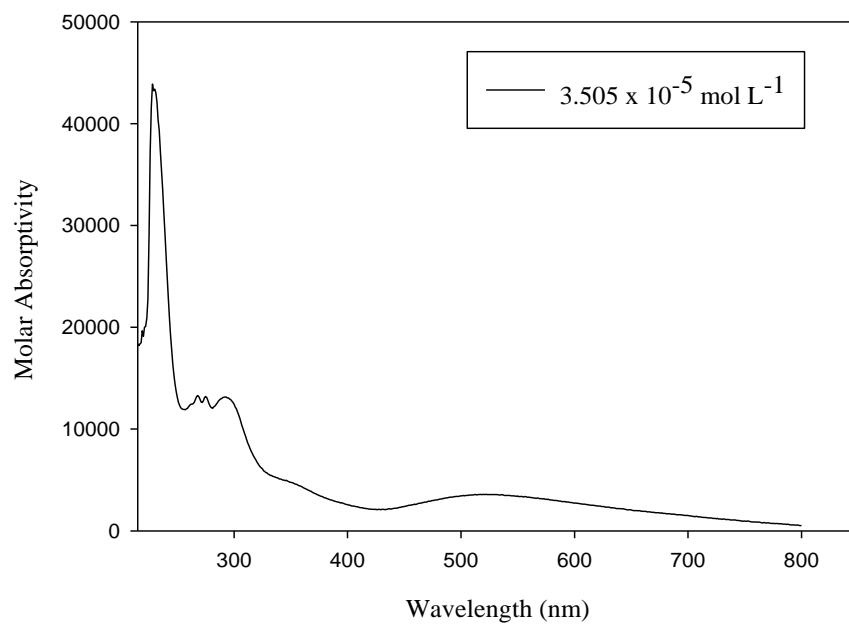


Figure 6.9: UV-vis spectrum of **2.4** in CH_2Cl_2

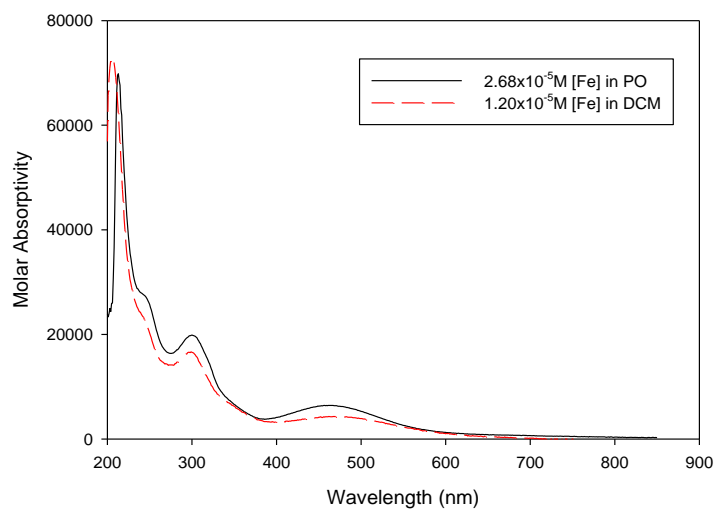


Figure 6.10: UV-vis spectrum of **2.2** in CH_2Cl_2 overlaid with **2.2** in PO

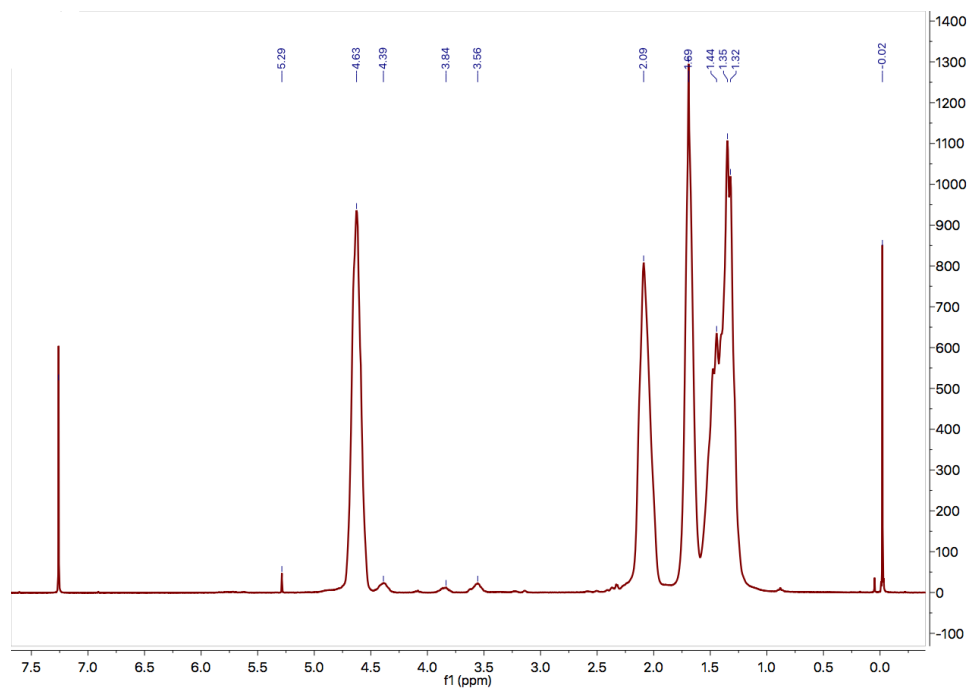


Figure 6.11: ^1H NMR spectrum of isolated polycarbonate in CDCl_3 (Table 4.1 Entry 3)

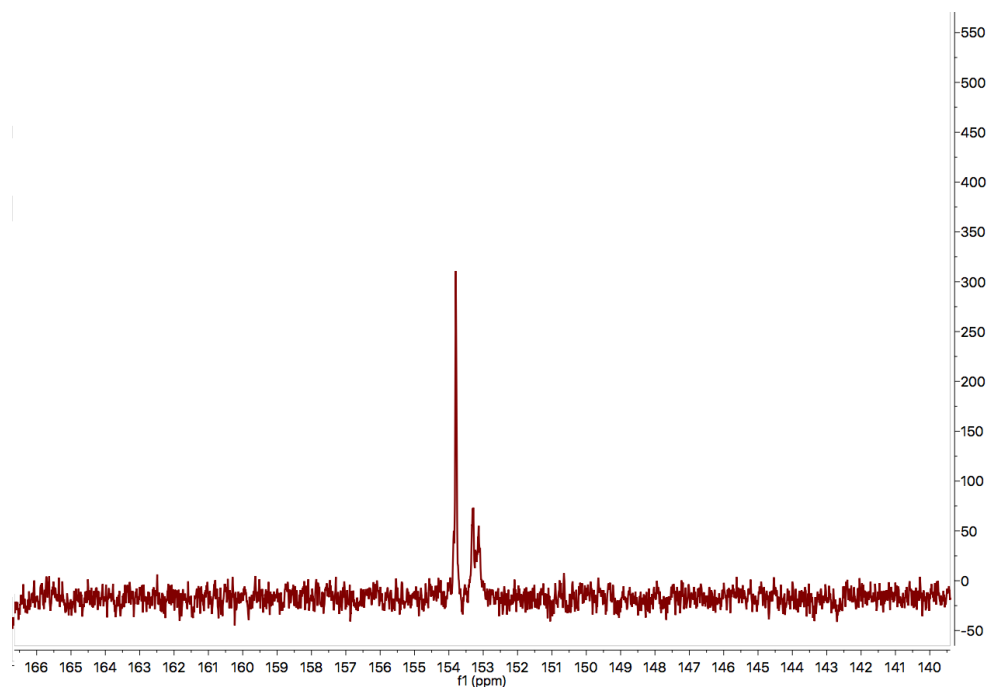


Figure 6.12: Magnified $^{13}\text{C}\{^1\text{H}\}$ NMR spectrum of isolated polycarbonate in CDCl_3 (Table 4.1 Entry 3) demonstrating atactic stereoselectivity

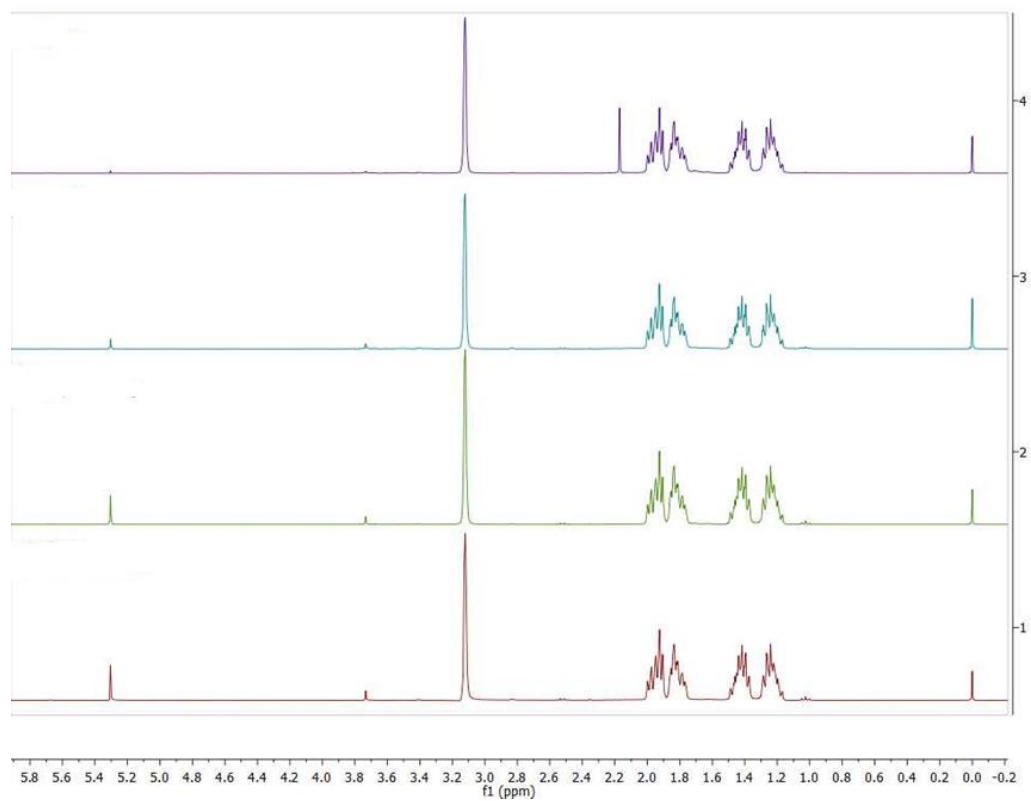


Figure 6.13: ^1H NMR spectra of attempted homopolymerization reactions of CO_2 and CHO using **2.4**; from bottom to top: 25 °C, 40 °C, 60 °C, and 80 °C